Investigation of composite electrolytes with structured silica materials for lithium ion batteries

Dissertation zur Erlangung des Doktorgrades der Chemie des Fachbereichs 8 der Justus-Liebig-Universität Gießen

vorgelegt von

Kerstin Sann

wohnhaft in Offenbach am Main

Gießen 2016

Dekan / dean: Prof. Dr. Volker Wissemann

1. Gutachter / 1st reviewer: Prof. Dr. Jürgen Janek
2. Gutachter / 2nd reviewer: Prof. Dr. Bernd Smarsly

eingereicht am / submitted on 28.06.2016

Ich erkläre:
Ich habe die vorgelegte Dissertation selbständig und ohne unerlaubte fremde Hilfe und nur mit den Hilfen angefertigt, die ich in der Dissertation angegeben habe. Alle Textstellen, die wörtlich oder sinngemäß aus veröffentlichten Schriften entnommen sind, und alle Angaben, die auf mündlichen Auskünften beruhen, sind als solche kenntlich gemacht. Ich stimme einer evtl. Überprüfung meiner Dissertation durch eine Antiplagiat-Software zu. Bei den von mir durchgeführten und in der Dissertation erwähnten Untersuchungen habe ich die Grundsätze guter wissenschaftlicher Praxis, wie sie in der "Satzung der Justus-Liebig-Universität Gießen zur Sicherung guter wissenschaftlicher Praxis" stehen, eingehalten.

(I declare that I have completed this dissertation single-handedly without the unauthorized help of a second party and only with the assistance acknowledged therein. I have appropriately acknowledged and cited all text passages that are derived verbatim from or are based on the content of published work of others, and all information relating to verbal communications. I consent to the use of an anti-plagiarism software to check my thesis. I have abided by the principles of good scientific conduct laid down in the charter of the Justus-Liebig-University-Gießen "Satzung der Justus-Liebig-Universität Gießen zur Sicherung guter wissenschaftlicher Praxis" in carrying out the investigations described in the dissertation.)

Gießen, 2016

Kerstin Sann

“In der Mitte von Schwierigkeiten liegen die Möglichkeiten”
(*Opportunities are to be found amidst difficulties*)

Albert Einstein

Abstract

Composite electrolytes, consisting of an organic lithium electrolyte with dispersed filler material therein, were experimentally studied concerning their electrochemical behavior. The influence of added filler material (isolating particles) on a liquid lithium electrolyte, especially boundary layer phenomena, the influence of surface charge, viscosity trends and electrochemical stability were evaluated. Hence, different types of silica filler material, mesoporous and surface designed silica as well as commercially available silica, were systematically deployed with a range of pore geometry, pore size and specific surface area. The crucial role of the chemical composition of the filler surface exposed to an electrolyte of 1 M lithium hexafluorophosphate ($LiPF_6$) in a solvent mixture of ethylene carbonate (EC) and diethylene carbonate (DEC) at the ratio 3:7 was investigated.

Besides different measurements (conductivity, zeta potential, viscosity, electrochemical window) and material variations (cf. fig. 0.1), some formal considerations were done like the calculation of the conductivity decrease with volume exclusion assumptions and estimation of activation energies for the movement of the ions in solution or the number of possible adsorption sites on the silica surfaces.

These formal considerations were only helpful to a certain extent. The conductivities varied much between the systems and therefore, they differed more or less from the theoretical volume exclusion assumptions. The characteristics of the calculated activation energies could hardly be linked with the measured conductivities. Most of the dispersions had the same activation energy as the pure electrolyte, when taking measurement deviations into account. The calculation of silica surface sites showed, that the number density of ions in the used 1 M electrolyte is one order of magnitude higher than the number density of possible adsorption positions on the silica surfaces in the dispersions.

The conductivity decreased with addition of silica filler material but varied considerably for the different fillers. Due to the sedimentation of the silica,

stirring was necessary whereby no particulate network was formed. Several materials showed deviations from the the conductivity trend expected from calculation of volume exclusion. Hence, boundary layer effects or interaction of electrolyte ions with the silica surface (filler material) are assumed. Accordingly, zeta potential measurements showed partially trapping of Li^+ ions on the silica surface dependent on the surface functionalization and therefore the surface charge. As the Li^+ ions are the essential charge carrier in lithium electrolytes this adsorption reaction is unfavorable.

Viscosity studies showed mainly Newtonian behavior of the composite dispersions with a liquid organic electrolyte, which again proves that no attractive particle network was formed. However, the mechanical properties of the electrolytes changed significantly in some systems with the amount of filler material, with only little change of the conductivity.

Determination of the electrochemical window showed a slight widening for one system, maybe due to special morphology of the silica material Cab-O-Sil in this work, whereby most of the dispersions exhibited the same electrochemical window as the pure electrolyte.

Within all the measurements and results no clear trend for the behavior and characteristics of silica filler materials in a liquid lithium electrolyte could be observed. The conductivities varied between the composite electrolytes, but showed a conductivity decrease, which was stronger than the expected decrease with volume exclusion assumptions. With the used silica materials no particle network was formed, but different influences depending on the characteristics of the silica materials could be observed. Hence, one can conclude that the surface chemistry and morphology of the silica filler materials influence the electrochemical behavior of liquid lithium electrolytes, which can be positive as well as negative. Improvement of good liquid lithium electrolytes with addition of silica as filler material did only lead to marginal changes in this work.

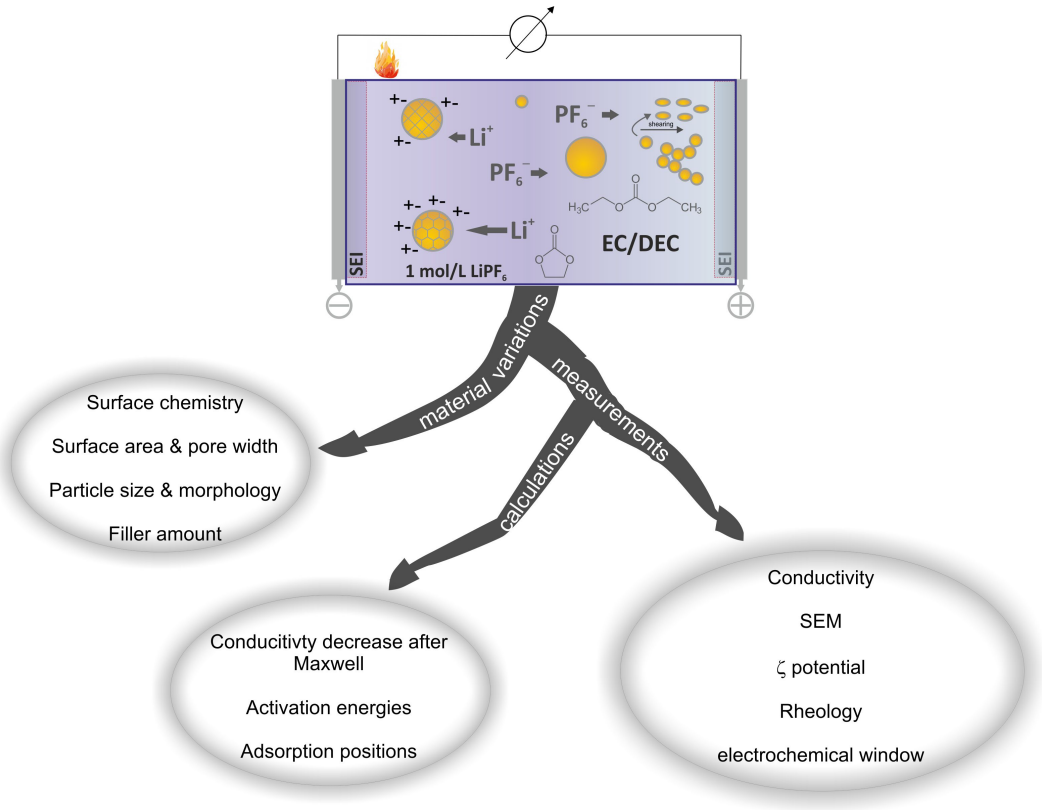

Figure 0.1: Summary of variations, measurement methods and calculations used in this work.

Zusammenfassung

Komposit-Elektrolyte, bestehend aus einem organischen lithiumhaltigen Elektrolyten mit verschiedenen darin dispergierten Silica-Materialien (Füllmaterial), wurden in dieser Arbeit hinsichtlich ihres elektrochemischen Verhaltens experimentell untersucht (vgl. Bild 0.2). Dabei war der Einfluss der hinzugefügten Silica-Materialien auf den flüssigen Lithium-Elektrolyten, bestehend aus 1 M Lithiumhexafluorophosphat ($LiPF_6$) in einem Lösemittelgemisch aus Ethylencarbonat (EC) und Diethylencarbonat (DEC) in einem Mischungsverhältnis von 3:7, von Interesse. Vor allem Leitfähigkeiten, Grenzflächen-Phänomene, Einfluss von Oberflächenladungen, Viskositätsverhalten und die elektrochemische Stabilität wurden untersucht. Dafür wurden systematisch unterschiedliche Silica-Materialien eingesetzt, sowohl mesoporöse und oberflächenmodifizierte Silica, als auch kommerziell erhältliche Silica-Materialien, mit verschiedenen Porengeometrien, Porengrößen und spezifischen Oberflächen.

Innerhalb der durchgeführten Messungen und theoretischen Berechnungen konnte kein eindeutiger Trend für das Verhalten von Silica-Materialien dispergiert in einen flüssigen Lithium-Elektrolyten festgestellt werden. Die Leitfähigkeiten variierten zwischen den verschiedenen Elektrolyt-Systemen, wobei die Zugabe der Silica-Materialien zu einer Leitfähigkeitsabnahme geführt hat, die teilweise stärker war, als durch Berechnung des Volumenausschlusses angenommen. Mit den verwendeten Silica-Materialien wurde kein partikuläres Netzwerk erhalten, jedoch konnten verschiedene Einflüsse, abhängig von den Charakteristiken der zugesetzten Silica, beobachtet werden. Zusammenfassend kann gesagt werden, dass die Oberflächenchemie und Morphologie der Silica-Materialien das elektrochemische Verhalten eines flüssigen lithiumhaltigen Elektrolyten sowohl positiv als auch negativ beeinflussen können. Insgesamt hat die Zugabe der Silica-Materialien nur zu geringen Änderungen der Eigenschaften des flüssigen Elektrolyten geführt. Die Verbesserung eines gut leitenden flüssigen Lithium-Elektrolyten durch Zugabe von Silica-Materialien erscheint damit wenig möglich.

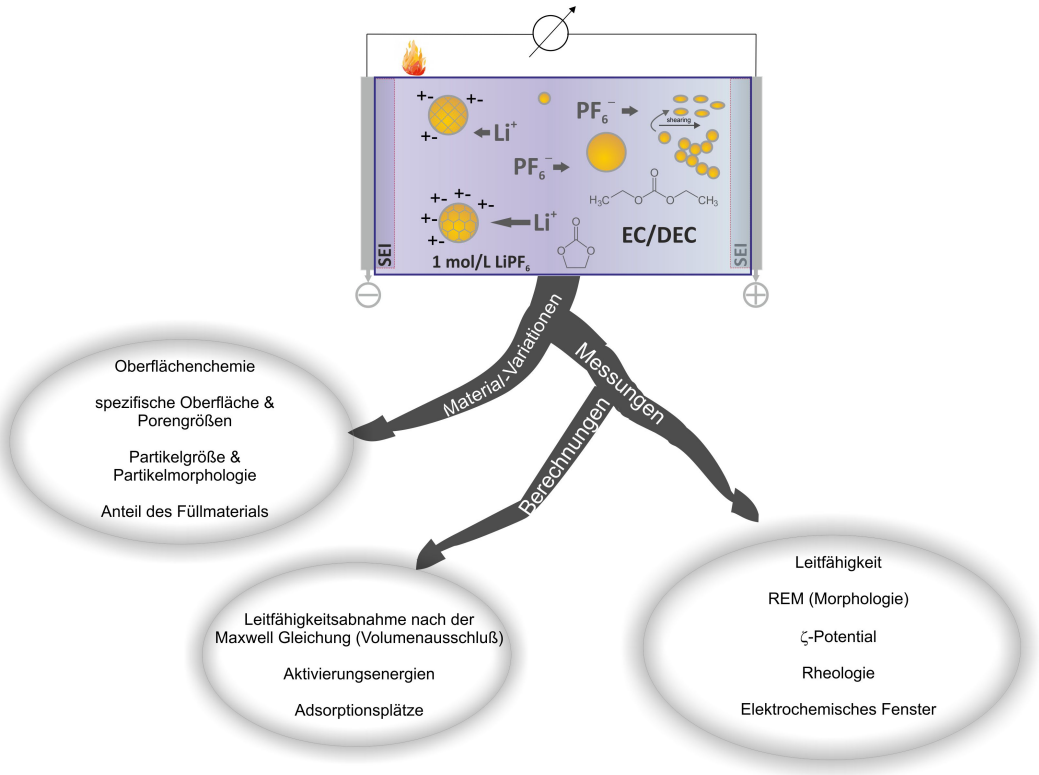

Figure 0.2: Grafische Zusammenfassung der in dieser Arbeit genutzten Material-Variationen, der durchgeführten Messungen und der vorgenommenen theoretischen Berechnungen.

List of Abbreviations

AC	Alternating current
CPE	Constant phase element
CV	Cyclic voltammetry
DC	Direct current or continouus current
DEC	Diethyl carbonate
EC	Ethylene carbonate
EIS	Electrochemical Impedance spectroscopy
IL	Ionic liquid
IR	Infrared spectroscopy
LDV	Laser doppler velocimetry
LIB	Lithium ion battery
LSV	Linear sweep voltammetry
MCM-41	Mobil´s Composition of Matter
MS	Mass spectrometry
NMR	Nuclear Magnetic Resonance
pfg-NMR	Pulsed field gradient NMR
SBA-15	Santa Babara Amorphous type material
SEI	Solid electrolyte interphase
SEM	Scanning electron microscopy
VFT	Vogel-Fulcher-Tammann
XRD	X-ray diffraction

List of Symbols

D_j	diffusion coefficient
ε	volume fraction of the second phase
E_A	activation energy
E_g	electrochemical window
e_o	elementary charge
Φ	work function
$\dot{\gamma}$	shear stress
η	viscosity
I	current
$l/A = C_{cell}$	cell constant
$\tilde{\mu}$	electrochemical potential
n_i	number of ions
ρ	specific resistance
R	resistance
R	ideal gas constant
σ	conductivity
t	transference number
τ	shear rate
T_{FP}	flash point
T_g	glass temperature
U	voltage
u_i	ion mobility
ω	mass fraction
Ψ_S	Stern potential
ζ	zeta potential
z_i	ion charge

Contents

1 Introduction

The markets and applications for lithium ion batteries (LIB's) are still growing, and therefore, the search for improvements continues. Lithium ion batteries are the power source of choice for the portable electronic market, especially cellular phones and laptops. In this field, the current LIB technological status fulfills the requirements. Besides, the effective storage of electrical energy is a main factor for future politics in energy. Efforts in efficient use of renewable energy sources and replacement of combustion engines with electric motors is necessary. For the energy efficiency in the use of renewable energies like solar, wind and geothermal energy, the side support with storage systems to compensate intermittent characteristics is essential. The LIB is of paramount importance for the expansion of the electromobility market as well as for stationary intermediate storage of renewable energies, since a battery is a device that provides two functions, namely, the energy storage and energy conversion. Moreover, it is a portable device and capable to deliver the stored energy with high conversion efficiency and without gaseous emission [1]. Various problems prevent the large-scale application of LIB's for this use, mainly the energy density (and therefore the specific capacity), the rate capability, the safety and the costs. Generally spoken their lack of economic viability as well as limits in performance have prevented it from making a breakthrough. Hence, an improvement of the present LIB technique seems to be the fastest and easiest way of progress and there is still much potential for upgrading, before new and promising battery systems are sufficiently investigated to be applicable.

There is also a great potential for further development of new battery systems, especially concerning the lithium/sulfur and the lithium/air battery. However, in order to make them operational, a lot of research is needed as there are still serious problems to be dealt with. The lithium/sulfur battery is suffering from the formation of polysulfides for example, which easily dissolve in the electrolyte [2] [3], whereas the severe issues of the lithium/air battery are the reactivity of the anode, the poor reversibility and the poor

efficiency of the oxygen electrode [4].

Advancements in the lithium ion technology are relevant especially concerning enhanced energy density and the material chemistry [5]. The electrode chemistry for instance passes from intercalation to conversion chemistry [6]. The energy density of current LIB's is in the range of 150 Wh kg^{-1} - 200 Wh kg^{-1}, whereby the batteries can differ in cycle stability. Prototypes of Li-S-batteries already exhibit 350 Wh kg^{-1}. Batteries with energy densities more than 350 Wh kg^{-1} are needed in order to reach high energy batteries. With lithium/sulfur and lithium/air batteries even higher energy densities are expected.

Lithium with its low molar weight (6.9 g/mol), high specific charge (3862 Ah/kg) and negative electrode potential ($-$ 3.05 V) is in theory well suited for the use in batteries. Although the lithium metal is thermodynamically unstable in non-aqueous electrolytes, it is kinetically stable in appropriate electrolytes due to the formation of a protective layer. This protective layer, called solid electrolyte interphase (SEI), is built up at the interface between electrode and electrolyte and is permeable for lithium ions. Dependent on the type of electrolyte, the SEI consists of organic and inorganic components like LiF, Li_2CO_3 etc. The secondary lithium battery with lithium metal as anode was not marketable due to the growth of dendrites, resultant loss of capacity and risk of short-circuits. The breakthrough of the rechargeable lithium ion battery for portable applications was achieved by Sony in 1991 with intercalation materials as cathode material instead of metallic lithium. The charge and discharge process is ensured by the transport of Li^+ ions between anode and cathode. Thus, the battery reaction is simple, as only Li^+ ions participate in the charge/discharge reaction:

$$\mathrm{Li_{1-x}MO_2 + Li_xC_n} \underset{\text{charge}}{\overset{\text{discharge}}{\rightleftharpoons}} \mathrm{LiMO_2 + C_n} \tag{1.1}$$

Most of the current battery systems contain solid electrodes, separated by special fiber mats (separator) soaked with liquid electrolytes [7]. Basically, in LIB's lamellar carbon materials like graphite are deployed as negative active mass, which can store and deliver Li^+ ions reversibly (cf. fig. 1.1). As positive active mass compounds transition metals of the type $LiMO_2$ (M = Ni, Co, Mn) are used. The currently used lithium ion battery consists of graphitic carbon as anode, predominately $LiCoO_2$ and other layered compounds of

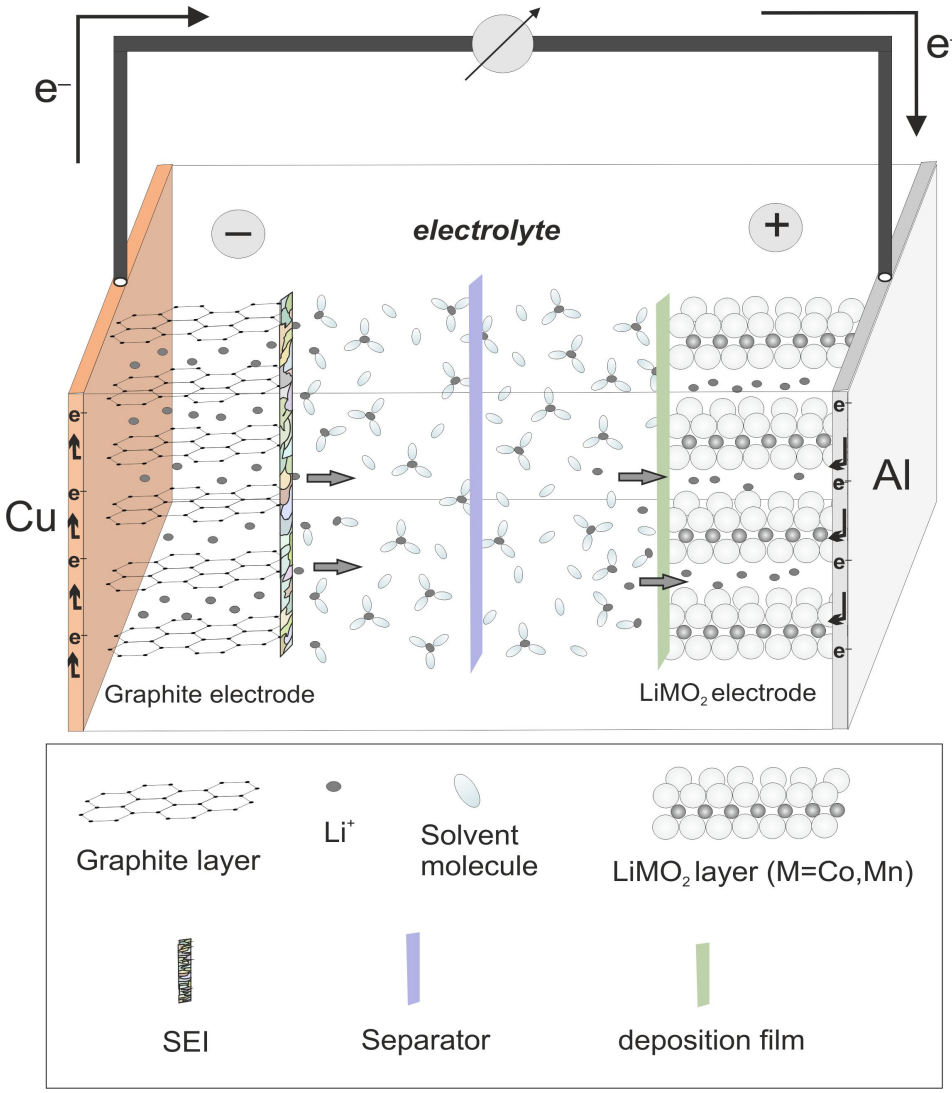

Figure 1.1: Schematic presentation of a lithium ion battery under discharge.

the type Li[Ni, Co, Mn]O_2 as cathode and mixtures of alkyl carbonates with the conducting salt $LiPF_6$ as electrolyte with additionally certain functional additives [8, 9]. This LIB is capable of a high performance with a minimal amount of side reactions. The electrode active materials must show a good reversibility and kinetics of the intercalation and deintercalation, as the lithium diffusion in and out of the electrode structures is the rate determining step.

In the present lithium ion battery technology a lot of work is done in finding new or improved electrode materials to enhance the energy density, especially cathode materials. The substitution of electrode materials does not mark the final solution for significant progress in the LIB technology. The electrolyte is also an important component, hence the improvement of the electrolyte is crucial, particularly for high power and large size applications. There is still a distinct search for convenient electrode/electrolyte pairs, because the matching of the battery components is decisive for advanced batteries. A major research issue is to improve the performance and safety of electrolytes as well as the electrochemical stability, and this issue was addressed in this work. In the following chapter the fundamental considerations concerning requirements, benefits and deficits of disperse electrolytes are discussed in-depth, in order to explain the motivation for this study.

2 Motivation

The choice of the right electrolyte for lithium ion battery systems must be done carefully and is more crucial than often considered [10]. Liquid electrolytes are well established and commonly used in lithium ion batteries. Polymer electrolytes are also used and represent the attempt to combine high mechanical, thermal and electrochemical stability. Solid electrolytes are outstanding in terms of safety but the application in batteries is problematic due to contact problems with the electrode [11] and typically a lower conductivity. Relatively new electrolyte components are ionic liquids (IL). They are promising as solvents as they have good safety features like low vapor pressure and inflammability as well as a good conductivity with the advantages of a liquid electrolyte [1]. All these types of electrolytes differ in conductivity. The highest ionic conductivity is offered by liquid electrolytes with the range of 10^{-2} S cm^{-1} - 10^{-3} S cm^{-1}, followed by polymer electrolytes and IL's in the range of 10^{-3} S cm^{-1} - 10^{-4} S cm^{-1} and by solid electrolytes around 10^{-4} S cm^{-1}, but fast tendency towards much higher conductivities.

However, still the liquid organic electrolytes are superior in conductivity at moderate temperatures to most of the other materials (see fig. 2.1). The ionic conductivity of electrolytes is of course the most important aspect for the use in lithium ion batteries since it determines the cell resistance together with the electrode resistances [12]. The solid and ionic liquid electrolytes that can compete with the conductivity of organic electrolytes at room temperature have to overcome serious problems in the battery like contact and formulation problems or cathodic stability for example. An additional issue is the current electrolyte production, which is fully based on liquid electrolytes. A change of the electrolyte to a non-liquid system would need a completely different production technology for the lithium ion battery. Therefore, there is a remarkable interest of the industry to use liquid electrolytes.

The deficits of non-aqueous liquid electrolytes are mainly their flammability and toxicity. Hence, the goal is to develop an electrolyte, which better fulfills the high safety requirements, high availability, easy processing and

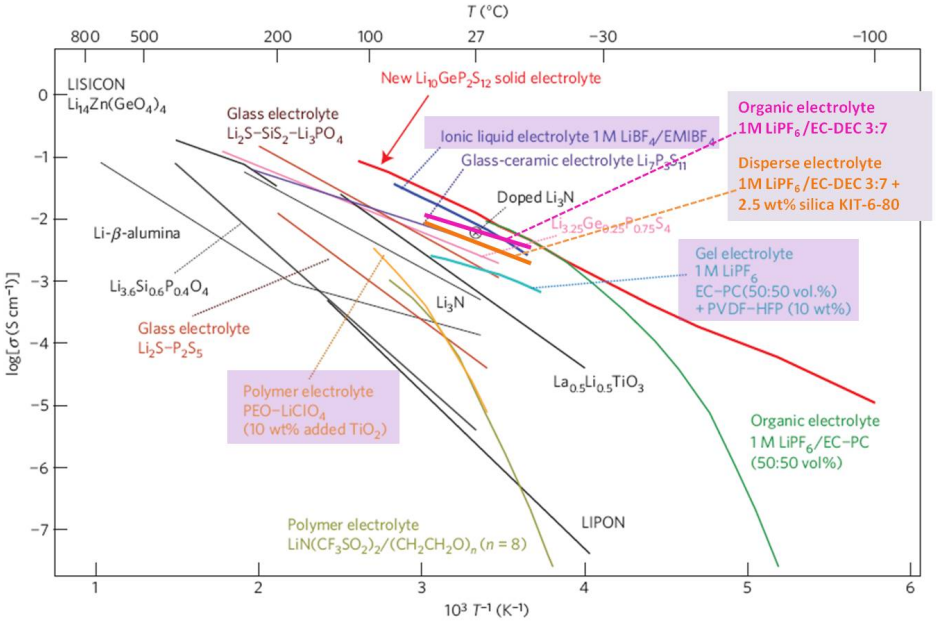

Figure 2.1: Electrical conductivities of various lithium electrolyte materials are shown. Liquid organic electrolytes, solid ion conductors and polymer electrolytes are compared in conductivity versus temperature (extended version of a graphic in source: [13]).

contacting with the electrodes and good conductivity.

The strategy to select electrolyte solutions for LIB's is based on four priorities [9]:

1. **Transport properties**: The high-current performance and high mobility of ions in battery electrolytes is essential for the function of batteries. Therefore, the optimization of transport properties such as transference number of the main charge carrier, salt diffusion coefficient and the salt activity are important.

2. **Safety features**: The flammability and toxicity of electrolytes should be reduced. Furthermore, the leakage of liquid electrolytes should be prevented.

3. **Electrochemical stability**: A battery electrolyte must be electrochem-

ically stable against the electrode materials. Especially for high-voltage systems stability in a wide electrochemical window up to 5 V will be necessary.

4. **Temperature range**: The surrounding and operational temperature for batteries fluctuates substantially and therefore the electrolyte should have good performance over a wide range of temperature without decomposition.

In recent years many efforts have been made to introduce new solvents [14], [15], salts [16] and additives [17] that may lead to an improvement and update of existing electrolyte system performances. Various additives with different functions are known like SEI modifier (tris(pentafluorophenyl)-borane (TPFPB)), salt stabilizer (LiF or tris(2,2,2-trifluoroethyl)phosphite - (TTFP)), cathode protection agents to scavenge water and acidic impurities (N-Si-based compounds), fire-retardants (cyclophosphazenes), ionic solvation enhancer (boranes, borates) or wetting agents (cyclohexane).

Besides the predominately liquid or soluble additives, the addition of inert solid particles to the liquid electrolyte is a promising idea that can affect several important issues at once ("nanofiller concept" for nanosized particles). The resulting colloidal dispersions are supposed to exhibit effects known from the heterogeneous doping of solids, which can enhance the conductivity [18]. Furthermore, in stable colloidal suspensions the electrochemical and thermal behavior may also be affected due to boundary effects and the influence of highly stable particles in a resulting particle network. The reduction of the organic fraction would also enhance the safety of the liquid electrolyte as the flammability and the leakage could be reduced.

The "doping" of solid electrolytes with inert and insulating solids and the resulting enhanced conductivity is known since the works of Liang back in 1973 [19]. In the 1980, Maier developed the concept of heterogeneous doping of solid electrolytes to improve their conductivity [18, 20, 21] with highly conductive space charge regions.

The effort to sustain highly conductive transport paths along internal interfaces also plays a key role in liquid composite electrolytes. Therefore, the high surface area and the various possibilities of systematic chemical structuring as well as surface modification of silica materials is advantageous. Recent works where this theory is transferred to liquid electrolytes refer to

the 'soggy sand' concept. This second phase effect on the conductivity of non-aqueous electrolytes firstly was reported by Bhattacharyya and Maier in 2004 [22–24]. However, the observed conductivity enhancements in various systems by Bhattacharyya must be viewed in a critical light, as these effects could not be well reproduced [12] and the mostly used conducting salts (e.g. $LiClO_4$) are of little significance for practical applications. But a second phase effect due to space charge regions around the filler material is still conceivable. As the formation of a space charge region is a surface effect, the use of mesoporous materials with higher specific surface area would lead to amplification of a conductivity enhancement. Silica materials appear to be beneficial as filler materials due to easy synthesis as mesoporous material and the easily done 'design' or modification of the surface.

Mesoporous materials as filler material are rarely investigated. The interest is currently growing, even in ionic liquids [25–30], although, the area of application are predominately polymer electrolytes [31–37]. In the case of polymer electrolytes, an enhancement of conductivity through dispersed particles is obvious due to hindrance of crystallization [38], which is clearly a different effect to those in liquids.

To study the influence of mesoporous silica with various characteristics on a standard battery electrolyte for lithium ion batteries, composite electrolytes consisting of an organic lithium electrolyte with dispersed filler material therein were prepared and examined concerning their electrochemical behavior. Therefore, different types of silica filler material, more precisely mesoporous and surface-designed silica as well as commercially available silica, were systematically deployed with a range of pore geometry, pore structure and specific surface area in the presented work. The crucial role of the chemical surface composition of the filler in an electrolyte with 1 M $LiPF_6$ and a mixture of ethylene carbonate (EC) and diethylene carbonate (DEC) at the ratio 3:7 was investigated experimentally (cf. fig. 2.2). Hence, the conductivity of the composite electrolytes with varying silica mass fraction was investigated as a function of temperature (and time) using impedance spectroscopy. To evaluate the observed effects, calculations with the Maxwell theory of exclusion volumes as well as the calculation of activation energies with the Vogel-Fulcher-Tamann (VFT) equation were performed. The surface charge of the silica particles in the used electrolyte were determined with zeta potential measurements. In this context adsorption considerations were applied and the number of silica surface sites were calculated.

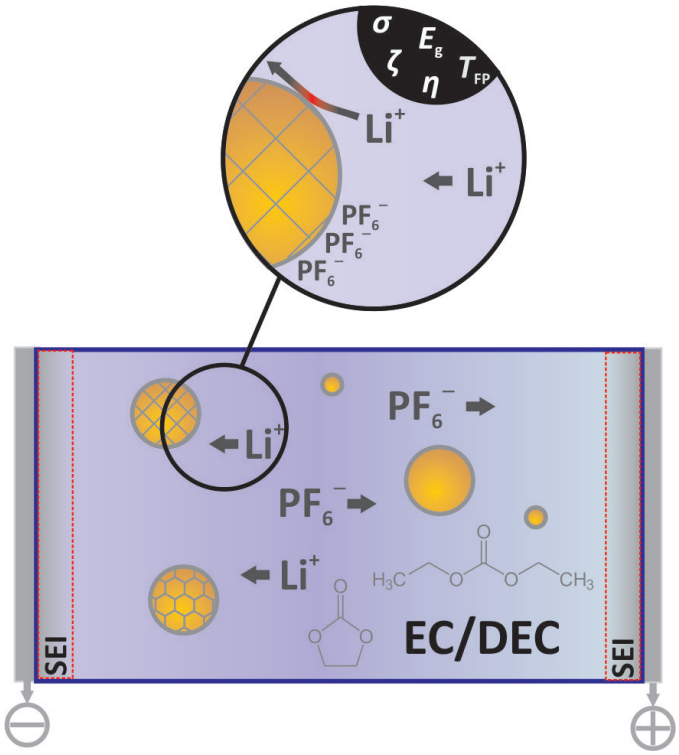

Figure 2.2: Schematic presentation of the basic experiment and considerations for composite electrolytes consisting of 1 M $LiPF_6$ in EC/DEC 3:7 with several silica filler materials. In the black area of the circle the measured parameters are mentioned (conductivity σ; zeta-potential ζ; viscosity η; electrochemical stability window E_g; flash point T_{FP}) [modification on the basis of a graphic drawn by Bjoern Luerßen].

Moreover, network structures and mechanical properties were examined via rheological measurements. Electrochemical and thermal stabilities were examined with linear voltammetry and flash point measurements.

This study was executed within a collaboration with the research group of Prof. Fröba, University of Hamburg, who took care for the structuring and functionalization of the silica materials. The particles were synthesized in Hamburg and have been subjected to the mentioned electrochemical measurements at the Justus-Liebig-University Gießen.

The aim of this work was to acquire an improved understanding of con-

ductivity phenomena in composite electrolytes and furthermore to examine silica filler materials concerning safety and mechanical features in liquid battery electrolytes. Nevertheless, the possible enhancement of electrochemical characteristics of present standard liquid electrolytes in LIB is one of the key questions. In general, the intention was to create electrolyte systems as reliable and stable as the present liquid organic electrolytes. The basic principles underlying these changes then had to be understood.

This thesis is structured in seven chapters. After the “Introduction” and “Motivation” section with general information, the “Theory” in chapter 3 comprises electrolytes for lithium ion batteries, especially conduction mechanisms and existing works. Additionally, conduction concepts for disperse electrolytes are specified. Chapter 4 describes the synthesis of materials, applied methods and used devices to obtain the required results. The received results are represented and discussed in chapter 5 and concluded in chapter 6, where an outlook for further work is given and the thesis is completed with a summary of the work in chapter 7. Relevant references are given in the Literature section at the end.

3 Theory

The focus of the following chapter are the basics of conduction phenomena and electrochemical characterization of electrolytes. Recent reviews of battery electrolytes and their properties, including next generation batteries, can be found in [39–43].

3.1 The electrolyte in a battery

To fulfill performance and safety requirements for lithium ion batteries, the electrolyte needs to meet demands like:

- high Li^+ ion conductivity
- wide temperature operation window
- high stability against the potential imposed by the positive electrode (wide electrochemical stability range); i.e. oxidation stability
- high chemical stability in general, but particularly against the anode
- beneficial interaction with electrodes; i.e. good SEI-forming properties
- no degrading interaction with Cu and Al
- acceptable viscosity such that the electrolyte can easily infiltrate into porous electrodes
- flame retardant $\rightarrow$ acceptable safety features
- cost-effectiveness

Consequently, the challenges for the construction of a high power battery are to develop a nonflammable electrolyte with a large electrochemical and thermal window, a good SEI-forming ability, and a high Li^+-conductivity (σ_{Li^+}

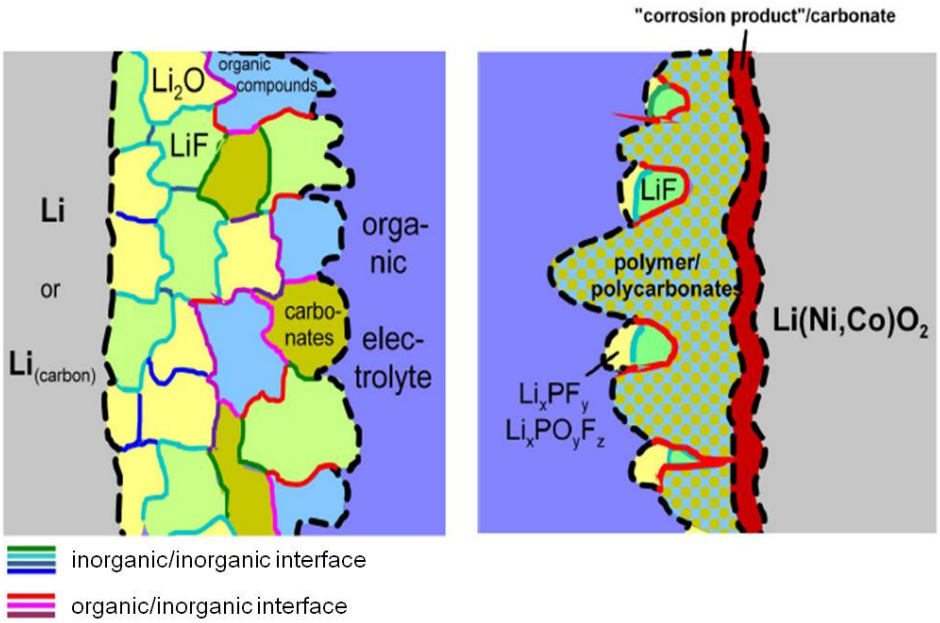

Figure 3.1: Possible composition of a SEI on the negative active mass (left) consisting of electrolyte reduction products and on the right side assumed compounds forming a deposition film on the positive active mass (taken from [44]).

>10^{-3} S/cm) in the electrolyte volume and across the electrode/electro-lyte interface [45].

Depending on the different applications and specific requirements the electrolyte composition may differ. The purity of all electrolyte components is crucial for the performance, especially a low water content. Electrolyte formulations are a compromise between various factors [46]. One critical parameter in electrolyte design is the formation of a good SEI and thus a good electrode/electrolyte contact and low charge transfer resistance. The SEI, formed by electrolyte decomposition products at the electrode surface (cf. fig. 3.1), has an important influence on parameters of the battery like capacity, cycling behavior and stability. The SEI influences the activation energies of interfacial lithium ion transfer as well [47]. Basically, this layer must block further chemical reaction between the electrode material and the electrolyte and must allow ionic transport, but prevent transport of electrons. This

layer acts as a second electrolyte in series with the primary liquid electrolyte. The composition and stability of the SEI is dependent on the electrolyte mixture as well as on the electrode surface structure. Therefore, the choice of solvents, salts and other additives within the electrolyte plays an important role in the formation of a SEI.

As the electrolyte is the link between the reactions at the anode and the cathode, it balances potential differences between the electrodes in the running cell. Hence, another important factor for the use of electrolytes in lithium-ion batteries is the range of potentials in which they are stable, the so-called electrochemical window. Fig. 3.4 shows, that the typically used electrode materials operate within the stability window of common organic electrolytes. In a battery the anode is the reductant and the cathode is the oxidant. The electrodes are electronic conductors with electrochemical potentials $\tilde{\mu}_A$ and $\tilde{\mu}_C$ (Fermi levels) as shown in fig. 3.2. The electrolyte shows an electrochemical window E_g in which it is stable. This “window"’ is given by the energy between the lowest unoccupied molecular orbital (LUMO) and the highest occupied molecular orbital (HOMO) [45]. Consequently, the electrolyte is reduced by an anode with $\tilde{\mu}_A$ above the LUMO and oxidized by a cathode with $\tilde{\mu}_C$ below the HOMO. This means the electrolyte solution is thermodynamically unstable at low and very high potentials vs. Li/Li^+.

With the first charge of the cell, the electrolyte starts to degrade by solvent and salt reduction processes. The organic and inorganic decomposition products are deposited on the electrode surface. Then, the SEI prevents the electrolyte against further reduction by imparting kinetic stability and therefore a larger V_{OC}. The limiting $\tilde{\mu}_C$ of the cathode can be determined by the HOMO of the salt and the solvents. Thus, it is a key task to design an electrolyte with an electrochemical window that fits to the chemical potentials of the anode and cathode. The evaluation of positive stability limits of a number of electrolytes showed, that mixtures of EC with DMC or DEC are kinetically stable up to the 5 V limit, although none of these solvents is thermodynamically stable at this potential [48].

Generally, four groups of electrolytes for rechargeable Li-ion batteries are in use or under development so far [49]:

1. **Liquid electrolytes** are solutions of lithium salts in aprotic organic solvents (usually solvent mixtures)

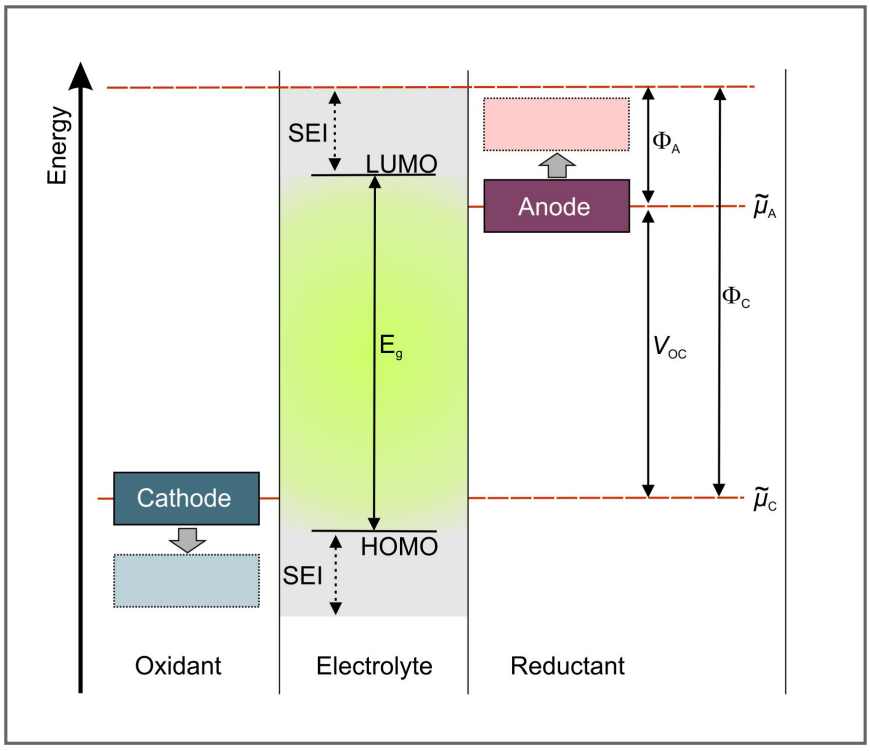

Figure 3.2: Energy diagram for an electrolyte with open-circuit conditions. It shows, that the electrochemical potentials of the anode $\tilde{\mu}_A$ and the cathode $\tilde{\mu}_C$ have to be in the range of the electrochemical window E_g of the electrolyte for thermodynamic stability. This window is expanded by presence of an SEI layer. Φ_A and Φ_C are the work functions of the anode and the cathode (graph after [45]).

2. **Polymer electrolytes** are formed by the dissolution of lithium salts in high molecular weight coordinating macromolecules (e.g. polyethyleneoxide (PEO))

3. **Ionic liquids** (IL's) - organic salts with high charge delocalization and steric hindrance

4. **Solid electrolytes** - solid lithium ion conductors, ceramics and glasses

Liquid electrolytes have one of the major advantages besides the considerably greater ionic conductivity, which is the ability to compensate volume

changes of the electrode materials during charge and discharge [7]. Well established liquid electrolytes for ambient temperatures consist of organic solvents with lithium salts like $LiPF_6$. The organic solutions are mostly binary solutions of a cyclic carbonate like ethylene carbonate (EC) or propylene carbonate (PC) and a linear carbonate like dimethyl carbonate (DMC) or diethyl carbonate (DEC) (cf. tab. 3.1). The mixing ratio of the solvents is chosen in a way, that the ionic conductivity and the viscosity are balanced. The problem is that high solvent polarity and therefore good salt solubility goes together with a strong solvent-solute interaction and consequently high viscosity. Alkyl carbonates are used because of their anodic stability, their high polarity and good conductivity. Also their reasonable range between boiling and freezing temperature, their low toxicity and their acceptable safety features are beneficial. EC is very attractive as electrolyte solvent, however, it has a high melting point, so that it must be combined with another solvent. PC as cosolvent was recognized to cause defoliation of the graphitic negative electrode [50]. Other possible solution components are ethers and esters, but alkyl carbonates have higher oxidation potentials.

To operate as an electrolyte, solvents have to be combined with lithium salts. Thereby, the lithium salt has to comply several criteria:

- high solubility
- good dissociation
- stable at electrode potentials
- non-toxic
- inert to other components of the cell
- formation of SEI

Most widely used is $LiPF_6$, especially in industry, but $LiClO_4$, $LiAsF_6$, $LiBF_4$, LiTFSI and LiBOB are also applied in various scientific publications, whereas all of them have advantages as well as disadvantages (see tab. 3.2). LiBOB and LiFAP seem to be the most promising alternatives to $LiPF_6$. LiBOB was studied for high temperature applications [52] and was found to be more stable than $LiPF_6$, to form a stable SEI and to have a wide potential window. The conductivity in comparable solvents, however, is smaller than

Table 3.1: Overview of typical solvents used in LIB's and their physical properties. Selected and supplemented Data from [51].

Solvent	Abbreviation	Mol. Weight /g · mol^{-1}	$T_{melting}$ / °C	T_{flash} / °C	η / cP [25°C]	ε_r [25°C]	ρ / g · cm^{-3} [25°C]	Remarks
Ethylene Carbonate	EC	88	36.4	160	1.90 (40°C)	89.78	1.321	good SEI
Propylene Carbonate	PC	102	-48.8	132	2.53	64.92	1.200	defoliation of graphite
γ-Butyro-Lactone	γ-BL	86	-43.5	97	1.73	39	1.199	
Dimethyl Carbonate	DMC	90	4.6	18	0.59 (20°C)	3.11	1.063	
Diethyl Carbonate	DEC	118	-74.3	31	0.75	2.81	0.969	
Ethyl methyl Carbonate	EMC	104	-53		0.65	2.96	1.006	
Ethyl acetate	EA	88	-84	-3	0.45	6.02	0.902	
Propylene Sulfite	PS	122.14		181.4			1.347	
Triethylenglycol-Dimethylether	TEGDME, Triglyme	178.23	-46	111		7.5	0.98	

that of $LiPF_6$. Merck's LiFAP salt seems to have even more promising electrochemical behavior, but suffers from high production and purification costs [53]. $LiClO_4$ has to be handled carefully due to potentially explosive character, $LiAsF_6$ is toxic and LiTFSI causes corrosion of the aluminum current collector in liquid electrolytes. $LiBF_4$ with its small anion size and therefore high mobility reacts with the aluminum current collector as well, but due to

Table 3.2: Overview of typical salts used in LIB's and their physical properties. Supplemented Data from [51].

Salt	Abbreviation	Mol. Weight / g · mol^{-1}	$T_{melting}$ / °C	$T_{decomposition}$ / °C (in solution)	σ / mS cm^{-1} (in EC/DMC; 1.0 M; 25 °C)	Remarks
$LiPF_6$		151.9	200	~ 80	10.7	thermal decomposition; hydrolysis
$LiBF_4$		93.9	293	>100	4.9	reaction with Al; low solubility
$LiAsF_6$		195.9	340	>100	11.1	poisenous
$LiClO_4$		106.4	236	>100	8.4	explosive
$LiSO_3CF_3$	Triflate	155.9	>300	>100		low conductivity
$LiN(SO_2CF_3)_2$	LiTFSI	286.9	286.9	>100	9.0	corrosive for Al
$LiC(SO_2CF_3)_3$						corrosive for Al
$LiB(C_2O_4)_2$	LiBOB	193.79		265		
$Li(C_2F_5)_3PF_3$	LiFAP					high production and purification costs

a passivation reaction it can be used. Nevertheless, the solubility and the SEI formation are still poor. Therefore, $LiPF_6$ is the best compromise at the moment. The problem with $LiPF_6$ is the decomposition caused by heat and moisture [54]. The decomposition products, e.g. HF, are highly reactive on the electrodes resulting in bad impact on the electrode performance [55]. Interestingly, it was found that small amounts of the resulting HF increase the battery cycle life, due to the formation of a very strong passive layer on the

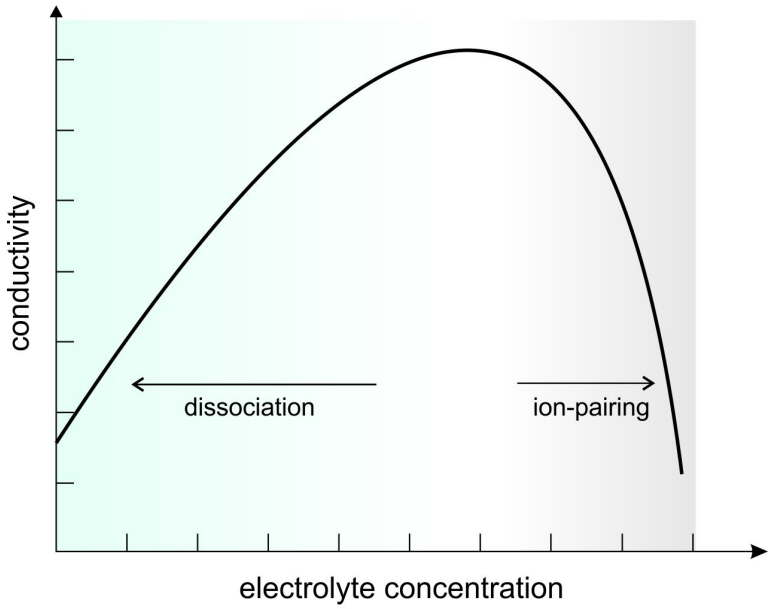

Figure 3.3: Conductivity behavior dependent on the concentration of salt in an electrolyte with low viscosity.

aluminum collector such as AlF_3 [56].

In general, the optimal salt concentration has to be determined to create a good electrolyte, since the conductivity of an electrolyte passes a maximum dependent on the salt concentration (see fig. 3.3). With increasing salt concentration the ion concentration increases until a maximum is reached. Then the formation of ion pairs outweighs the addition of free ions and thus the conductivity decreases. The concentration should be chosen in a way, that the conductivity maximum is reached.

Besides the search for new salts and solvents, the improvement of the electrolyte performance by additives is widely studied. Various additives are available, whereas each additive exhibits a unique function to improve the battery performance. Additives can be classified into the following categories [17]:

- SEI forming enhancer

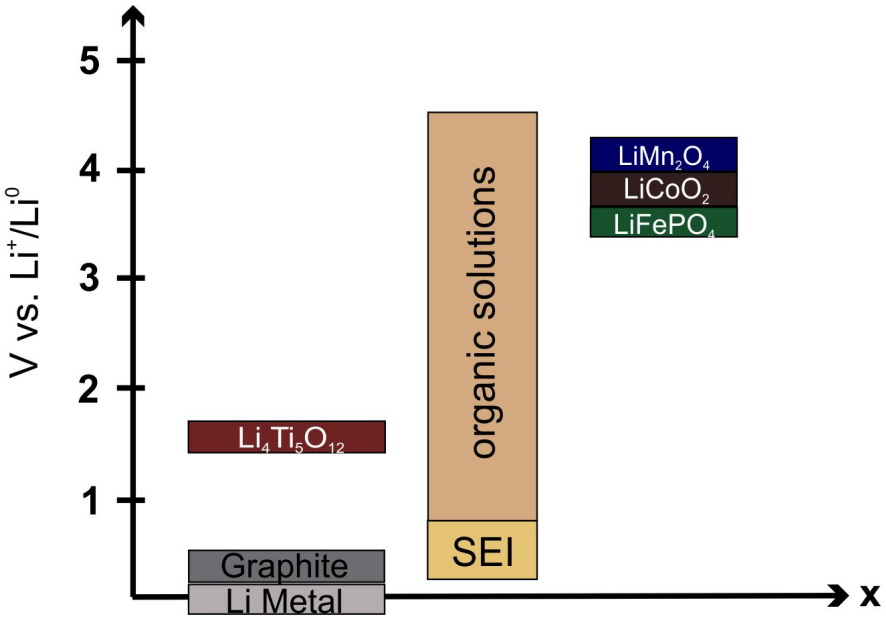

Figure 3.4: Stability window of liquid organic electrolytes in comparison with the potential vs. Li^+/Li^0 of common positive mass and negative mass materials.

- cathode protecting agent
- salt stabilizer
- safety protection agent (flame retardant, overcharge protector)
- Li decomposition agent
- solvation enhancer
- Al corrosion inhibitor
- wetting agent

The concentration of additives in the electrolyte is typically not more than 5 % in weight or volume. As additive often vinylene carbonate (VC) or vinyl acetate, for example, are used because the materials form insoluble, solid

products by reduction that cover the graphite electrode and increase the SEI stability. Sulfur-based additives like ethylene sulfite are added as reductive agents to assist the SEI formation. Even nitrate and nitrite or aromatic esters have been implemented to improve SEI formation, whereas boron-based compounds have been studied as additive to increase the cycle-life of batteries by stabilizing the SEI. An enormous number of materials is tested as additives, as the use of additives is an effective way to improve LIB performance.

Besides the liquid electrolytes, polymer electrolytes are a widely studied field of LIB electrolytes. With the discovery of ionic conductivity in alkali metal salt complexes of poly (ethylene oxide) (PEO) in 1973 by D. E. Fenton et al. [57], polymer electrolytes became interesting for the use in batteries. Polymer electrolytes combine the advantages of solid-state and liquid electrolytes and offer the easy processing of plastic materials (flexible geometry). Furthermore, with the mechanical features of polymer electrolytes, it is possible to omit the separator. Basically, polymer electrolytes are solid solutions of alkali metal salts in polymers, where either the cation or anion is covalently fixed to the polymer repeat unit. To facilitate the salt dissociation the lattice energy of the salt should be low and the dielectric constant of the polymer should be high. Compared to liquid electrolytes the polymer electrolytes have benefits in safety (e.g. no-leakage) but show a relatively poor conductivity at room temperature.

Different groups of polymer electrolytes are available: dry solid polymer electrolytes, gel polymer electrolytes and composite polymer electrolytes [58]. The dry solid ion-conducting polymers are in their simplest form polymer lattices with salt dissolved therein, acting as solid solvent, while no organic liquid is included. These polymer electrolytes, mainly in the form PEO-LiX, offer only a low ionic conductivity (10^{-6} S cm^{-1}) at ambient temperature [59, 60]. To obtain polymer electrolytes that operate at ambient temperature, the most common approach is the addition of low-molecular weight plasticizers (cyclic carbonic acid esters and chain-like esters like propylene carbonate) resulting in gel-type polymers [61]. They do not crystallize and they exhibit higher conductivities, because the amount of charge carriers is increased. The problem is their lack of chemical stability under working conditions.

One of the most promising ways to improve electrical and mechanical properties of polymer electrolytes is the addition of ceramic filler material [58] (see chapter 3.1.2). Besides the predominantly used PEO host material, Poly(vinylidene fluoride) (PVdF) is a promising material. Other employed polymers like poly(acrylonitrile) (PAN), poly(methyl methaycrylate) (PMMA) or poly(vinyl chloride) (PVC) have too many disadvantages like poor ionic conductivity or passivation of the electrode contact.

The increasing interest in ionic liquids as electrolytes for batteries results from their low vapor pressure and therefore high safety, as organic electrolytes are predominantly flammable and sometimes toxic. IL's have lower melting points than inorganic salts. Due to their large organic cations and high charge delocalization of the anions they are not flammable and thermally stable up to $400\ ^{\circ}\mathrm{C}$. Correspondingly, the larger the structural groups acting as ions, and the lower their electrical charges, the easier it is to break them apart with thermal energy. Furthermore, materials with ions that are less symmetrical tend to have lower melting points as they are more difficult to fit into crystal lattices. Both ions contribute to the charge transport. As cations quaternary ammonium groups R_4N^+ are widely used and as anions bulky ones like $F_3(CSO_2)_2N^-$, $BF_4{}^-$, $AlCl_4{}^-$, $PF_6{}^-$, butylpyrrolidinium and butylmethylimidazolium are used. The conductivity of the IL's in the mS/cm range depends on the chain length of the alkyl cation component. Nevertheless, the easy preparation and the variety of components that can be used and therefore the possibilities in "designing" IL's, makes them attractive as electrolyte material [62].

In several publications the reasonable behavior of IL's as electrolytes in lithium batteries was demonstrated [15, 63–69]. However, the interface structure between the electrodes and the IL is still not well understood and most of the IL's are not stable at reducing voltages, possibly due to impurities. Further, they are not prone to form a SEI layer without additives and moreover, their costs are high, hence they are marginally deployed in organic electrolytes to modify properties [70, 71].

Solid lithium ion conductors are not used as electrolytes in LIB's yet, because of two major reasons: Firstly, their conductivity is not as high as common organic electrolytes and secondly they cannot compensate the volume changes of the electrodes during the cycling and the resulting mechanical

stress. Solid lithium electrolytes might be useful in cells operating at elevated temperatures, where liquid electrolytes are no longer stable. They are essential for the development of thin film batteries and they are suitable for aggressive environments. Three compound classes are investigated as ceramic solid electrolytes in LIB's: sulfides, oxides and phosphates. There is a good overview provided by Fergus [11]. Several sulfide glasses or glass-ceramics like Li_2S-P_2S_5 or the so called thio-LISICON have been reported. There is no rule for the conductivity of those conducting glasses, as sometimes crystalline and sometimes amorphous phases show higher conductivities. Two oxide structures were considered to be appropriate as lithium ion conductors: on the one hand materials with perovskite structure of the type ABO_3 and on the other hand materials with garnet structure [72]. Additionally, there are good conducting phosphates, similar to the well known sodium-ion conducting NASICON. There, the highest conductivities are observed for the compound $Li_{1+x}Al_xGe_{2-x}(PO_4)_3$ (LTAP). One of the most promising glass ceramics is the so called Ohara glass with the crystalline phase $Li_{1+x+y}Al_x(Ti,Ge)_{2-x}Si_yP_{3-y}O_{12}$, but the instability against lithium metal is problematic [73].

3.1.1 Ionic conduction mechanisms of liquid, solid and polymer electrolytes

Basically, the dissolution of salts in solvents leads to charged and solvated particles through dissociation. The existence of ions in solution can be proven by conductivity measurements, as the ions move through the electrolyte driven by an applied electric field. The conductivity σ of a liquid electrolyte is described by the following equation:

$$\sigma = \Sigma\, z_i \cdot e_0 \cdot n_i \cdot u_i \tag{3.1}$$

The ion charge number z_i, the elementary charge e_0, the concentration of ions n_i and their mobility u_i determine the conductivity. The conductivity is measured via the electric resistance of a defined amount of electrolyte. Therefore, two electrodes (e.g. platinum) are immersed into the solution and high-frequent alternating current (AC) is applied, as continuous current (DC) leads to polarization and electrolysis at the electrodes [74].

The electrolyte resistance is given by:

$$R = \frac{1}{\sigma}\frac{l}{A} \tag{3.2}$$

In this case, l/A is the cell constant with the distance between the electrodes l and the area of the electrode A. $1/\sigma$ is also termed the specific resistance ρ. The SI unit for the specific conductivity σ is S m^{-1}. The specific conductivity depends on the concentration of ions in solution and thereby on the salt concentration. The mobility of ions is dependent on the solvent by the viscosity η and therefore also dependent on temperature and pressure, whereas it is inversely proportional to the hydrodynamic radius R_j of the ions in a simple model:

$$u_j = \frac{v_j}{E_{\text{field}}} = \frac{z_j e}{6\pi\eta R_j} \tag{3.3}$$

The Li^+ ion has a high charge density. In liquids, migration and diffusion processes are assisted by solvent reorientation. The mobile charge is surrounded by a solvent sheath, which has to be sheared off for any transfer across the electrolyte interface like intercalation. Non-aqueous electrolytes are used in lithium ion batteries because of the high reactivity of lithium and the low decomposition potential of water. In non-aqueous electrolytes the concentration has a higher impact, so that the specific conductivity is lower compared to aqueous electrolytes in the same concentration range [75]. For the case that the hydrodynamic radius is unchanged in a given temperature range, the temperature dependence of the mobility can be attributed to the viscosity. Hence, the viscosity of liquids decreases with increasing temperature ($\eta \propto \exp\ (E_A/RT)$), and therefore the ionic conductivity increases. Besides the electric field as a driving force for ion migration, ions can move due to diffusion, i.e. driven by concentration differences. The direction for diffusion is given by the negative concentration gradient. The Einstein relation connects the diffusion coefficient D_j and the ion mobility u_j:

$$D_j = \frac{u_j RT}{z_j F} \tag{3.4}$$

The extended Nernst-Einstein equation connects the diffusion coefficient with the molar limiting conductivity and thus, the diffusion coefficient can be determined via conductivity measurements, if the charge carrier concentration is known. Further, the Stokes-Einstein relation links the viscosity coef-

ficient with the diffusion coefficient, but this relation is valid for not too small spherical particles.

The charge transport is not shared equally by all ions in electrolyte solutions. The individual ion conductivity can be described with the transference number *t*. This is the is the fraction of the total current *I* carried in an electrolyte by a given ion, meaning the cations I_+ or the anions I_-.

$$t_+ = \frac{I_+}{I} \quad and \quad t_- = \frac{I_-}{I} \tag{3.5}$$

For the characterization of electrolytes for LIB's the transference number is essential, because the Li^+ ions are the relevant charge carriers and therefore the transference number of the Li^+ ions has to be specified. There are several methods (potentiostatic or galvanostatic polarization, electromotive force, pfg-NMR) that can be used, but each of them has noticeable inaccuracies [76]. Moreover, for liquid-solid composite electrolytes the determination of the Li^+ transference number seems to be even more difficult.

The conduction in solid materials differs from liquids. In solid materials electrons and holes as well as ions can contribute to the conductivity. Depending on the conduction mechanism, solid materials are classified into metals, semiconductors and isolators and their conductivity can be explained by the energy-band model. The ionic motion in solid electrolyte materials corresponds to the displacement of "bare" ions, residing in potential wells to overcome energy barriers through thermal activation [7]. Other components of the lattice structure are immobile. Accordingly, ion motion in solid materials is provided through lattice defects. Hence, ideal crystals without defects are isolators. Real crystals always exhibit defects at temperatures exceeding 0 K for entropic reasons. The number of defects grows with increasing temperature, as entropy and enthalpy contributes to the total energy. Basically, variable defects in different dimensions can occur, whereas point defects (0-dimensional defects) [77] show the greatest influence. Within the point defects a distinction is made between Frenkel- and Schottky-type defects [78–80]. In both cases, the ion transport is correlated with an activated change of positions and are exponentially temperature dependent. In conclusion the conductivity in solids is dependent on the number of available charge carriers and therefore on the defect concentration and moreover on the height of the activation barriers.

There are other variables for the conductivity in polymers (see fig. 3.6): the degree of crystallinity and the glass transition temperature T_g. At T_g the mechanical and thermodynamic properties of polymers and glasses change substantially. Polymer-salt complexes are either semi-crystalline or amorphous, whereas in crystalline regions and complexes no ionic conductivity was found. This means, the ionic transport occurs exclusively in amorphous regions, where the segmental motion of the polymer host matrix has been identified as the main parameter controlling the conductivity.

The glass transition temperature is dependent on the structure of the polymer. The glass transition temperature is lower, the more flexible the main chains are. The side chains (in cross-linked polymers) lead to a low T_g, if the distance between them is far. With an increasing number of side chains, the glass transition temperature therefore increases. The motion of ions is coupled with the segmental motion of chains above T_g, in the so-called rubbery state. That is why "low-T_g" materials are searched for an efficient ion transport in polymers [81]. Moreover, plasticizers are used to work as internal "lubricant" and ingredient to decrease T_g. Large weight fractions of additives like TEGDME, PC and EC are used. This results in gel electrolytes with a "swollen" polymer network [81]. The effect of plasticizers can be enormous, so that room-temperature conductivities of sol gel electrolytes are in the range of liquid organic electrolyte conductivities. The room temperature conductivities of polymers are at least two orders of magnitude lower in value than those of liquid organic electrolytes. Ionic conductivities of 10^{-3} Ω cm $^{-1}$ are reached at temperatures around $80\ ^{\circ}\mathrm{C}$ - $120\ ^{\circ}\mathrm{C}$ without electronic contribution (cf. fig. 3.5). The ionic conduction proceeds via a worm-like solvation-desolvation process along the chains above T_g. In this case, the solvent is "immobile", as in inorganic solid electrolytes. Some cations in polymers are too strongly attached to the chains, however the singly charged Li^+ is not immobilized. The Li^+ ion motion follows this solvation-desolvation process along the chains. There are indications, that solvated salt units aggregate into dimers and trimers, acting as temporary cross-links for polymer chains. Hence, an increase of salt concentration leads to an increase in chain stiffness. Nevertheless, the correlation between the ion motion and the segmental motion of the macromolecules is expressed in laws for the temperature-dependent conductivity of amorphous systems.

The temperature dependence of the conductivity for liquid and polymer

electrolytes above the glass transition temperature is often inadequately described by a simple Arrhenius expression, since the temperature dependence of the pre-exponential factor σ_0 is not taken into account. While the Arrhenius theory remains the best approach for solid electrolytes, empirical laws including the glass transition temperature (Vogel-Fulcher-Tamman VFT [82–84] or Williams-Landel-Ferry WLF [85]) apply widely to disorganized matter, polymers and to liquids as well. Hence, a variety of empirical descriptions have been developed to describe the temperature dependence of ionic conductivity, like the VFT equation. This equation was introduced to describe the viscosity of glasses and polymers dependent on temperature, but is also used to describe the temperature dependence of the conductivity. In its modified form, a temperature dependence of the prefactor is assumed:

$$\sigma = \sigma_0 \, T^{-1/2} \cdot e^{-\frac{E_\mathrm{A}}{R(T-T_\mathrm{g})}} \tag{3.6}$$

The additional parameter in the VFT equation compared to the Arrhenius equation is T_g. Killis et al. demonstrated that this model expresses the correlation between the mechanical properties of a polymer and the ionic conductivity for a wide variety of compositions [86].

3.1.2 Disperse electrolytes

The conductivity enhancing effect of a dispersed (insoluble, isolating) second phase (filler material) in a solid electrolyte material is well known as heterogeneous doping since many years. Wagner has already published a paper in 1972 with the title: “The Electrical Conductivity of Semiconductors Involving Inclusions of Another Phase” [88]. There, he summarized classical approaches known for two phase mixtures since Maxwell [89]. With the increased ionic conductivity of LiI due to the dispersion of Al_2O_3 particles in it, published by Liang in 1973 [19], the reasons for these conductivity effects of heterogeneous doping have been widely studied in the 1980’s by Maier and Wagner, predominantly [21, 90]. Several material combinations were studied to clarify the transport phenomena in solid two phase mixtures. CuCl, AgI and AgBr were used for example as matrix material and as filler material particles of Al_2O_3, TiO_2 and SiO_2 were dispersed therein. Various models were developed to explain the enhancing effect on the conductivity. The main assumption is a space charge region at the interface of the

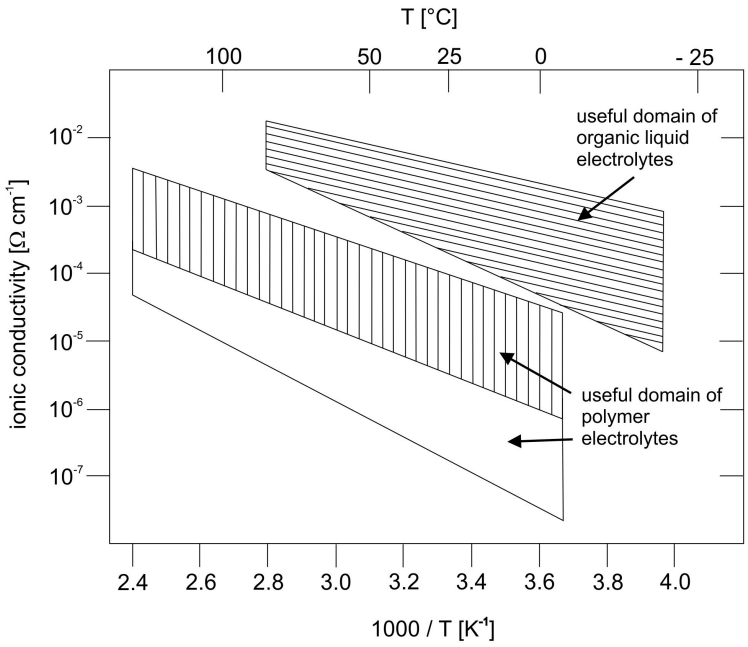

Figure 3.5: Conductivity range dependent on the temperature for polymer electrolytes compared to organic liquid electrolytes (Source: [87]).

two materials with surface interactions. This is further explained in section 3.1.3. The conductivity enhancing effect is thought to be a result of surface induced defects [18]. However, this model is only effective with small defect concentrations.

The concept of heterogeneous doping was also transferred to polymer electrolytes. The addition of an inert filler to a polymer matrix was first introduced by Weston and Steele in 1982 [91]. The idea was to improve mechanical characteristics in the way that a solid-like support matrix is provided by the fillers, allowing the amorphous parts of the polymer to maintain its liquid-like character in terms of fast ionic mobility [92]. A rigid structure out of particles and polymer can be formed, which is more permeable for ions than the pure polymer. The observed conductivity increase in composite polymer electrolytes is explained by an enhanced degree of amorphocity

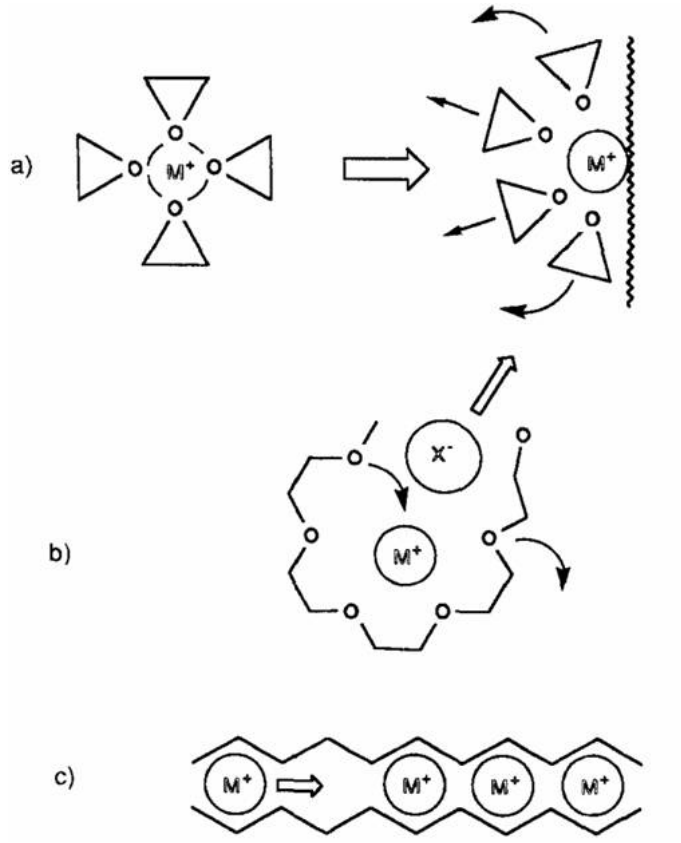

Figure 3.6: Schematic presentation of the different conduction mechanisms in a) liquids, b) polymers, c) crystalline solids (Source: [87]).

or a hindered recrystallization (cf. 3.1.1). In polymer electrolytes the concept of heterogeneous doping with filler materials is now widely applied for over 20 years [38, 93–96] and Stephan and Nahm give a good overview for lithium ion conducting composite polymer electrolytes until 2006 [58]. Besides the use of polymer electrolytes in LIB's, they are commonly used in solar cells [97–99] and applied in fuel cells [100, 101]. The possibilities for filler materials are manifold, so that even inorganic-organic nanotubes [95] and polyanilin nanofibers [102] are used. The role of ceramic fillers in gel electrolytes, which are a combination of polymer and liquid electrolytes, has also been addressed [103].

For liquid electrolytes the concept of heterogeneous doping with inert solid particles was introduced in 2004 by Bhattacharyya et al. [23]. The authors formulated the concept of “soggy sand“ electrolytes [24], where liquid organic electrolytes are mixed with oxide particles to achieve improved ionic conductors. Compared to polymer electrolytes, these electrolytes have higher conductivities with good mechanical properties. Inorganic filler materials may help to fulfill some of the requirements for liquid electrolytes in lithium ion batteries, as they reduce the volume fraction of the inflammable phase while the conductivity is barely affected. The use of surface functionalized filler materials might even enhance the ionic conductivity due to extra inter-facial pathways for the lithium ions. In the concept of “soggy sand” ion conductors the conductivity enhancement is thought to be caused by adsorption interactions of the ions in solutions with the surface of the oxide particles [104] and furthermore by percolation pathways along connected particles [24] [105]. Basically, an electrolyte consists of ion pairs besides a few free ions. In the space-charge-region-model the oxide surface may adsorb the anions of the electrolyte, and therefore the required lithium charge carrier for LIB’s could dissociate out of the ion pairs. This would result in an enhanced concentration of free charge carriers in a space-charge region around the oxide filler particle (see fig. 3.7). Nevertheless, the published conductivity enhancement by Bhattacharyya [23] for dispersed oxide particles in concentrated electrolytes could not be reproduced in this work [12].

The concept of heterogeneous doping is even applied to ionic liquids [106]. In this case, the filled ionic liquid electrolytes offer a specific mechanism to suppress the formation of lithium dendrites in lithium metal based batteries. Furthermore, the composite ionic liquid electrolytes are also conceivable for lithium ion batteries [29]. As the lithium ions in ionic liquids are highly coordinated by the anions and therefore hindered in migration, interaction with the filler material can be helpful. Either the filler surface can interact with the anions to break up the lithium anion complexes or they can interact specifically with the lithium ions to allow migration as free ions. Eventually, an interface effect can be observed, but this effect has to be characterized carefully as it seems to be very different to the one observed in conventional liquid electrolytes.

A new class of electrolyte systems, which are disperse electrolytes in the broadest sense, are “solvent-in-salt” electrolytes. Suo et al. introduced

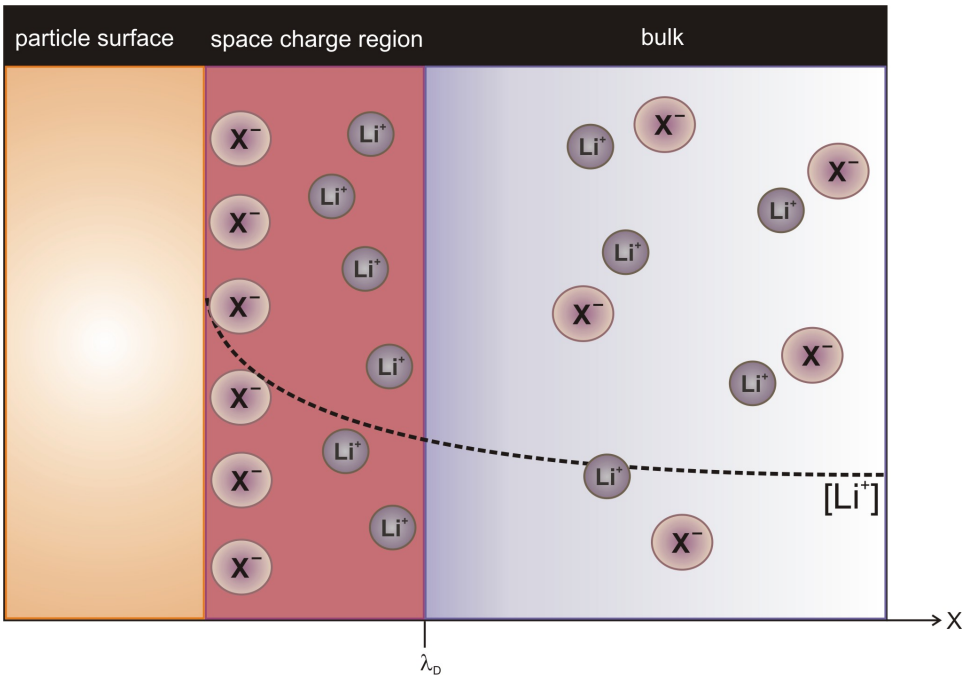

Figure 3.7: Schematic presentation of the assumed characteristics in the space charge region of a liquid electrolyte filled with silica particles. One particle surface is considered exemplary. The anions of the electrolyte are assumed to be adsorbed on the silica surface, so that the concentration of Li^+ ions is enhanced in the space charge region. The width of the space charge region is in the range of the Debye length λ_D.

highly concentrated electrolyte systems, which were classified as “solvent-in-salt” systems [107]. There, the concentration of the salt can reach up to 7 mol L^{-1} and the solvent-in-salt system exhibits high lithium transference numbers up to $t_{Li^+} = 0.73$. With high salt concentrations of 5 mol L^{-1} the physicochemical properties of the electrolyte changes, as the salt dominates the solution in weight and volume. The authors present the decreasing number of solvated lithium ions with increasing salt concentration as an explanation for the higher Li^+ transference number. Additionally, Watanabe et al. investigated equimolar mixtures of glymes with lithium salt [108]. The authors succeeded in developing a new family of ionic liquids, as the glymes are supposed to act like chelat ligands which form a complex with lithium

ions.

In general one can say, several systems with dispersed particles have been studied and reported in the literature. Supported by these observations, the noticed change in conductivity is dependent on the surface area of the dispersed particles, although the conductivity mechanisms in the systems (solid, polymer, liquid) are different.

3.1.3 Conduction concepts for disperse electrolytes

Several observations have been reported wherein the transport properties of a material (matrix material) are changed by the presence of a second phase (filler). Classical approaches could not explain the often observed increase in conductivity. The classical approaches by Maxwell [89] and Lord Rayleigh [109] calculate the conductivity of two phase mixtures using the bulk conductivity of each phase. Electrical double layers or fast conductivity paths at the interface of two phases are not taken into account. Hence, three complementary conduction concepts are discussed in the following chapters. Firstly, the general volume exclusion assumptions by Maxwell for heterogeneous systems are presented. Secondly, the concept of space charge regions between two solid phases with a fast transport path for ionic defects is introduced and lastly the percolation theory as explanation for fast ionic movement in heterogeneously systems is reviewed.

3.1.3.1 Volume exclusion assumptions

The calculation of the conductivity of dispersions is a long known problem. Most research was focused on the limit regions, which are called “wet-limit” and “dry-limit” region [110]. A second phase, usually gas or liquid bubbles or spherical solid particles, is mixed into the volume of a liquid or a solid matrix. In the “wet limit” the fraction of the added second phase is low, so that the particles are widely separated, while in the “dry limit” the volume fraction of the matrix material is low. For the calculation of the resulting conductivity σ in the “wet limit”, Maxwell has derived the following equation in 1892 [89]:

$$f_\sigma = \frac{\sigma_{sample}}{\sigma_{matrix}} = \frac{2\varepsilon}{(3-\varepsilon)} \tag{3.7}$$

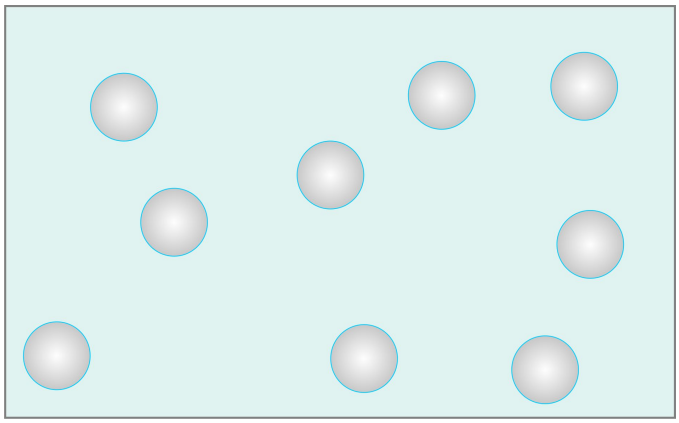

Figure 3.8: Graphical considerations to the volume exclusion assumptions of Maxwell .

where ε is the volume fraction of the matrix phase. This equation is based on the assumption of an electric field in and around isolated spheres. The radii of the isolating spheres must be small compared to their distance. Maxwell investigated the electric conduction through a low concentrated dispersion with non-interacting insulating spheres of conductivity σ_s [89] (cf. fig. 3.10). These spheres are embedded within a conductive medium with conductivity σ_f. For the potential of a single sphere in unbound space he stated that

$$\varphi_K \rightarrow \frac{2\sigma_f + \sigma_s - 2(\sigma_f + \sigma_s)(1-\varepsilon)}{2\sigma_f + \sigma_s + 2(\sigma_f + \sigma_s)(1-\varepsilon)} \tag{3.8}$$

when $\varepsilon \rightarrow 1$. For dielectric spheres (σ_s = 0) this equation reduces to equation (3.7). Surface effects are neglected. Considering the conductivity of the second phase (filler material) the following equation is achieved because of ϑ = 1 - ε, with ϑ as the volume fraction of the filler material.

$$f_\sigma = 1 - \frac{3}{2}\vartheta \tag{3.9}$$

Maxwell's formula is the earliest and best-known formula for the calculation of the conductivity of a heterogeneous medium consisting of a dilute suspension of insulating spheres. Duan et al. presented a scheme that

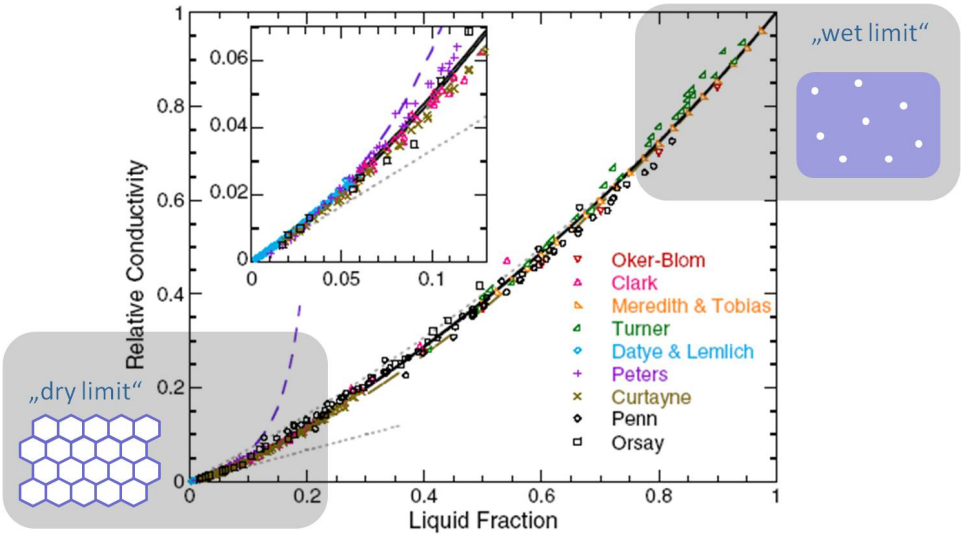

Figure 3.9: Measurements of Feitosa [110] and collected data of measurements in the "'wet limit"' region and the "'dry limit"' region of several two-phase-mixtures, with a graphical demonstration of particle distribution in the limit regions.

generalizes the Maxwell formula for the case of heterogeneous media containing multiple inclusions considering the orientation of the inclusions [111]. For the “dry limit” the equation of Lemlich is used:

$$f_\sigma = \frac{1}{3}\varepsilon \tag{3.10}$$

This formula describes the opposite limiting case of Maxwell and corresponds rather to foam-like and “soggy sand”-type microstructures. It results from the assumption of random orientation of plateau borders. The conduction is supposed to occur only through these plateau boarders (and not through lamellar films). Lemlich found this equation for foams with low bulk density [112] and it is based on a model proposed for liquid foams with bubbles of any polyhedral shape. For the intermediate region between “wet” and “dry” limit an empirical formula, with analysis of several measurements shown in fig. 3.9, was reported by Feitosa et al. [110].

These first considerations have to be regarded as guidelines to evaluate

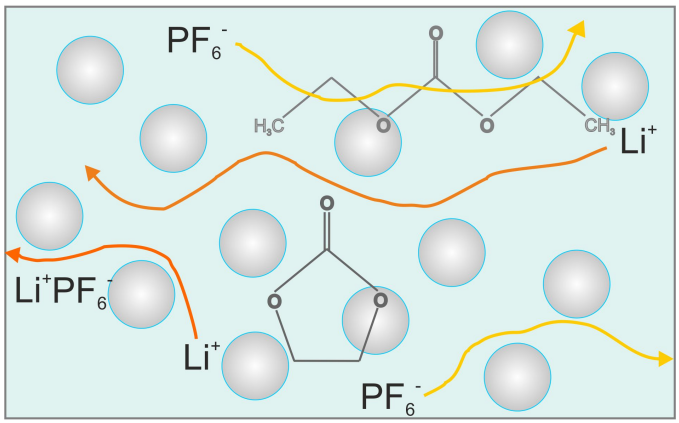

Figure 3.10: Graphical considerations to the volume exclusion assumptions transferred to the present electrolyte system in this work.

the effect of any kind of filler due to simple volume exclusion assumptions. The described assumptions do not include percolation effects or interfacial conductivities in boundary regions. Once the mean conductivity is higher than expected by volume exclusion considerations, interface and percolation effects have to be taken into account.

3.1.3.2 Space charge regions

Interfaces appear as a boundary separating two different phases. In terms of different states of matter this boundary is called the “surface”. The influence of interfaces is often observed in heterogeneous systems [113]. Interfaces exhibit special thermodynamic properties beside the structural differences to the bulk. The chemical potentials for charge carriers and defects as well as the concentration and mobility of the charge carriers at the interface differ from those in the bulk. Thus, special ionic and electronic conductivities occur and multiphase systems with two or more coexisting phases are more than simply the sum of its parts. Heterogeneously doped materials consist mostly of an insulating phase dispersed in the matrix of an ionic conductor (two ionic conductors in contact are also possible). These dispersions show in many solid/solid mixtures an enhancement of the ionic conductivity. Many published papers report enhancement effects achieved by dispersing insu-

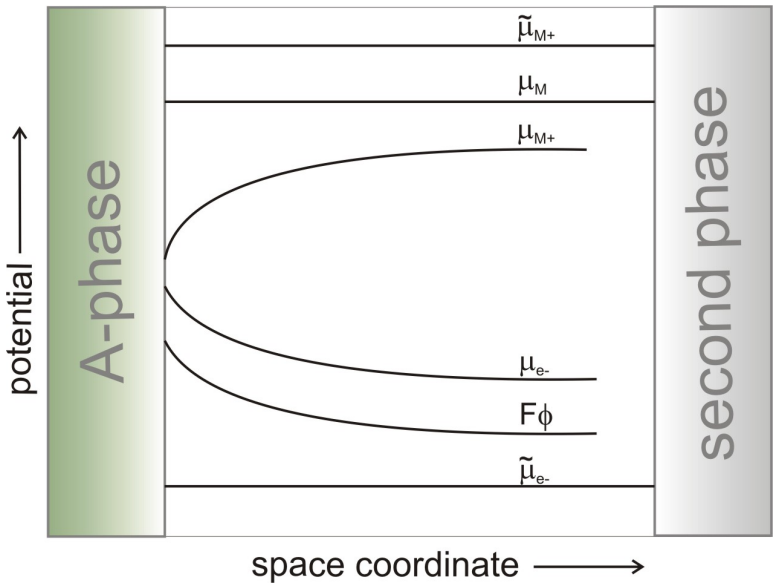

Figure 3.11: Electrochemical potentials in boundary regions with an insulator A (Graphic after [120]).

lating oxides like Al_2O_3 and SiO_2 in moderate ion conductors, mostly Li-, Cu-, and Ag-halides. Especially in ceramic materials, the concept of heterogeneous doping has been well proven. Several theoretical models have been proposed to explain the conductivity enhancement in heterogeneously doped solid electrolytes [20, 114–117]. The majority of the models assume a space charge zone as origin for the conductivity enhancement in two-phase systems. These space charge layers act as a path for the fast transport of ionic and electronic point defects. Important theoretical work in this field was published by Maier and Wagner Jr. [21, 90, 118, 119].

The space charge concept is based on adsorption of defects at surfaces and resulting differences in the local free energy of defects in the bulk and at the surface. The space charge potential depends on the charge density and therefore on the number of mobile (newly formed) charge carriers. It represents the natural extension of volume-defect thermodynamics [119]. With a surface reactive second phase a great effect is expected, because the mobile ions are either stabilized or destabilized at the interface, so that the respective concentration of vacancies or interstitials is enhanced. In

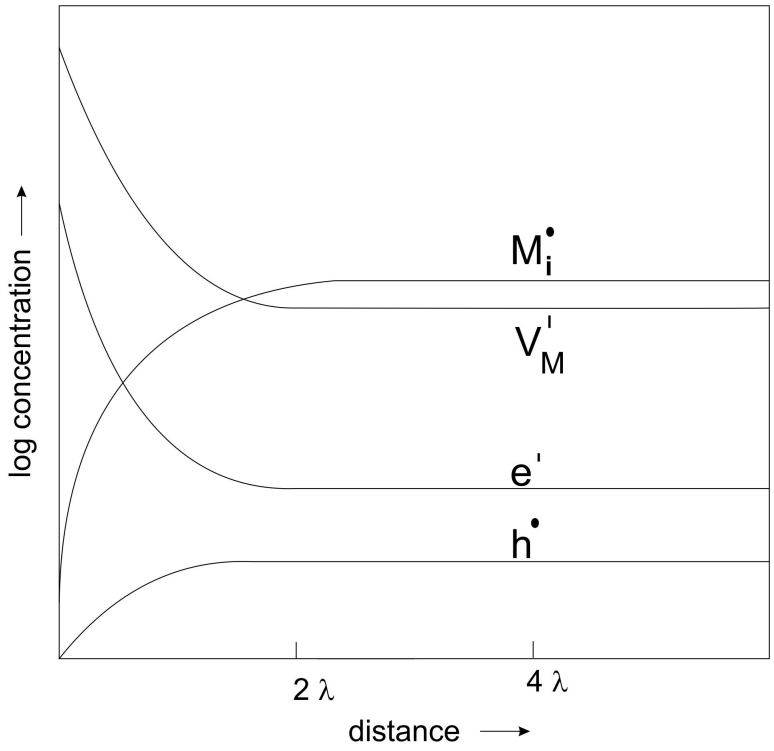

Figure 3.12: Logarithmic profile of the defect concentrations in the boundary regions of a Frenkel disordered solid MX (Graphic after [120]) with the following indications: $M^{\cdot}{}_i$ interstitial defects, $V^{'}{}_M$ M-vacancy, e' excess electron, $h^{\cdot}$ defect electron.

boundary regions with the assumption of an ideal insulator, meaning not influencing the chemical potential of the components (μ_M, μ_X), an electric field arises due to the zero-gradient of the electrochemical potential ($\tilde{\mu}$) of the mobile ions as shown in fig. 3.11. Consequently, the profile of the defect concentrations split up as shown in fig. 3.12.

3.1.3.3 Percolation theory

The percolation theory is a macroscopic model based on the statistical treatment of conductance resulting from a random distribution of second phase and matrix particles. The percolation model and the space charge layer

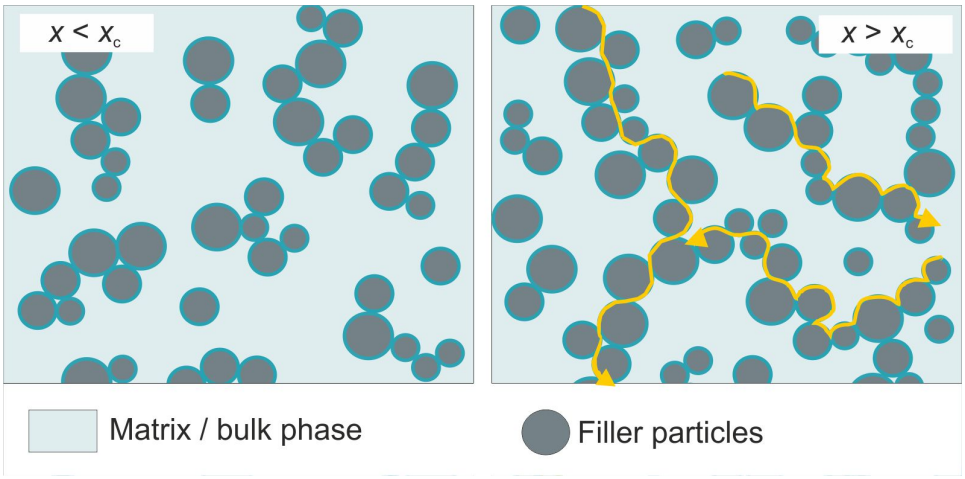

Figure 3.13: With a sufficient amount of filler material x_c, above a percolation threshold, percolating pathways arise.

model need to be linked in typical filled electrolytes, as the space charge layer is a microscopic model only explaining the formation of a surface film, whereas the percolation model couples these individual surfaces to an extended path [118]. Percolation models are relevant for compact mixtures of conducting and non-conducting materials or homogeneous two-phase systems in which one phase is much more conductive than the other. Such mixtures often exhibit a percolation threshold. Conduction thresholds in mixtures of conducting and non-conducting materials have been well reported in the literature [118, 119, 121–131]. The highly conducting boundary layers of isolated particles embedded in a conducting matrix do not provide a perceptible contribution to the overall conductivity. The effect is only strong, if continuous paths are formed (percolation paths, cf. fig. 3.13). The percolation theory requires threshold values at which the behavior of the system changes qualitatively (first percolation threshold) [119]. A percolation model starts with a collection of points distributed in space and certain pairs that are supposed to be adjacent or linked. There may be many paths between a given pair of points, but if there is at least one path, the points are said to be connected [121]. Some basic percolation lattice models shall be mentioned in order to consider the conduction in the presence of randomly distributed excluded volumes under a variety of statistical constraints.

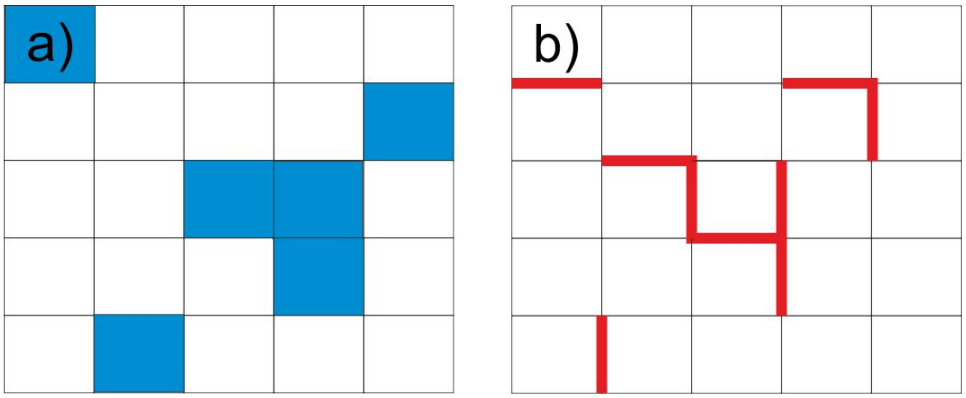

Figure 3.14: Different models for percolation; (a) Bond percolation model; (b) Site percolation model

1. The Bond percolation model (cf. fig. 3.14 a): In the simplest case a random fraction of bonds is chosen. All properties are studied as a function of the remaining bonds. The remaining fraction of bond corresponds to the conducting volume fraction.

2. The Site percolation model (cf. fig. 3.14 b): The fraction of removed sites is selected. There is a strong spatial correlation to absent or present nearby bonds.

3. The Correlated Bond percolation model: Random numbers for the bonds are calculated and all bonds greater than some selected limit are removed. Therefore, there is a statistical correlation. In this model the remaining bonds are clustered together, whereas in the site percolation model the missing bonds cluster. Thus, if a bond is present, its neighbors have a great probability of also being present.

For interfacial conductivity percolation behavior is typical. Hence, the conductivity percolates as soon as the particles reach an adequate narrow spacing. A conducting boundary layer formed around isolated particles in a conducting matrix material can also affect the conductivity in the way that the transport is blocked. Blocking of pathways by dry oxide particles can occur with higher volume fractions because porosity effects are involved (second percolation threshold). With increasing number of linkages, the cluster

size increases. Basically, the transition from a non-percolating to a percolating state is a kind of phase transition [121]. Studies of percolation on lattices have been carried out with numerical and analytical techniques. There are different percolation theories like the “effective medium theory” or the “time-dependent percolation theory”. The models based on bond percolation are well described by a simple effective medium theory, except close to the threshold value. The effective medium transport theory is applicable to an extremely wide class of systems. Broadbent and Hammersly [122] were the first to formally study percolation thresholds in 1957. They introduced simplified lattice models for the flow of a fluid through a porous (static random) medium. They showed that no fluid will flow, when the concentration of the active material is smaller than the threshold value. They also considered a percolation probability for a given region of the active medium to be well connected to the rest and therefore available for conduction. Furthermore, for low fractions of oxide filler material the double layer repulsion works against the percolation leading to small conductivities [123]. Based on a few works a spatial picture of the percolation threshold has emerged [124]. The stages of site percolation are described using a lattice with N sites (N is a large number). For low particle concentrations ($x \ll x_c$) the allowed sites x occur in small isolated clusters of adjacent sites. Larger clusters occur as x increases and therefore the average size of a cluster increases constantly. When x_c is reached the larger clusters start to merge, creating a few very large clusters. For the limit $N \to \infty$ the mean cluster size diverges at x_c. Then a complete path of allowed sites is formed, and the macroscopic flow through the system becomes possible. The path appears as soon as $x > x_c$.

In conclusion, all of the three conduction concepts are not perfectly applicable for the investigations in the following work. As the described measurements in this work show that the filler materials decrease the conductivity of the pure electrolyte, the volume exclusion after Maxwell was calculated. In some cases the conductivity trend differed from these estimations and therefore the model of space charge regions was taken into account. Percolating pathways cannot be excluded, but seem to be improbable for the examined composite electrolytes, as the volume fraction up to 7.5 wt% is assumed to be too low for the built-up of a percolating network.

3.1.4 Silica materials as filler

Several inorganic materials like inert oxide particles TiO_2, Al_2O_3 or SiO_2 are used as filler materials in electrolytes to improve characteristics like conductivity or mechanical behavior. Most of these filler materials are cheap, available in large quantities and harmless. Silica materials are widely used, as they have some major advantages. Actually, silica materials can easily be produced with varying surface areas, particle sizes, pores and surface functionalizations, as shown in fig. 3.15. This means that silica materials can be tailored to the requirements of different systems. The grafting procedure shown in fig. 3.15 is a simple method to modify silica materials, retaining the silica structure. Mainly organosilanes of the type $(R^2O)_3SiR^1$ are used to functionalize free silanol-groups on the inner surfaces of mesoporous silicas. A broad variation of the organic rest R is possible, though the porosity of the mesoporous material is reduced. Silica particles can interact in several ways with a head group of a surfactant, dependent on the pH (cf. fig. 3.16). The dominating interactions are of electrostatic nature (fig. 3.16 a-d), but with the use of non-ionic surfactants attractive interactions are mediated through hydrogen bonds. The reactions can take place under acidic and basic conditions, whereby in some combinations a mediator ion is necessary (b; c).

Especially the simple synthesis of mesoporous silica materials makes them attractive as filler material. As the surface area of mesoporous materials is high, the surface functionalization can be very effective. The resulting organic-inorganic hybrid materials can have enormous influence on the movement of ions and they can be produced with special characteristics. Due to the manufacturing process it is easy to vary the particle size within a wide range by changing the synthesis temperature. Silica materials can also be synthesized with a variety of morphologies. Additionally, the porous silica materials can be produced with different pore geometries (e.g. SBA-15 and MCM-41 have hexagonal pore systems; KIT-6 has a cubic pore system).

Particularly polymer electrolytes have been well studied with silica materials as fillers. Silica materials in polymers reduce the degree of crystallinity, as already mentioned in chapter 3.1.1. In general the segmental motion of polymer chains in amorphous regions contribute more pronounced to the ionic conductivity. There, fumed silica materials are widely used. The in-

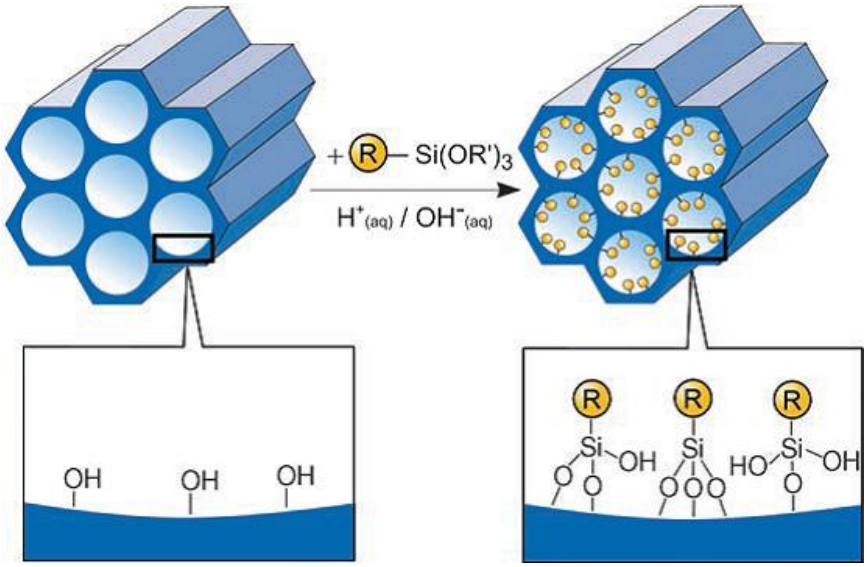

Figure 3.15: Schematic presentation of the grafting procedure with organosilanes to reach silica material with organic surface functionalization; source: [132].

terest in fumed silica as filler material is a result of its unique ability to form network structures in liquids [92]. The silanol groups have hydrophilic character for the polymer matrix material, but they can be replaced by hydrophobic ligands. Therefore, these materials are inserted into a polymer electrolyte to enhance the ionic conductivity, mechanical properties and even chemical stability [133–138] or to inhibit dendrite formation in lithium metal batteries [139]. Additionally, mesoporous SBA-15 as well as MCM-41 silica material were added to PEO-based electrolytes to improve electrochemical properties and stability towards the lithium electrode [140–142]. Core-shell structured silica particles were added as well [143]. With addition of silica nano-particles to the polymer electrolyte an all solid-state polymer battery has been constructed [144, 145].

In methanol fuel cells silica are applied to the membrane to reach higher operation temperatures and better oxidation kinetics [146], whereas the use of silica materials (fumed silica) in photoelectrochemical cells leads to the solidification of ionic liquid electrolytes with good results [147]. Even amine group-functionalized silica were tested [148]. Furthermore, silica nanoparti-

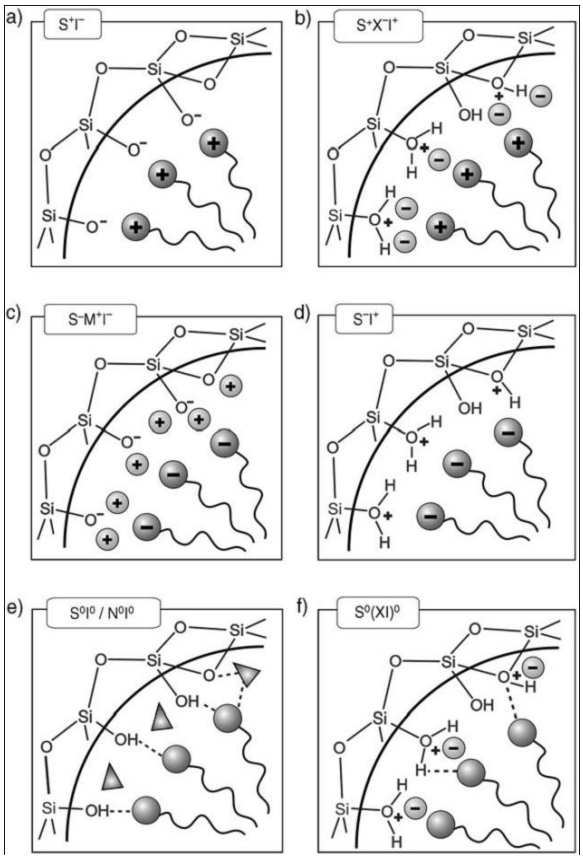

Figure 3.16: Possible interactions between the head group of a surfactant and the inorganic species in acidic, basic or neutral medium through electrostatics S^+I^- (a), $S^+X^-I^+$ (b), $S^-X^+I^-$ (c), S^-I^+ (d) or hydrogen bonds S^0I^0/N^0I^0 (e), $S^0(NX)^0$ (f); source: [132].

cles are used in electrolyte membranes to minimize the water uptake [149] or to act as trapping medium for impurities, again mainly water, in electrode materials and electrolytes [145]. For the electrode application a porous film of the nanostructured silica materials covers the electrode [150]. As a result, the fumed silica material seems to have a stabilizing effect (enhanced cyclability, reduced interfacial resistance) on the cell performance of a lithium battery [151].

A remarkable application of silica materials is the use of silica glasses. A

network is filled with ionic liquid, whereby high ionic conductivity is combined with high mechanical strength in a solid electrolyte material [152].

The confinement of ionic liquids within a silica-derived network results in so-called ionogels [153]. These were found to have the same conductivity as pristine IL's and excellent thermal stability. Correspondingly, the group of Archer investigated a new organic-inorganic hybrid electrolyte, where the ionic liquid 1-methyl-3-propylimidazolium bis(trifluoromethanesulfone)-imide was tethered to silica nanoparticles (SiO_2-IL-TFSI) [154]. These materials have more than three orders of magnitude enhanced ionic conductivities relative to either of the mixture components and they exhibit high thermal stability. This concept is called "salt-in-filler" concept.

Filler materials are scarcely used in liquid electrolytes. The known application as fillers are the "soggy sand" electrolytes [23], but the conductivity effect seen with this composite electrolytes is controversial and still under investigation (cf. chapter 3.1.2). An enhancement of the conductivity is explained with space charge regions and percolation effects, whereby silicas were thought to be superior to other oxide filler materials like TiO_2 and Al_2O_3 due to their higher acidity and therefore better adsorption of the anion. The addition of filler materials to liquids is problematic due to segregation and stability. Especially in organic electrolytes used in batteries the silica materials react under decomposition.

In conclusion, silica materials as fillers have a proven and positive influence on the conductivity of polymers. For applications as trapping medium of impurities like water, silica materials are well suited. Even for gelation or to enhance the thermal stability, silica materials as filler can be implemented. In liquids, segregation has to be avoided by using surface functionalization.

4 Materials and methods

The electrochemical and mechanical behavior of disperse composite electrolytes for lithium ion batteries with different silica materials as filler materials were investigated systematically. KIT-6, MCM-41 and SBA-15 silica as well as commercial available silica particles were inserted into an electrolyte consisting of 1 M $LiPF_6$ in EC/DEC 3:7 in their basic form but predominately with surface modification. The ionic conductivities were studied with impedance spectroscopy, surface potentials were examined via zeta potential measurements and viscosity was studied with rheological methods. Moreover, changes of the electrochemical window were determined via voltammetry measurements and the morphology of the silica materials was investigated with SEM.

4.1 Silica materials

Several types of silica as filler materials have been used: mesoporous and non-porous silica with different pore geometries, pore diameters, specific surface areas and varying surface functionalization groups (listed in tab. 4.1). Spherical silica particles have been purchased from different companies (SiO_2 nanopowder and SiO_2 S5631 from Sigma Aldrich, Cab-O-Sil M-5 from Fluka, silica gel 60 from Merck KGaA). Mesoporous silica materials SBA-15, KIT-6 and MCM-41 were synthesized by slightly modified procedures applying different temperatures resulting in different pore sizes with respect to the literature [155–157]. The synthesis, modification and characterization of the non-commercial silica materials, have been carried out in the work group of Prof. Fröba at the University of Hamburg as a part of a cooperation project. Thereby, the surface modification was achieved via a post-synthetic grafting procedure [12, 158, 159]. The mesoporous silica nanoparticles were synthesized in accordance to the literature [160], whereas the preparation of the spherical nanoparticles was done by Stöber synthesis [161]. All silica were characterized with nitrogen physisorption. Characterization of silanes

was done by ^{1}H and ^{13}C nuclear magnetic resonance (NMR) and mass spectrometry (MS). The silica were analyzed with infrared spectroscopy (IR), powder X-ray diffraction (XRD) and thermal analysis with mass spectrometry (TG-DTA-MS).

For labeling of the filler materials the differences in synthesis temperatures and surface groups were utilized (cf. tab. 4.1). The base material (e.g. MCM-41) is always the first information. The notation KIT-6, MCM-41 and SBA-15 are very common and well-reputed, because they are acronyms for the places of synthesis and do not describe characteristics of the materials (e.g. SBA-15: Santa Barbara Amorphous type material). Following this, the commercial materials are named with their trade name, whereas S5631 is the product number for better differentiation. The in-house synthesized materials are distinguished with their synthesis temperature in $^{\circ}\mathrm{C}$, followed by the surface functionalization group as required. The MCM-41 materials are differentiated with the lengths of the used precursor molecule (e.g. C12). Im13 is the abbreviation for a imidazole surface group followed by the counter ion hexafluorophosphate ($\mathrm{PF_6^-}$).

4.1.1 Morphology of silica materials

SEM pictures to study the morphology of the silica materials were recorded with a MERLIN microscope (Zeiss). For that purpose, the silica particles were fixed on carbon pads and covered with platinum by sputtering.

4.2 Preparation of the dispersions

The organic electrolyte 1 M lithium hexafluorophosphate ($\mathrm{LiPF_6}$) in a mixture of ethylene carbonate (EC) and diethylene carbonate (DEC) at the ratio 3:7 (w/w; >99.5 %, UBE Industries, Ltd.) was opened in the glovebox and used as received. The water content of the pure electrolyte was determined by coulometric Karl Fischer titration and was <15 ppm. The silica materials were vacuum-dried (glass oven Büchi B-585) for at least 24 h at $60\,^{\circ}\mathrm{C}$, $80\,^{\circ}\mathrm{C}$ or $120\,^{\circ}\mathrm{C}$ (surface-modified materials) and $300\,^{\circ}\mathrm{C}$ (non-modified silica), respectively. For the preparation of the disperse electrolyte samples, the appropriate amount of silica material was added to the suitable mass of electrolyte solution and dispersed with an ultrasonic finger (Hielscher, UP100H).

Table 4.1: Investigated filler materials with their average pore widths, specific surface areas and specific pore volumes, each determined by nitrogen physisorption. The item '/' means, that these materials are non-porous and therefore have no values for characterizing pores.

material	average pore width / nm [a]	specific surface area / m^2g^{-1} [b]	specific pore volume / cm^3g^{-1} [a]
SiO_2 nanopowder	/	658	/
SiO_2 S5631	/	156	/
silica gel 60 (Kieselgel 60)	7.0	376	0.734
Cab-O-Sil	$\sim$ 46 [c]	224	1.532
MCM-41-C12	3.2	1034	0.648
MCM-41-C14	3.5	1266	0.876
MCM-41-C16	4.3	1141	0.991
MCM-41-C18	4.4	1153	1.153
SBA-15-50	5.1	348	0.372
SBA-15-140	10.1	392	1.003
SBA-15-140-aminopropyl	6.8	364	0.816
SBA-15-140-methyl	10.1	421	1.044
SBA-15-140-octyl	7.4	467	1.152
KIT-6-80	7.0	876	0.934
KIT-6-100	8.5	862	1.248
KIT-6-120	9.1	684	1.295
KIT-6-140	10.9	491	1.346
KIT-6-140-sulfonyl	8.8	509	1.041
KIT-6-140-aminopropyl	9.4	385	1.018
KIT-6-140-methyl	9.4	445	1.080
KIT-6-140-octyl	9.1	426	1.021
KIT-6-140-hexyl	8.5	669	1.166
KIT-6-140-Im13-sulfonic acid	8.8	391	0.802
KIT-6-80-PEO1000	7.0	271	0.462
KIT-6-120-PEO1000	8.1	299	0.617
KIT-6-140-Im13-PF_6	8.8	362	0.877
KIT-6-140-Im13-PF_6-HDMS	9.1	343	0.902
KIT-6-140-Im13-Cl	8.8	350	0.842
SiO_2-nano	/	290	/
SiO_2-nano-Im13-PF_6	/	315	/
SiO_2-nano-SNP20	/	355	/
SiO_2-nano-porous	11.7 [c]	516	1.614

[a] from Density Functional Theory (NLDFT) analysis of desorption data

[b] using BET method

[c] wide distribution 7 nm - 70 nm

More precisely, mass fractions of approximately 1 %, 2,5 % and 5 % were adjusted based on the following equation:

$$\omega_{\text{silica}} = \frac{m_{\text{silica}}}{m_{\text{silica}} + m_{\text{electrolyte}}} \tag{4.1}$$

Complementary measurements were partially executed with a mass fraction of 0.5 % and 7.5 % as well as 10 %, but only if it was possible due to dispersing and material availability. All composite electrolytes were prepared in a glovebox under argon atmosphere. The amount of water and oxygen in the atmosphere was controlled and below 3 ppm.

4.3 Impedance spectroscopy

Classical methods in electrochemistry work with constant voltage (e.g. chronoamperometry) or with alternating voltage of defined frequency combined with high amplitudes (e.g. cyclovoltammetry). However, the electrochemical impedance spectroscopy (EIS) is more frequently used since measuring instruments and software are easier to operate and faster. Especially in terms of surface and interface research (corrosion processes, batteries, sensors) the EIS is deployed [162].

Basically, for EIS measurements an alternating voltage (sinusoidal signal) with varying frequency and small amplitude is applied to the analyzed system. Since the frequency dependent impedance (AC resistance) of a system is recorded, dynamic processes of charged particles can be observed. The impedance spectra in Nyquist representation can consist of semi-circles and lines. An equivalent circuit is often used to analyze and describe the electrochemical system. Actually, the connection of impedance elements, either parallel or in series, like ohmic resistance, capacitor etc. should exhibit the same frequency dependent impedance behavior like the analyzed system. In line with this, the impedance elements are attributed to physical characteristics of the system. Nevertheless, this comparison is possible as long as the charge carriers (ions) in the electrochemical system show similar impedance behavior like electrons in resistances and capacitors, which is often problematic. Hence, material constants (conductivity, dielectric constant), interface processes as well as the capacity of interfaces can be investigated and the differentiation between several sub-processes is possible [163]. For the ex-

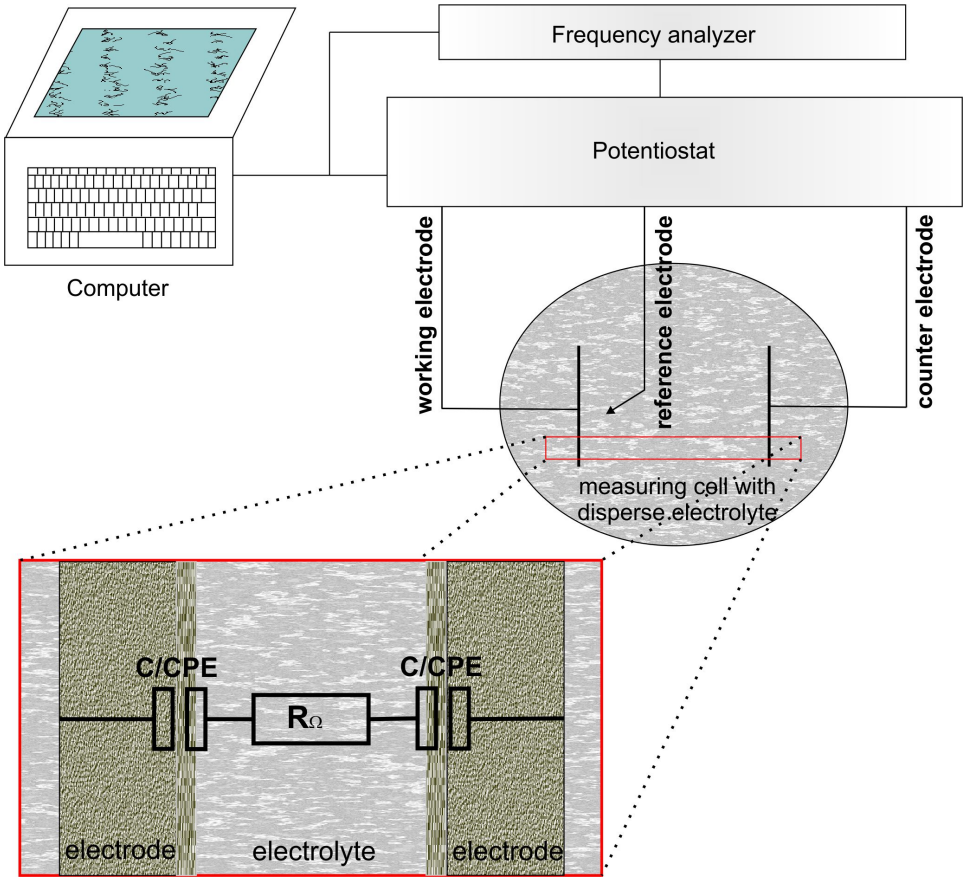

Figure 4.1: Experimental set-up of an EIS measurement with disperse electrolytes and three-electrode array.

ploitation, the behavior of current I and voltage U under alternating current in an electric circuit must be known. Ohm's law only applies to AC current measurements, if ideal resistances R are present. Thus, current and voltage oscillate out of phase, when capacities or inductivities are existent. This means a description of U and I is possible with complex numbers solely. Basically, U and I can be expressed with application of the angular frequency ω:

$$U = U_0 e^{i\omega t} \text{ and } I = I_0 e^{i\omega t + i\varphi} \tag{4.2}$$

The complex resistance, known as impedance *Z*, is defined as:

$$Z = \frac{U}{I} = \frac{U_0}{I_0} e^{-i\varphi} \tag{4.3}$$

Hence, with Euler's formula ($e^{ix} = \cos x + i \sin x$) the impedance can be split into the real component *Z*' and the imaginary component *Z*":

$$Z = Z' + i\,Z'' \quad \text{with} \quad Z' = \frac{U_0}{I_0} cos\varphi \quad \text{and} \quad Z'' = -\frac{U_0}{I_0} sin\varphi \tag{4.4}$$

Therefore, impedance spectroscopy is the measurement of impedance at several frequencies. Accordingly, in a liquid sample two electrodes, more precisely the working and the counter electrode, are immersed. The electrodes can be well described as capacitors *C*, due to the formation of the electrochemical double layer (cf. 4.1). With applying an alternating voltage to the system, reversible processes at the electrode are initialized. The exchange of electrons between electrode and ions can be represented as charge-transfer-resistance *R*. In line with this, the systems observed in the present work, consisting of dispersed electrolytes, can be described with an equivalent circuit out of a serial connection with two capacities (electrode/electrolyte interfaces) and an ohmic resistance (electrolyte). Hence, a perpendicular line in the Nyquist plot is expected for such an equivalent circuit. However, a slightly curved trend is observed for the dispersions, as the electrodes are not perfect capacitors. Therefore, constant phase elements (CPE) as impedance elements are used for polarizable electrodes like the platinum electrodes. The CPE is composed of several small elements arranged in a defined way and is used to describe inhomogeneities of the electrode material and their influence on the impedance [164].

4.3.1 Conductivity measurements

The electrical conductivity experiments were performed by potentiostatic electrochemical impedance spectroscopy using a BioLogic SP150 potentiostat/galvanostat (BioLogic Science Instruments) controlled by the software EC Lab and an EG&G Potentiostat/Galvanostat Model 283 (Princeton Applied Research) with PowerSuite 2.45 as software. Conductivity cells equip-

ped with platinum ring electrodes (Mettler Toledo, C_{cell} = 0.8 cm^{-1}) were immersed into the sample in temperature-controlled glass bins inside the glovebox. Actually, a minimum of 4 mL of electrolyte was needed to cover the electrodes. For the first measurements an immersion measuring cell with opposed platinated electrodes (Metrohm) was used. Most of the organic dispersions were stirred during the measurements to avoid sedimentation. Although this influences the measurements in terms of percolating path, stirring was unavoidable. Temperature was controlled between $0\,^{\circ}\text{C}$ and $60\,^{\circ}\text{C}$ with a silicon oil filled thermostat (Julabo F32). Accordingly, the measurements were performed in steps of $5\,^{\circ}\text{C}$ and the exact temperature was determined with a thermocouple dipped into the dispersion. The set-up is shown in fig. 4.2.

The impedance measurements were carried out between 100 kHz and 500 Hz with an amplitude of 50 mV and the resistance as equivalent circuit was determined in the Bode plot with an ohmic resistance in a frequency range at a 0 ° phase angle. The resistance could be measured with an accuracy of 2 Ω and therefore the conductivity shows deviations at $25\,^{\circ}\text{C}$ of 0.3 mS/cm which corresponds to an uncertainty of approximately 5 %. The conductivity σ was determined by dividing the cell constant C_{cell} with the measured resistance R.

$$\sigma = \frac{1}{R} \cdot \frac{l}{A} = \frac{1}{R} \cdot C_{\text{cell}} \tag{4.5}$$

The cell constant was determined using a 0.1 M aqueous potassium chloride solution with the same conductivity cells. Deviations were around 3 %. The potassium chloride solution (Certipur) was purchased from Merck KGaA with a nominal conductivity of 12.8 mS/cm.

4.4 The Zeta potential

The stability and homogeneity of colloidal suspensions is most affected by the surface of the suspension particles. In simple material systems the electrostatic repulsion of the particles contributes essentially to the stability, which can be influenced externally. In this case methods like electrophore-

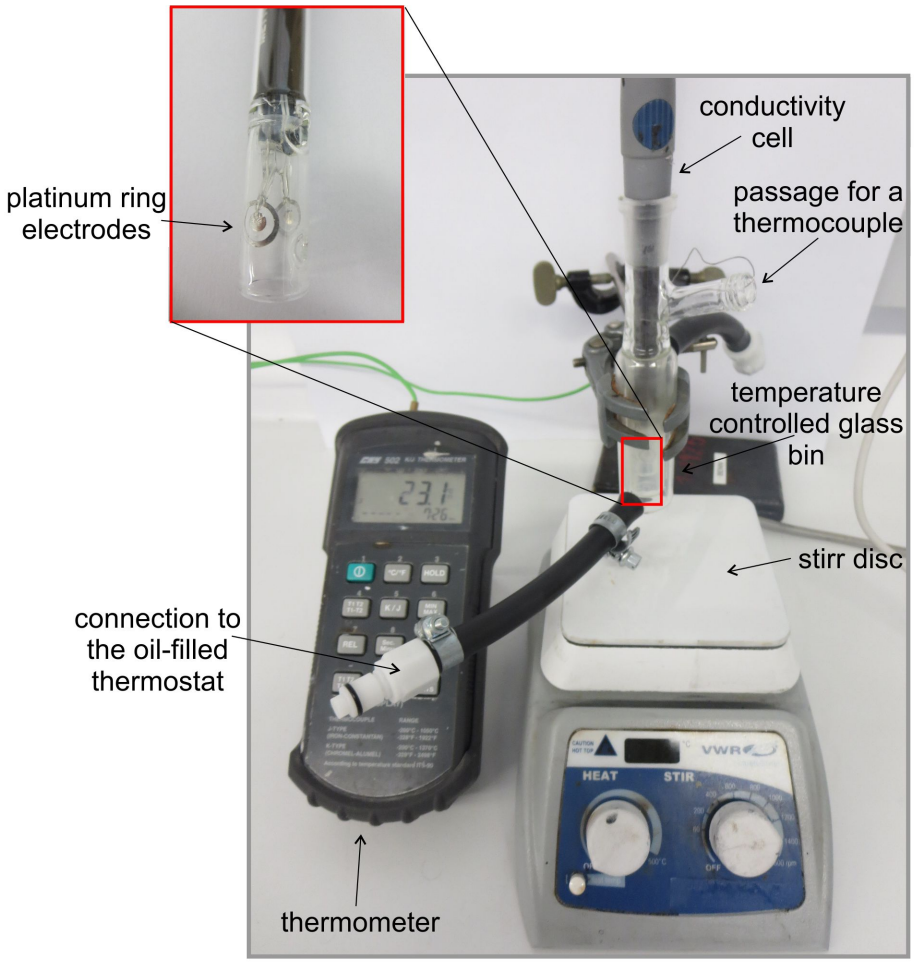

Figure 4.2: Experimental set-up for the conductivity measurements.

sis, acoustic and streaming potential methods can be used to characterize the surface potential of colloids. Actually, electrophoresis is the most commonly used method, whereby the so called zeta potential is derived from the electrophoretic migration velocity and cannot be measured directly. The charge conditions at the particle surface are influenced by the electrochemical situation of the surrounding liquid, above all the pH value and the electrolyte concentration, which defines also the conductivity [165]. The particle

size and even the shape are also decisive.

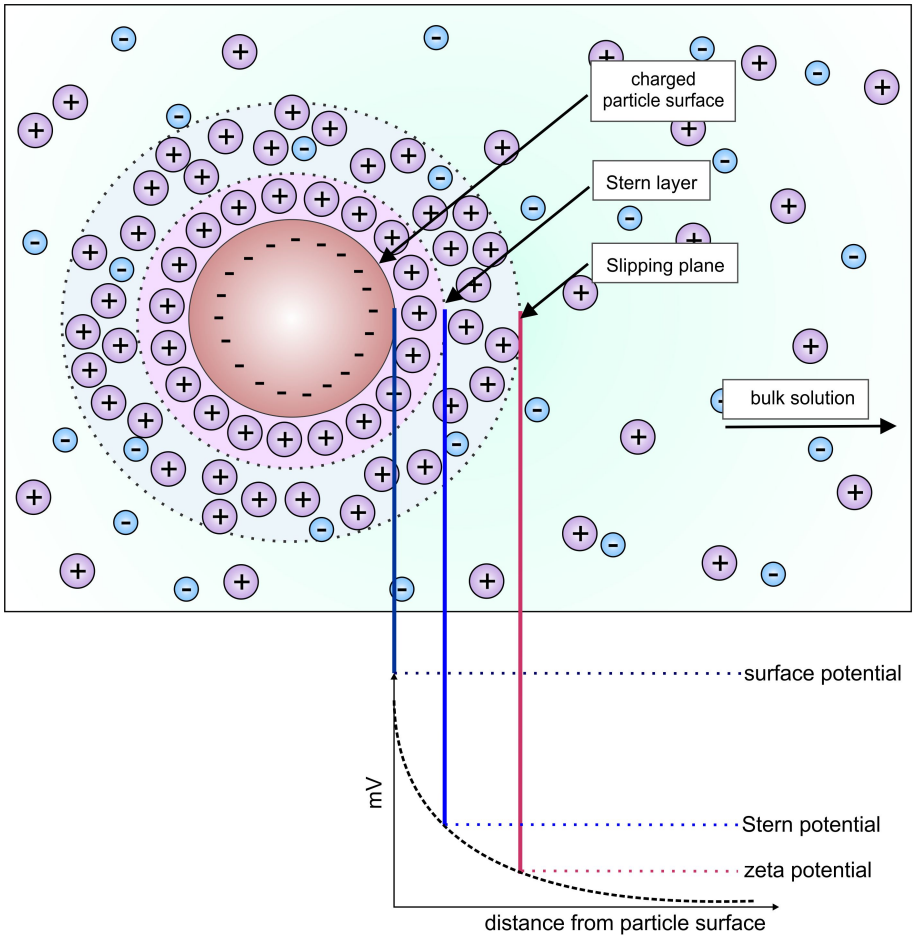

Figure 4.3: Schematic presentation of the zeta potential. With distance from the charged surface the Stern layer with the Stern potential is followed by the slipping plane with the zeta potential before the bulk solution begins.

The zeta potential is the electrical potential at the shear layer of a moving particle in a suspension as can be seen in figure 4.3. The first layer surrounding a particle in a liquid consists of ions adsorbed at the surface due to chemical interaction, called the Stern layer. The second layer of ions is loosely associated with the particle via coulomb force. Hence, this diffuse

layer can be sheared off during the movement through a medium due to friction and therefore, the particle exhibits a surface potential (zeta potential) at the shear plane. The zeta potential is the electrical potential at the shear layer of a moving particle in a suspension and is a function of charge density at this shear plane, whereas the magnitude of zeta potential is lower than the surface potential as the shear plane is located in a unknown distance from the surface in the diffusive part of the double layer. The decay of the electrostatic potential with increasing distance from the surface is shown in fig. 4.4. A difference can be seen between specific and non-specific adsorption. The differences in Stern potential Ψ_s and zeta potential ζ are substantially. The zeta potential varies for the non-specific adsorption with the concentration of the suspension. The zeta potential delivers information about the magnitude of repulsion and attraction between particles and insight into dispersion mechanisms. Statements about the systems stability of colloid suspensions are possible as it is a key for electrostatic dispersion control. Moreover, in this work the adsorption of ions on the surface of the silica materials and a possible space charge region should be clarified.

In simple systems the zeta potential corresponds to the surface potential of the particle. The received values have a sensitive dependence on the concentration and type of ions in the solution. Hence, the zeta potentials vary in a wide range with the surface conditions of the silica materials and the solution medium. Normally, zeta potentials are measured in water but would be meaningless for the observed dispersions as a non-aqueous electrolyte was used. Therefore, to get a more realistic picture of the silica surface potential in the observed dispersions, the zeta potentials were determined with a highly diluted electrolyte solution. In order to obtain a correct zeta potential, it is necessary to maintain the phase composition and distribution. However, samples have to be highly diluted, as with increasing concentration the double layer thickness decreases. The zeta potential decreases when the concentration of free ions increases. At high enough salt concentrations the double layer becomes very narrow and van-der-Waals forces overcome charge repulsion. Hence, electrostatically stabilized colloidal suspensions become unstable with addition of too much salt, called “salting out”. This effect has to be considered when analyzing the electrolyte dispersions.

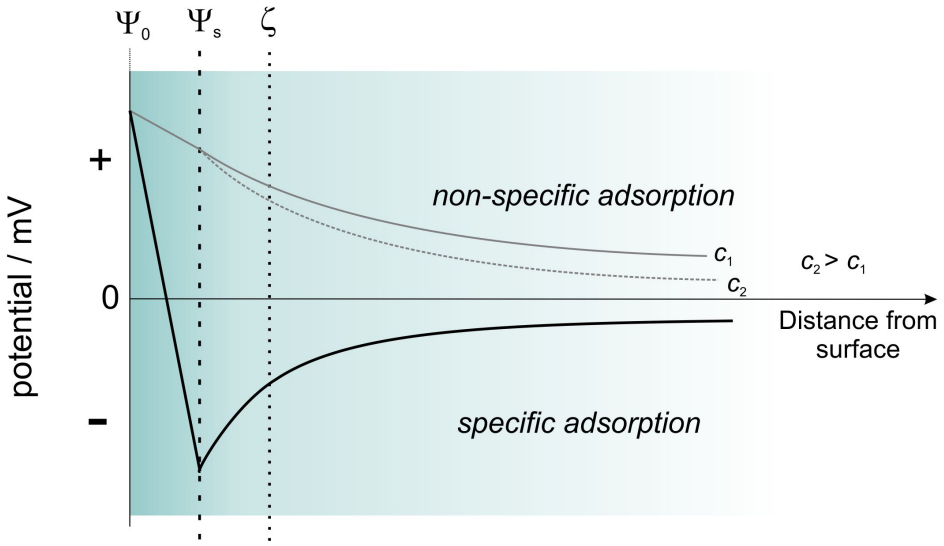

Figure 4.4: Schematic presentation of the electrochemical potential trend with increasing distance from the particle surface for non-specifically adsorbed ions and the case of specifically adsorbed ions. Ψ_0 is the surface potential, Ψ_s the Stern potential and ζ the zeta potential.

A difference has to be made between specific adsorption of ions and non-specific adsorption. Without specifically adsorbed ions on the surface, the corresponding ions (from suspension or added salt) gather near the surface. With diffusion (thermally-driven) the random distribution of ions increases with distance from the surface. Thereby, the surface potential is decreased to zero far away from the surface. The specific adsorption of counterions leads to reversal of the sign of the zeta potential. The shear plane is then shifted out further and has, for example, a negative potential if the surface is positively charged.

The difficulty in measuring zeta potentials of suspended particles in non-aqueous media is the low particle mobility. The understanding of electrophoresis in non-aqueous systems is difficult, but empirical understanding of stability and surfactant adsorption is possible.

Basically, an electrical field in an electrophoresis arrangement drives charged particles between electrodes. The zeta potential is optically measured as the electrophoretic mobility U_E. Hence, the zeta potential can be obtained by measurement of the electrophoretic mobility and by application

of the Henry equation afterward:

$$U_{\mathrm{E}} = \frac{2\varepsilon\ \zeta\ f(\mathrm{Ka})}{3\eta}$$

ζ : zeta potential
U_{E} : electrophoretic mobility
ε : dielectric constant
η : viscosity
f(Ka) : Henry's function

The case of f(Ka) = 1.5 is referred to as the Smoluchowski approximation. This equation applies to dispersions where the particle radius is much larger than the double layer thickness which is generally the case for particles greater than 0.5 µm and an electrolyte concentration lower than 10^{-3} mol·L^{-1}. For small particles in media with small dielectric constant f(Ka) becomes 1.0, which is referred to as the Hückel approximation. This is generally valid for small particles with relatively thick double layers.

The method used in this work was Laser Doppler Velocimetry (LDV) (cf. fig. 4.5). Here, a capillary cell with electrodes at both ends is used to which a potential is applied. Ergo, particles move toward the contrary charged electrodes. Therefore, an incident beam is focused on the sample and the light scattered at the particles is detected at an angle of 17°, compared to a reference beam. The fluctuating intensity is particularly characteristic for the frequencies of the signal. The intensity is proportional to the speed of the particles and is extracted by a digital signal processor. A system refinement modulates one of the laser beams with an oscillating mirror, to get an unequivocal measure of the sign of zeta potential. In order to perform measurements at any point within a cuvette a special technique, the M3-PALS technique, is used.

4.4.1 Measurement of the surface potential

Surface potentials were obtained from electrophoretic zeta potential measurements (Zetasizer Nano ZS, Malvern Instruments). A solution of 2 mM $LiPF_6$ in EC/DEC at the ratio 3:7 (w/w) was prepared and a silica mass fraction of 0.05 wt% was added. The dispersions were prepared inside an

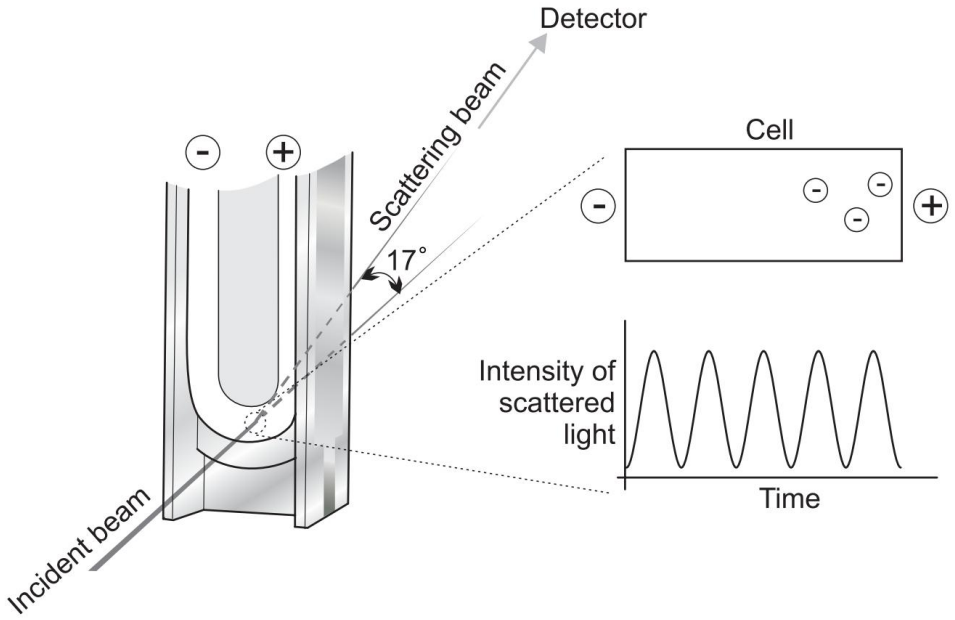

Figure 4.5: Schematic presentation of the method LDV to determine surface potentials; source: [165].

argon-filled glovebox and transferred into sealed capillary cuvettes. To clarify the effects of the conducting salt, zeta potentials were also determined in the pure solvent mixture EC/DEC 3:7 (w/w) without conducting salt. All the measurements were carried out at $25\,^{\circ}\mathrm{C}$. The zeta potential was calculated from the measured electrophoretic mobilities using the Smoluchowski model.

4.5 Rheology

Rheology is the field which deals with flow properties of materials. Samples like solids, liquids or colloidal materials deform with stress due to external forces. Correspondingly, viscoelastic and viscous properties of materials are determined [166]. The measurement of the viscosity η is in rotational rheometers dependent on the angular rate Ω and the torsional moment M, where k is a constant depending on the used measuring system:

$$\eta = k\frac{M}{\Omega} \tag{4.6}$$

Furthermore, the viscosity is dependent on the shear stress τ and the shear rate $\dot{\gamma}$ in the following way:

$$\eta = \frac{\tau}{\dot{\gamma}} \tag{4.7}$$

The shear stress is a basic information to describe material properties as it is directly proportional to the measurable force. Basically, a sample is placed in a measuring geometry, for example between two plates (or a cone-plate geometry; geometries are shown in fig. 4.6). Then, the upper plate is moved with the force $\vec{F}$ into an arbitrary direction and therefore the material in the shear gap is deformed. Hence, if the force impact is vertical to the surface normal, this motion is designated as shear strain. In accordance, the relation of the force $\vec{F}$ to the area A is labeled as shear stress τ. Generally, different measurement systems are used, dependent on the range of viscosity and particle size.

Three geometries are used mostly: The plate-plate-geometry (fig. 4.6a) is used for soft solids and samples with big particles. Unfortunately, the shear rate is dependent on the particle radii. The cone-plate-geometry (fig. 4.6b) has a shear rate independent of the particle radii and was developed for high shear rates ($\gamma < 10^6$ s^{-1}). Actually, it is used for highly viscous samples and for measurements with a low amount of material. The coaxial cylinder geometry (fig. 4.6c) is implemented for materials with low viscosity. Furthermore, a distinction is made between several coaxial geometries. The material can be sheared either continuously or oscillating. This results in measurement dependent either on the shear rate, shear deformation or shear stress. Linear or logarithmic ramps can be chosen, whereas for time-dependent phenomenons one dimension needs to be changed abruptly. For oscillating or dynamic measurements a sinusoidal deformation is used. Hence, different experiments like amplitude tests or frequency tests can be implemented.

The ideal liquid is the Newtonian fluid, which shows only viscosity and no elastic and plastic deformation. In addition, linearity between shear stress and shear rate with the viscosity as constant of proportionality is essential for ideal liquids under steady flow (see fig. 4.7). Furthermore, for elastic materials the deformation is reversible like for a spring, whereas the plas-

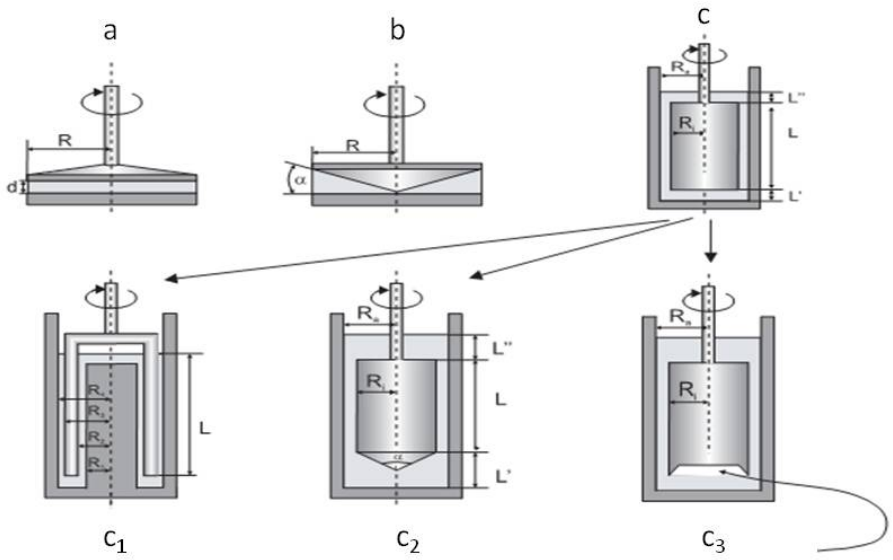

Figure 4.6: Different measurement geometries used for rotational rheometers [166]: a) plate-plate, b) cone-plate, c) coaxial cylinder geometry, c_1) dual gap, c_2) ISO3219, c_3) with air cushion

tic deformation is characterized with a present flow limit τ_0 .This flow limit denotes the range where the reversible elastic deformation ends and the irreversible deformation begins. Above all, constant viscosity with increasing shear stress is termed as Bingham behavior. However, for the rheological classification of materials the dependence of the shear stress on the shear rate is used.

Regarding fig. 4.7 it becomes obvious that materials do not always behave ideal under steady flow. Besides the Newtonian behavior, shear thinning (viscosity decreases with increasing shear rate) and shear thickening or dilatancy (viscosity increases with increasing shear rate) is possible. Soggy sand for example shows the rare shear thickening. For the case of an existing flow limit and change in viscosity with the shear rate one speaks of non-linear plastic behavior. For the visco-elastic behavior the material characteristics are dependent on time.

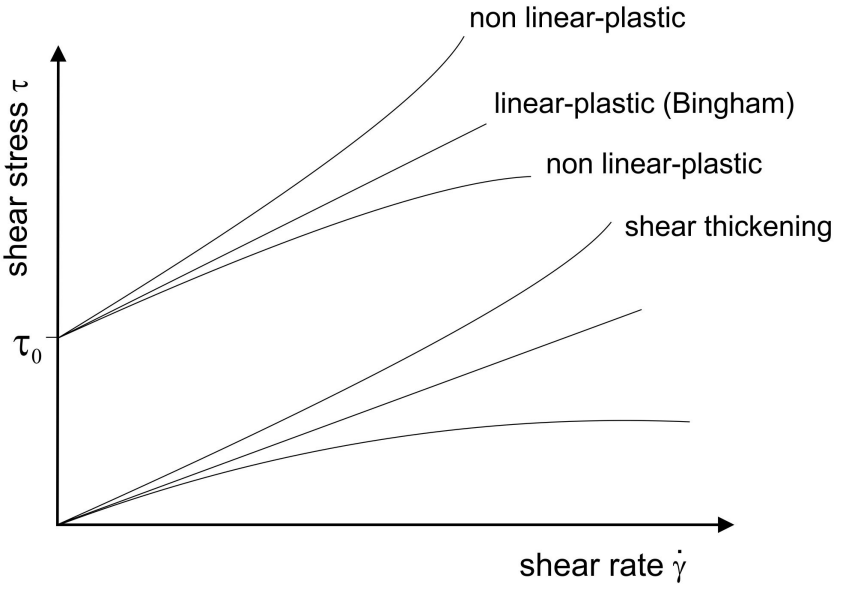

Figure 4.7: Classification of materials on the basis of the characteristics of the shear stress dependent on the shear rate.

4.5.1 Viscosity measurements

The viscosity was determined with an Anton Paar MCR 302 rheometer in a dry room ("Batteries and Electrochemistry Laboratory" (BELLA), Institute of Nanotechnology, KIT, Karlsruhe, Germany). Thereby, samples were mixed in a glovebox under dry argon atmosphere. The organic composite electrolytes with variying silica mass fraction and several silica materials were measured with plate-plate geometry at $25\,^{\circ}\mathrm{C}$ and a 1 mm gap. A shear rate between 0.001 s^{-1} and 1000 s^{-1} was chosen with a logarithmic ramp.

4.6 Voltammetry

Voltammetry is a generic term for an electroanalytical method, where the dependency between current and voltage is observed in order to clarify reaction mechanisms and chemical composition of materials as well as electrochemical stability, generally to investigate thermodynamics and kinetics

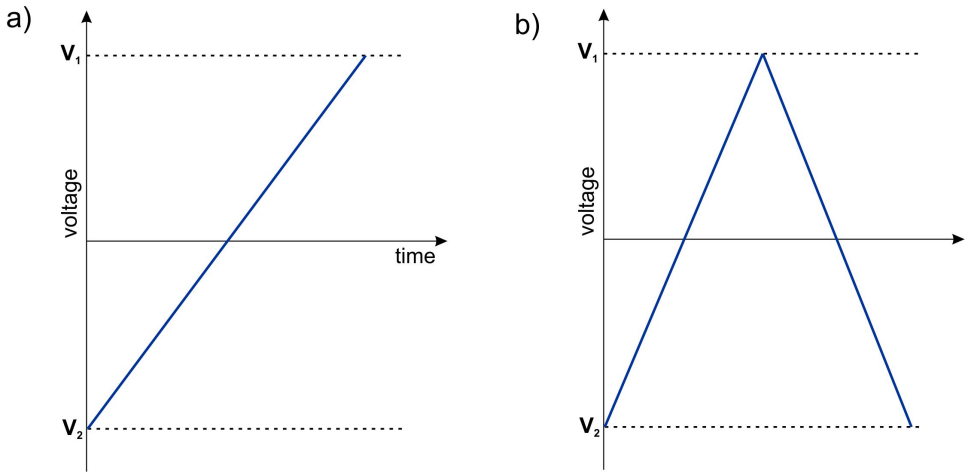

Figure 4.8: Schematic presentation of the voltage variation against time for a) linear sweep voltammetry (LSV) and b) cyclic voltammetry (CV).

of chemical reactions. Cyclic voltammetry (CV) is the most commonly used voltammetry technique, whereas the linear sweep voltammetry (LSV) is the simplest one. Basically, for the LSV measurement the working electrode potential is varied linearly in a fixed potential range as a function of time, as shown in fig. 4.8 a.

Therefore, the voltage is normally scanned from a lower limit to an upper limit and the current response is recorded. Relatively slow scan rates are implemented, so that the electrode is in equilibrium with the surrounding bulk solution. The characteristics in a recorded linear sweep voltammogram are dependent on factors like the chemical reactivity of the electroactive species, the rate of the electron transfer reaction and the applied scan rate. For the very similar CV method a linearly increasing voltage is applied to the working electrode, which means that the potential is ramped to a given value and then returned to the starting potential with the same rate (cf. fig. 4.8 b). Accordingly, the responding current is recorded and plotted against the applied voltage. In case of chemical reaction, peaks in current are observed. These current peaks can be used to characterize the type of occurring reaction, the concentrations of reactants and the type of the electroactive species. Furthermore, the electron transfer rate constant can be estimated by analyzing the variation of peak positions as a function of varying scan rates. For cases

with a non-reversible electron transfer considerably different behavior from the reversible counterparts can be observed. The current peaks result from the depletion of reactive species at the surface with achieving the reaction potential. Critical parameters for a reproducible measurement are the purity of the examined materials, the electrode and the choice of the scan rate and the potential limits. The potentiostatic measurement is normally performed with a three electrode arrangement, whereas the interesting reactions are observed at the working electrode consisting commonly of an inert noble metal like platinum or gold.

4.6.1 Voltammetry measurements

The linear voltammetry experiments were carried out in a sealed micro cell (TransMit - Project Division for Electrochemical Materials Research and Interface Characterization, Marburg, Germany), shown in fig. 4.9. The disperse electrolyte was kept in a platinum crucible which has a volume of 0.6 mL - 1.8 mL acting as counter electrode. In the cap glassy carbon (3 mm diameter) acting as working electrode is embedded and a lithium reference electrode is included. The reference electrode consists of a nickel wire with a nickel clip in which a piece of lithium foil was fixed. The cell was filled inside the glovebox with electrolyte solutions consisting of 1 M $LiPF_6$ in EC/DEC 3:7 and 2.5 wt% of silica material. The temperature was kept constant at $25\,^{\circ}\mathrm{C}$ using a Peltier element. The voltage was increased from 0.5 V to 7 V with a scan rate of 5 $mV \cdot s^{-1}$.

4.7 Supplementary measurements

Additional measurements were done in terms of the electrolyte safety with flame point measurements and in terms of examination of the basic mechanistic model of dispersions with adsorption measurements.

4.7.1 Flash point measurements

Flash point measurements are interesting in terms of electrolyte safety. Hence, it was investigated whether silica as filler material can increase or generally influence the flash point of organic electrolytes. A higher flash point

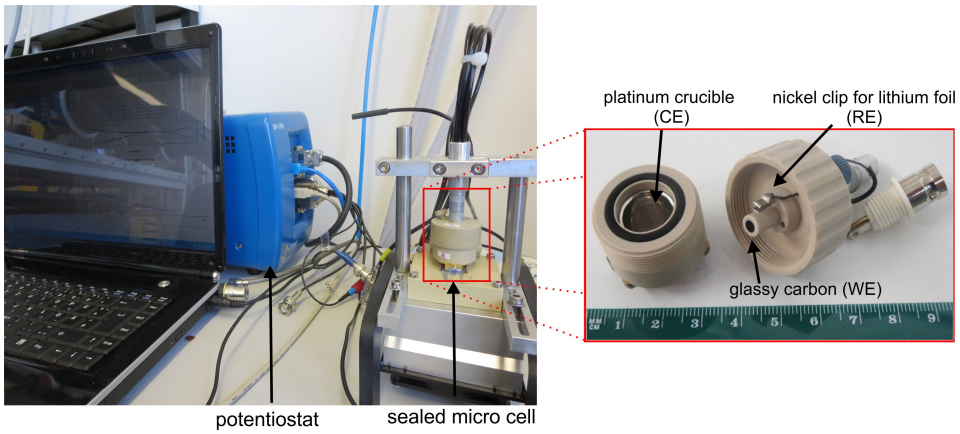

Figure 4.9: Setup with a sealed microcell to determine the electrochemical window by linear voltammetry.

would mean the electrolyte is less easy to inflame and therefore safer in the later application. Flash point measurements were performed in an Elcometer 6910, Setaflash series 3 (Stanhope-seta) with a closed aluminum cup. Several dispersions with varying silica material and silica mass fraction as well as the pure electrolyte 1 M $LiPF_6$ in EC/DEC 3:7 were measured after calibration. Therefore, the temperature was increased in steps of $1\,^{\circ}\mathrm{C}$ and around the flash point in $0.5\,^{\circ}\mathrm{C}$ steps. After each temperature step the flame of the Setaflash was shortly dipped into the cup with the sample, to screen whether the flash point was already reached. In case of the reached flash point, the equipment gave a clear signal, because a thermally activated detector determined the flash point. Thus, the risk of operating errors and the inhalation of vapors were minimized. Butane (lighter fuel) was used as gas for the flame and a sample volume of 2 mL approximately was needed. A temperature range of $0\,^{\circ}\mathrm{C}$ - $300\,^{\circ}\mathrm{C}$ was possible. The measurements were carried out with air environment.

4.7.2 Adsorption experiments

Adsorption measurements were performed to investigate the of ion adsorption at the silica surface. Therefore, varying electrolyte dispersions with different silica and silica mass fractions were made. Then, the conductivity

of the pure electrolyte was measured followed by the determination of the disperse electrolyte's conductivity. After two hours without stirring or mixing, most of the silica material had segregated and the conductivity of the residual liquid electrolyte was determined. Finally, the conductivity measurement of the organic phase was repeated after a waiting period over night with unaffected samples.

5 Results and Discussion

In this chapter the measurements that were performed to characterize the disperse electrolytes, consisting of silica particles and the liquid organic electrolyte 1 M $LiPF_6$ in EC/DEC, are presented and evaluated. First of all, morphology investigations by SEM are shown followed by a graphical analysis of numerous conductivity measurements executed with impedance spectroscopy. Within this processing the conductivity trends are correlated with surface areas and pore width of the silica materials. Furthermore, the activation energies for the migration of ions through the solution are calculated with the Vogel-Fulcher-Tammann (VFT) equation. In the following, the results of zeta potential measurements and the effects on the network structure of the disperse electrolytes as well as the possibility of an adsorption mechanism of electrolyte ions at the silica surface are discussed. The evidence of network structures within the silica particles was further investigated by rheological measurements, with the focus on viscosity. Some supplementary measurements are described at the end of this chapter, i.e. flash point testing.

5.1 Morphology of silica materials

The morphology of filler materials in dispersion may have significant influence on the colloidal behavior and therefore the conductivity behavior. Hence, SEM pictures of several used silica materials were recorded in order to be aware of strong differences. In fig. 5.1, SEM pictures of basic materials are shown with different magnifications. It can be seen that the KIT-6-40 material consists of individual particles with a spherical structure, whereas the SBA-15-140 material is composed of long chains which form elongated particles. In comparison, the SiO_2 S5631 and the MCM-41-C18 material show large agglomerates with porous surface structure. In fig. 5.2, more SEM pictures of materials with special morphology are shown. The SBA-15-140-octyl silica illustrates, that the elongated structure of the basic

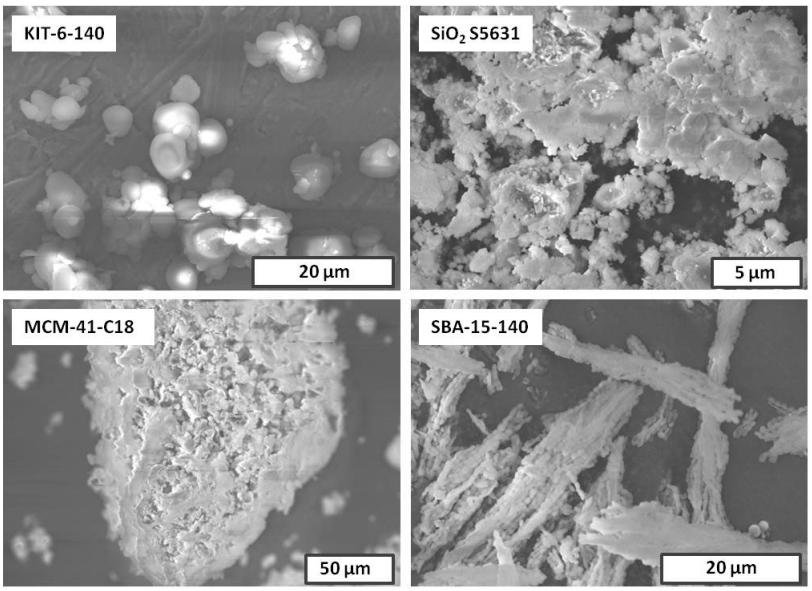

Figure 5.1: SEM pictures of non-modified silica materials illustrating evident differences in morphology. Scaling is not the same in the pictures, but in each case in the µm-range.

SBA-15-140 material is preserved with surface modification. Also, the fluffy surface of the aerogel Cab-O-Sil is shown and the rough surface of silica gel 60. The appearance of KIT-6-140 silica functionalized with imidazolium is interesting, as isolated particles with clearly defined planes are present. This differences in particles sizes and surface structures as well as agglomerate formation are significant for the stability of colloids as intermolecular forces are decisive. Therefore, the different morphology of silica materials will play a role in the following discussion of the results.

5.2 Conductivity measurements

The conductivities σ of silica materials were measured systematically dependent on temperature T and filler content ω, whereby the materials differ in their porosity, pore sizes, specific surface areas, surface functionalizations

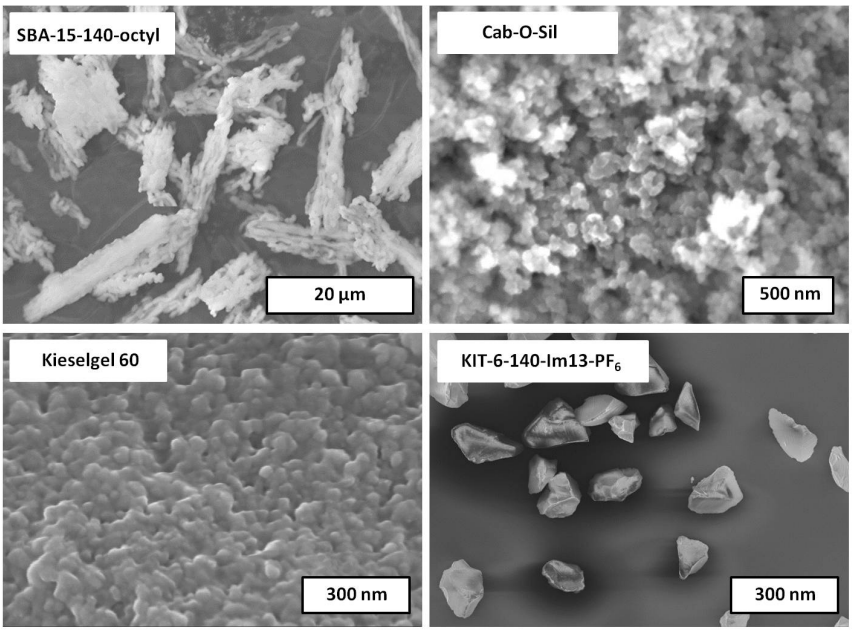

Figure 5.2: SEM pictures of various silica materials showing differences in morphology. Scaling is not the same in the pictures.

(see tab. 4.1) and morphologies. The results of the conductivity measurements are shown graphically in the following. As can be seen in fig. 5.3, the conductivity of electrolytes typically increases with increasing temperature. The measurements were stopped before the decomposition temperature was reached. The conducting salt $LiPF_6$ decomposes at $76\,^{\circ}\mathrm{C}$, hence the temperature dependent conductivity measurements were performed between $0\ ^{\circ}\mathrm{C}$ and $60\ ^{\circ}\mathrm{C}$. Variations in linearity, as can be seen for KIT-6-80 in the highest silica mass fraction of 7.0 wt% and temperatures higher than 300 K, result from segregation and starting decomposition phenomena. To avoid deviations because of sedimentation, dispersions were stirred throughout the measurements.

During the measurements, the decomposition of $LiPF_6$ followed by the degradation of silica material was observed. This was caused by higher temperatures on the one hand and by traces of water in the electrolyte and on the silica surface despite of intensive drying on the other hand. Basically,

PF_5 is formed by dissociation of $LiPF_6$, which reacts with water [167].

$$LiPF_6 \rightleftharpoons LiF + PF_5$$

$$PF_5 + H_2O \rightarrow POF_3 + 2HF$$

Thereby, HF is produced which reacts with SiO_2:

$$4HF + SiO_2 \rightleftharpoons 2H_2O + SiF_4 \uparrow$$

This reaction leads to decomposition of the silica material after decomposition of the conducting salt until filler and salt are consumed with water acting as catalyst. With starting of the decomposition reaction gas formation (bubbles) and an increase of the sample resistance was observed. However, the decomposition started mostly at higher temperature and long measuring times. Therefore, the surface of the silica materials were functionalized to avoid or decelerate decomposition, leading to an increased stability. The water amount of several dried silica materials was proven with TG-MS measurements and was low, but still the water deposits were sufficient for the activation of decomposition reactions.

The room temperature conductivities varied dependent on the age of the electrolyte between 6.5 mS/cm and 7.2 mS/cm. In fig. 5.3, it can be seen that the conductivity decreases with increasing silica mass fraction, which is most obvious at temperatures above room temperature. Below room temperature the conductivity varies for all silica mass fractions in a small range. Taking measurement uncertainties into account, no significant difference in conductivities is observed at low temperatures. Nearly similar scaling in the diagrams was chosen to have a better comparison between the dispersions.

In the following, the relative conductivities at room temperature of electrolyte dispersions with various silica materials depending on the added silica mass fraction are shown. Thereby, the relative conductivities are normalized to the conductivity of the pure electrolyte σ_0 because of the mentioned variations in the electrolyte conductivity depending on the electrolyte age. Furthermore, the change in conductivity compared to the pure electrolyte can be easily recognized.

Fig. 5.4 shows the decrease of the relative conductivity at room temper-

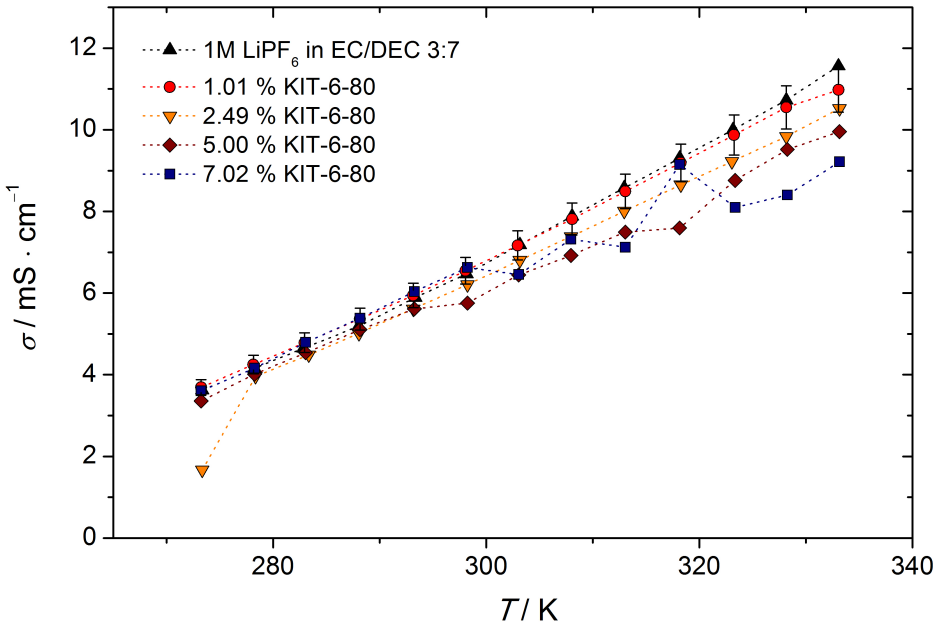

Figure 5.3: Temperature dependence of σ in the range of 273.3 K and 333.3 K (0 °C to 60 °C) exemplified for KIT-6-80 silica in various mass fractions. Abbreviations are shown exemplary for the dispersion with 1.0 wt% silica mass fraction. The dotted lines do not represent a functional relation between conductivity and temperature, they are just added as guide to the eye.

ature dependent on the content of KIT-6 material in dispersion compared to the pure electrolyte, whose σ/σ_0 value is 1.0. The gray line is the supposed conductivity decrease of the Maxwell calculation with the assumption of a volume exclusion due to isolating filler particles (cf. chapter 3.1.3.1). A linear decrease of conductivity with increasing silica mass fraction is expected according to the calculation of Maxwell. Most of the silica dispersions show a nearly linear conductivity dependence on the silica mass fraction. However, KIT-6 silica with different pore diameters show nonlinear behavior for their ionic conductivity, dependent on the mass fraction. For a silica mass fraction of 1 wt% a minimal conductivity enhancement (except for KIT-6-120) is observed. This conductivity increase amounts to 2.3 % for the KIT-6-140

silica. This increased conductivity for low silica mass fractions is not consistent for the whole measured temperature range and therefore not reliable. With increasing silica mass fraction the conductivity decreases almost linearly but much stronger than expected by Maxwell calculations. For mass fractions higher than 7 wt% the measurements showed stronger deviations from linearity. This might be due to adsorption or further blocking effects of the charge carriers. Additionally, it seems that in higher silica mass fractions other effects due to interactions of the silica particles with the electrolyte become relevant, like a higher degree of segregation on the one hand and faster decomposition promoted by higher water content of silica surfaces on the other hand.

The comparison between the KIT-6 materials shows that KIT-6-140 and KIT-6-120 have the smallest decrease of conductivity compared to the pure electrolyte conductivity. The higher number indicates higher synthesis temperature and therefore bigger pore diameters, whereas the pore diameters differ for all KIT-6 silica at within 4 nm (10.9 nm for KIT-6-140 and 7.0 nm for KIT-6-80). The specific surface area of KIT-6-80 is nearly 400 m^2g^{-1} higher than for KIT-6-140 (cf. tab. 4.1). Though, the conductivity differences among the dispersions are only marginal as the measuring deviance's are approximately 5 % at $25\,^{\circ}\mathrm{C}$. Therefore, pore sizes and surface modifications seem to have no strong influence on the properties of KIT-6 as filler material in liquid electrolytes. Basically, KIT-6 silica exhibit a three-dimensional bicontinuous cubic ($Ia\bar{3}d$) periodicity of the pore system instead of a hexagonal one as for SBA-15 and MCM-41 silica, which can be decisive for the ion movement.

The decrease of the electrolyte conductivity with addition of silica materials is stronger in the case of MCM-41 materials (cf. fig 5.5), whereas the initial drop with 1 wt% mass fraction is unclear. May be a process like adsorption takes place where ions are hindered to contribute to conductivity. However, after this drop the conductivity decreases only minimally but linearly for MCM-41-C16 (10 % drop) and MCM-41-C18 (6 % drop) with silica mass fractions until around 5 wt%. MCM-41-C12 shows a strong decrease of conductivity of 1.5 mS/cm from the beginning until a silica amount of 2.5 wt% is reached. In higher mass fractions around 7.5 wt% the same problem of deviations as with KIT-6 materials gets obvious due to faster decompositions and segregation phenomena. Indeed, the decomposition reaction of MCM-41 silica was faster compared to other materials. The overall conductivity is

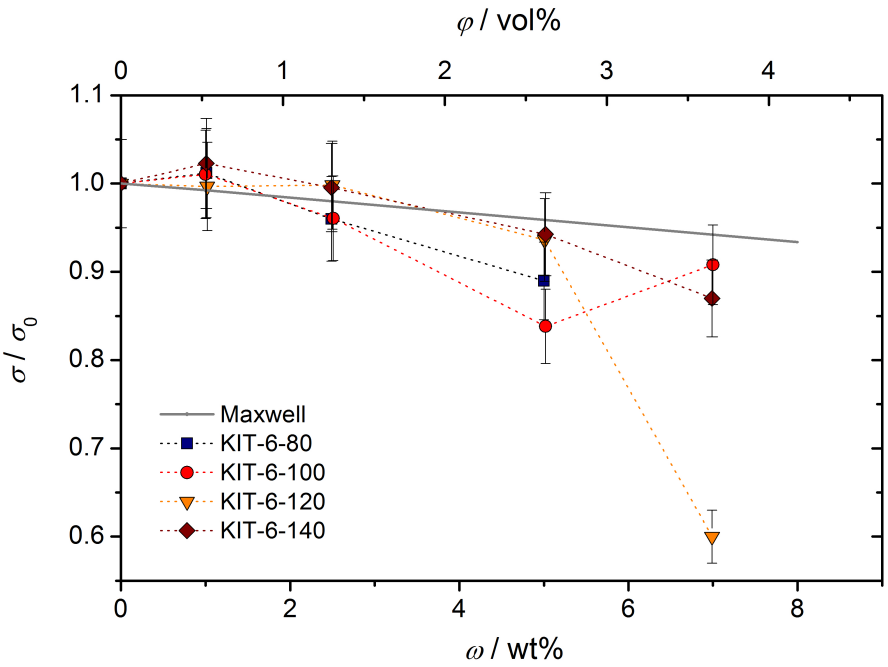

Figure 5.4: Relative conductivities σ/σ_0 (normalized to the conductivity of the pure electrolyte σ_0) of composite electrolytes with KIT-6 silica materials in 1 M $LiPF_6$ in EC/DEC 3:7 at room temperature dependent on the silica mass fraction ω. The dotted lines were added as a guide to the eye, and do not represent a functional relation between conductivity and silica content. The gray continuous line shows the calculated conductivity decrease after the Maxwell theory by the addition of an isolationg second phase to a conducting phase.

smaller than expected based on Maxwell calculations. MCM-41 silica have a more pronounced effect on the conductivity compared to KIT-6 silica, actually they cause the strongest decrease of conductivity in dispersion within all observed materials.

They are synthesized in a basic process different to all the other materials. Compared to the other materials they have extremely high surface areas, three times higher on average. The pore sizes around 3.5 nm are small. They form large particle agglomerates as can be seen compared to the other silica materials in fig. 5.1.

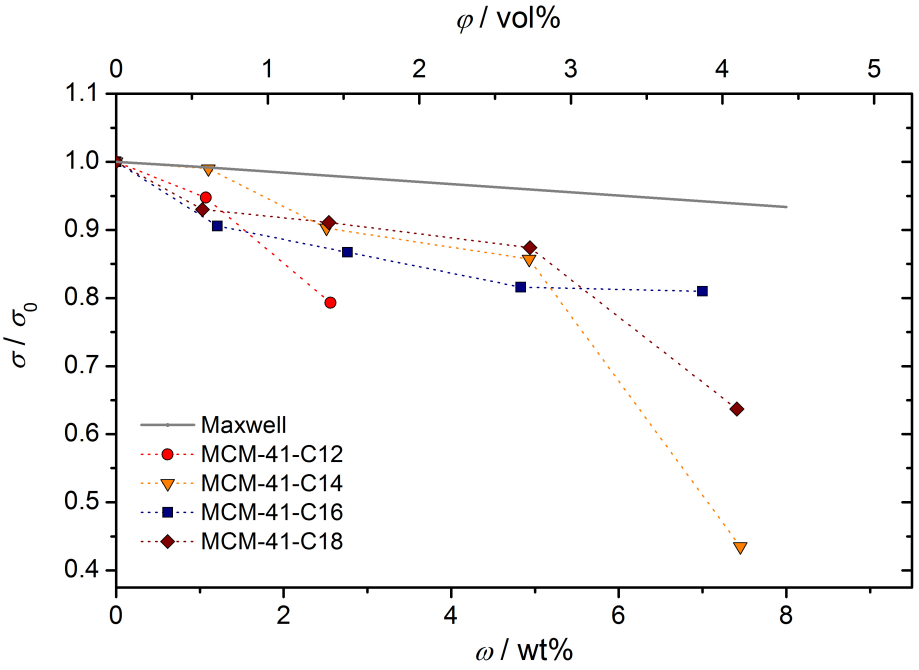

Figure 5.5: Relative conductivities σ/σ_0 of composite electrolytes with MCM-41 silica materials in 1 M $LiPF_6$ in EC/DEC 3:7 at room temperature dependent on the silica mass fraction ω.

Commercially available non-porous silica were investigated as comparison to the mesoporous silica materials (cf. fig. 5.6). SiO_2 nanopowder and SiO_2 S5631 show nearly the same decrease in conductivity, however, higher mass fractions of the SiO_2 nanopowder could not be dispersed since the decomposition reaction with the electrolyte occurred too fast. This shows that the different particle sizes (10 nm - 20 nm for SiO_2 nanopowder and 1 µm - 5 µm for SiO_2 S5631) have no influence on the conductivity behavior in dispersions of these commercial silica. The non-porous SiO_2 nanopowder and SiO_2 S5631 show only a small decrease of conductivity compared to the porous materials even with high silica mass fractions up to 10 wt% (in the case of SiO_2 S5631 a drop of 0.7 mS/cm or 9.5 % between 0 wt% and 10 wt%). The specific surface area of the silica materials seems to have no crucial effect on the conductivity as the SiO_2 nanopowder shows a significantly higher value (658 m^2g^{-1}) than SiO_2 S5631 (156 m^2g^{-1}, cf. tab. 4.1).

Thus, the bulk and the surface composition of the material seem to play the crucial role. The particle morphology of SiO_2 S5631 was observed with SEM. In fig. 5.1 it can be seen that the particles have frayed and no clear edges contrary to the KIT-6 silica particles for example. The particles are more fluffy. Besides, an advantage of the small particles (nanoparticles, nanopowder) is the better stability of the resulting dispersions. In this case, no stable dispersion was obtained with the used silica as they segregated rapidly. The time until segregation was individual for every silica material and differed between seconds and hours. Thus, all dispersions were stirred during the measurement.

Silica gel 60 and Cab-O-Sil are also commercially available silica materials but they are porous (in contrast to SiO_2 nanopowder and SiO_2 S5631). Silica gel 60 shows an unusual constant conductivity (variations around 1 %) with increasing silica mass fraction up to a silica content of 5 wt%; afterwards the conductivity decreases. Cab-O-Sil shows a conductivity decrease of 5 % already with 2.55 wt% of silica mass fraction. The specific pore volume of Cab-O-Sil is very high and the pore distribution is wide (1.532 cm^3g^{-1}; 46 nm). Furthermore Cab-O-Sil shows a special morphology as aerogels have a superlattice. Considering the measuring deviations, the commercial materials nearly show theoretical Maxwell behavior.

Within various nanoparticles the porous particles reduce the conductivity more severely than the commercially available nanopowder in the mass fraction of 2.5 %, as can be seen in fig. 5.7. The addition of 2.5 wt% of the porous nano-material leads to a conductivity decrease of 1.2 mS/cm or 20 %. Actually, they were difficult to disperse as a homogeneous dispersion was received only after 2 hours of treatment with a ultrasonic finger. The decomposition of the particles in the electrolyte started during the measurement and determination of conductivity with higher mass fractions was not possible due to fast decomposition. The surface of SiO_2-nano-Im13-PF_6 was specially modified with anion-catching imidazolium groups, but the stronger conductivity decrease compared to pure nanoparticles suggests negative influence of this surface group on the conductivity of the pure electrolyte. Possibly, the charge carriers are adsorbed. In contrast, the non-modified self-synthesized SiO_2 nanoparticles (SiO_2-nano) behave extraordinary as filler material as they do not affect the conductivity but maintain better mechanical electrolyte properties. Even with silica mass fractions of 7.5 % the conductivity of the dispersion is the same as for the pure electrolyte, which

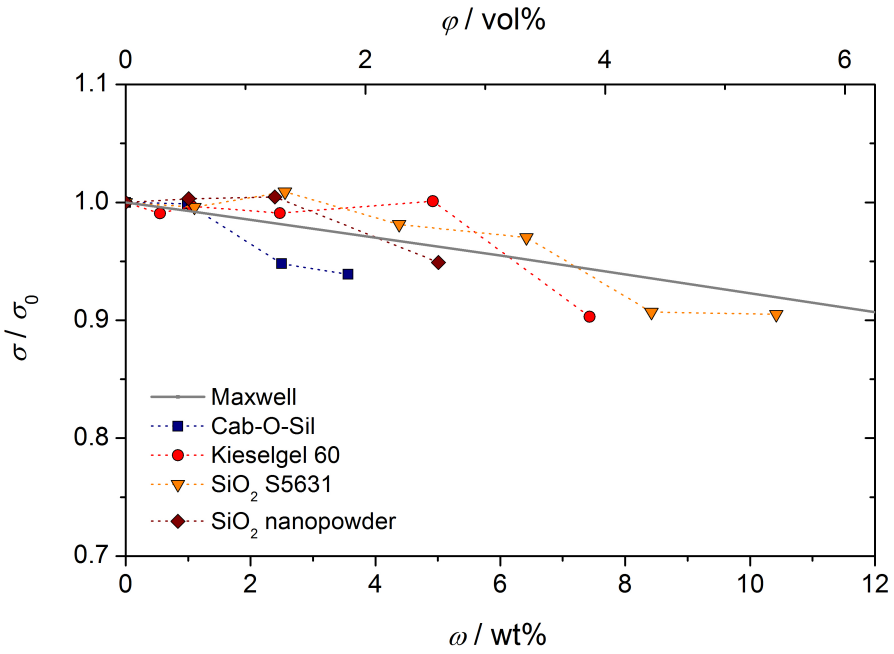

Figure 5.6: Nominal conductivity of commercial available silica materials dispersed in the electrolyte 1 M $LiPF_6$ in EC/DEC 3:7 dependent on the added amount of silica material at room temperature.

means a positive deviation from the considered decrease after Maxwell.

In order to examine the influence of standard organic surface groups on the conductivity behavior of electrolyte dispersions, the surface of KIT-6-140 was modified with various simple organic groups (methyl, hexyl, octyl, aminopropyl and sulfonyl groups). The assumption was to create surfaces that are able to catch the anion of the conducting salt to achieve a higher amount of free lithium ions in the space-charge region as charge carriers on the one hand and to reach higher stability of the silica material due to a reduced amount of OH-groups on the surface on the other hand. These materials with surface modifications show only small decreases of conductivity in dispersion compared to the pure electrolyte (see fig. 5.8). Like the pure KIT-6 materials, the KIT-6-aminopropyl and KIT-6-octyl show minimal conductivity enhancement in dispersion of 2-3 % with small amounts (1 w%) of silica. The other functionalized materials show the expected decrease by

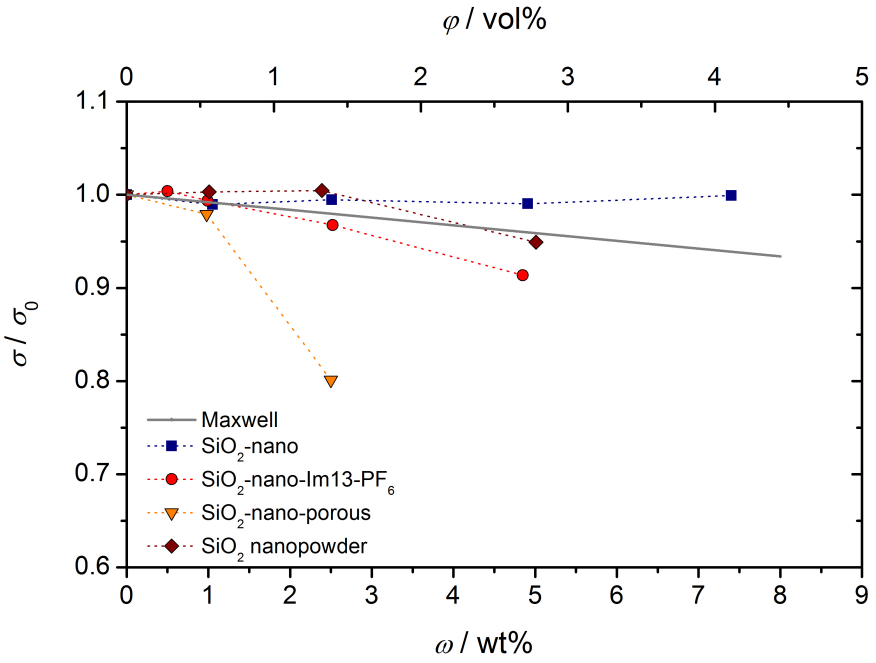

Figure 5.7: Relative room temperature conductivity of porous, non-porous and surface-modified silica nanoparticles. The conductivity is shown dependent on the added amount of silica. The continuous line represents the conductivity decrease calculated with assumptions of Maxwell.

calculation with the Maxwell equation. In the following, the modified KIT-6 materials show approximately the same values in conductivity with respect to the measurement errors as the differences in conductivity are at most 0.5 mS/cm with a silica mass fraction of 7.5 wt%. No surface group could be identified with obvious advantages in influencing the conductivity of a lithium electrolyte.

Comparable measurements were done in the diploma thesis of Kerstin Sann with SBA-15 materials (cf. [168]). There, the surface modification with aminopropyl and octyl groups enhances the decrease of conductivity compared to the non-modified materials but these fillers are more stable in the organic electrolyte than the pure SBA-15 materials (see fig. 7.1 in the appendix).

The surface groups were chosen as easiest attempt to reduce the den-

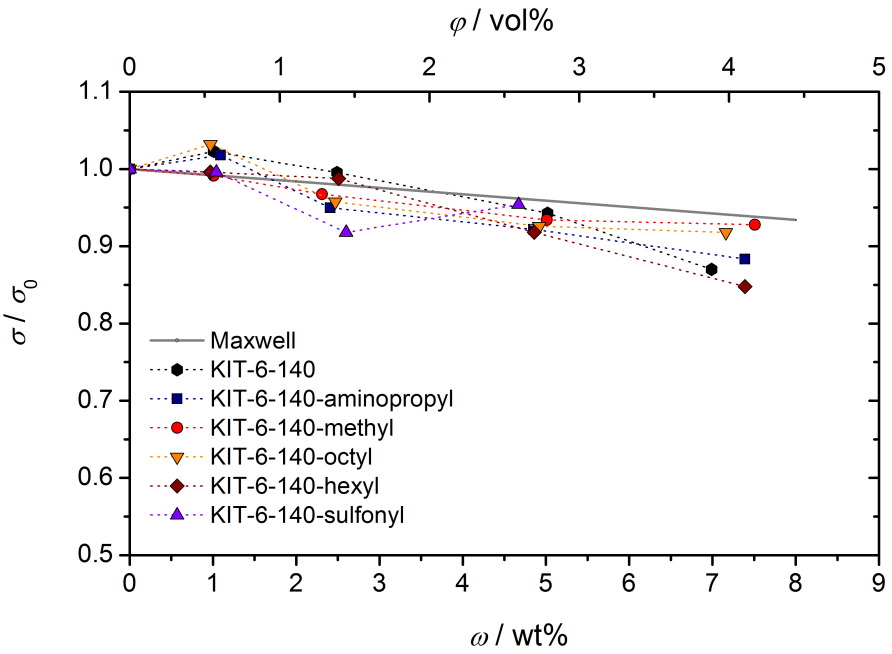

Figure 5.8: Room temperature conductivity relative to the conductivity of the pure electrolyte dependent on the added silica mass fraction ω of dispersions with alkyl and sulfonyl functionalized KIT-6 silica in 1 M $LiPF_6$ in EC/DEC 3:7. The solid line is the theoretical decrease of conductivity in dispersions calculated with the equation of Maxwell.

sity of silanol groups at the surface and therefore reach a higher stability. IR spectra of organically functionalized silica showed that the SBA-15-aminopropyl exhibits the lowest density of free silanol groups (Si-OH) at the surface, whereas SBA-15-octyl showed the highest. An explicit correlation between density of silanol groups and chemical stability against $LiPF_6$ containing electrolyte was found. SBA-15-aminopropyl with the lowest degree of silanol groups showed the highest stability and did not decompose during the measurement (approx. 4 hours).

Furthermore, the imidazolium group was tested as anion catching surface group on KIT-6 silica material. The imidazolium group needed to be chemically saturated to be stable. Therefore, the anion PF_6^-, also present in the conducting salt, was used. Cl^- was also tested as counter ion, but was then

rejected because of negative impact in an assembled lithium ion battery. As can be seen in fig. 5.9, the imidazolium modified materials have worse influence on the electrolyte than the pure KIT-6-140 material, especially in mass fractions until 2.5 wt%. A similar conductivity decrease with a mass fraction of 2.5 wt% and the following increase at a mass fraction of 5 wt% of KIT-6-140-Im13-PF_6 and KIT-6-140-Im13-Cl is noticeable. The conductivity trends of these materials vary around the Maxwell calculation up to a mass fraction of accordingly 5 wt%. There, effects like agglomeration and decomposition are more significant, whereas the pores of the KIT-6 materials are not taken into account for the calculation. Afterwards, the KIT-6-140-Im13-PF_6 was additionally treated with hexamethyldisilazan (HDMS) to saturate remaining silanol groups. Although this treatment was not convincing, a slight difference is obvious in the conductivity of the disperse electrolyte, as it does not show the conductivity decrease at the silica mass fraction of 2.5 wt%. Additionally, the material was easier to disperse.

Moreover, the KIT-6 silica materials were surface modified with polyethylene glycol (PEO) groups, in order to reach a network through cross-linked particles and therefore to avoid sedimentation. Hence, PEO1000 units were chosen. As can be seen in fig. 5.10 the conductivity of dispersions with this silica material is very similar to the pure KIT-6 materials. Small variations become obvious for higher silica mass fractions of 5 wt%. There, the PEO functionalized KIT-6-80 material does not exhibit the same conductivity decrease as seen for the pure KIT-6-80. All in all, the conductivity decrease is only slightly below the calculated decrease due to volume exclusion assumptions. The dispersions with PEO groups were not really higher in viscosity but harder to disperse and moreover, in dispersion the PEO-functionalized silica also showed sedimentation.

Finally, as comparison to the isolating silica particles, lithium ion conducting garnet particles of the type $Li_{7-x}La_3Zr_{2-x}Ta_xO_{12}$ (LLZTO; varying amount of Ta 0.375 < x < 1.5) were dispersed in the electrolyte. The particles sedimented quickly in a milky dispersion and the particles could hardly be distributed homogeneously. In fig. 5.11 the conductivity of the garnet dispersion is shown dependent on the filler mass fraction. It can be seen that the ion conducting particles also lead to a decreased conductivity, which is very similar to the decrease calculated with the Maxwell assumptions.

The fast decomposition of some of the silica particles in the electrolyte 1 M $LiPF_6$ in EC/DEC 3:7 motivated the use of a different electrolyte with

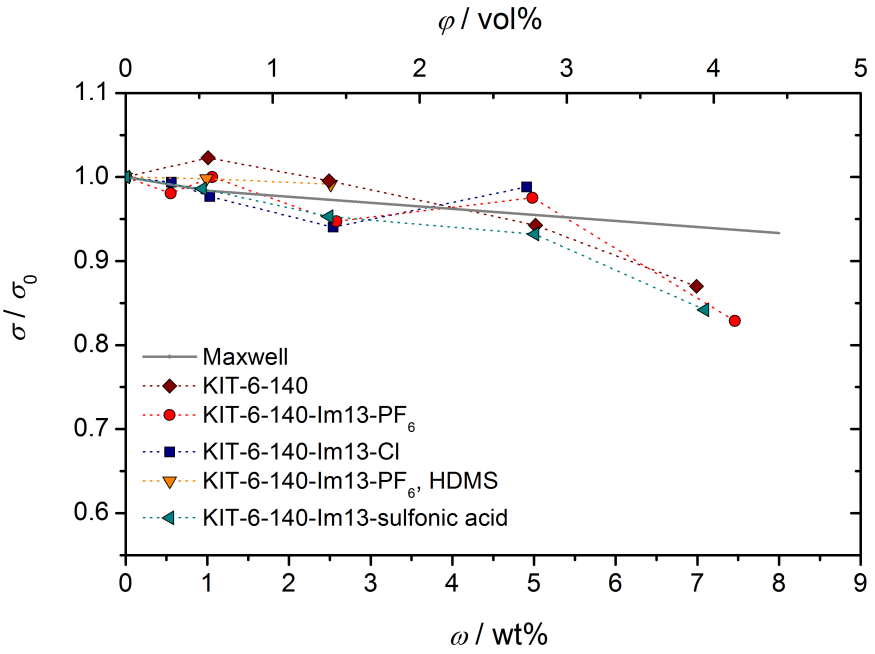

Figure 5.9: Nominal conductivity at room temperature dispersions with imidazolium functionalized KIT-6 silica dependent on the amount of silica material.

another conducting salt. The electrolyte SelectiLyte LF30 sold by Merck for a short time contained lithiumtris(pentaflouroethyl)trifluorophosphat (LiFAP) as conducting salt, which has higher moisture stability and releases less HF than $LiPF_6$ in solution. Therefore, this electrolyte was supposed to be an alternative, particularly since the conductivity of this electrolyte was in the same range as the used one, even slightly higher which can be seen in fig. 5.12. As the salt LiFAP is stable only in solution, a 1 M LiFAP solution in EC/DMC 1:1 (LF30) was chosen. Surprisingly, the conductivity of the electrolyte LF30 was nearly unaffected by the addition of silica material KIT-6-80. Up to 5 wt% silica mass fraction the conductivity was constant after a small initial decrease, although there was an obvious strong increase in viscosity. Hence, the LF30 electrolyte shows good performance in dispersions and further investigations would be interesting. However, the electrolyte was expensive.

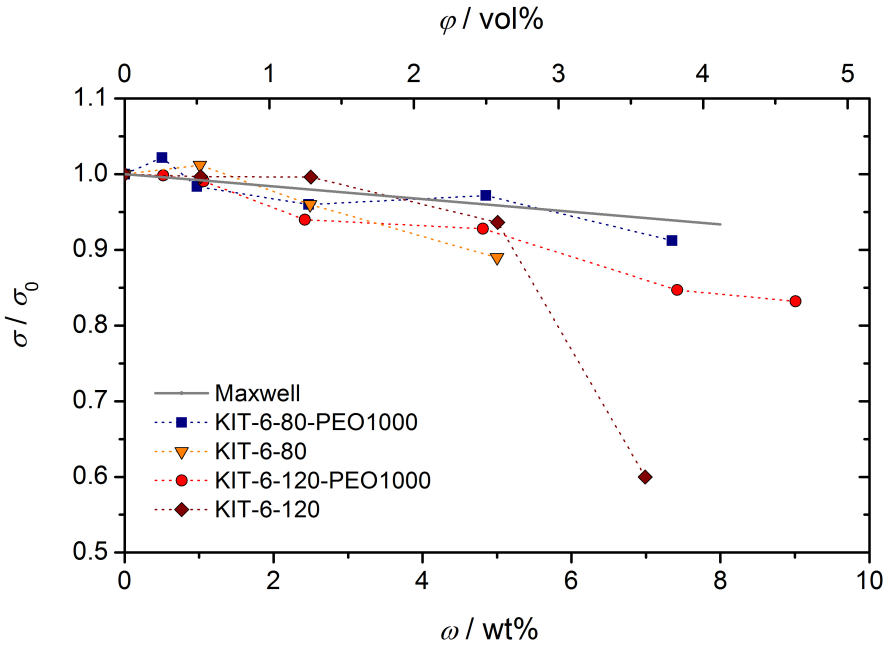

Figure 5.10: Relative room temperature conductivities of dispersions with PEO1000 functionalized KIT-6 silica as a function of silica mass fraction ω.

5.2.1 Correlation of conductivity with surface area and pore width

To clarify the possible influence of specific surface area and pore width of the silica materials on the conductivity in dispersion, selected correlations are shown. The correlation of the relative conductivity of all observed silica materials in the mass fraction of 2.5 wt% at $25\,^{\circ}\mathrm{C}$ with the specific surface area of the silica materials is shown in fig 5.13. There is no direct correlation between conductivity and specific surface area of filler materials as the conductivity shows large jumps with increasing specific surface area. General considerations originating from an adsorption mechanism of ions on the oxide surface had led to the assumption, that the adsorption of ions is more significant with larger specific surfaces. As the silica surfaces were modified with special surface chemistry it became obvious, that the influence of these surface gruops is stronger than the size of the surface area. There can be

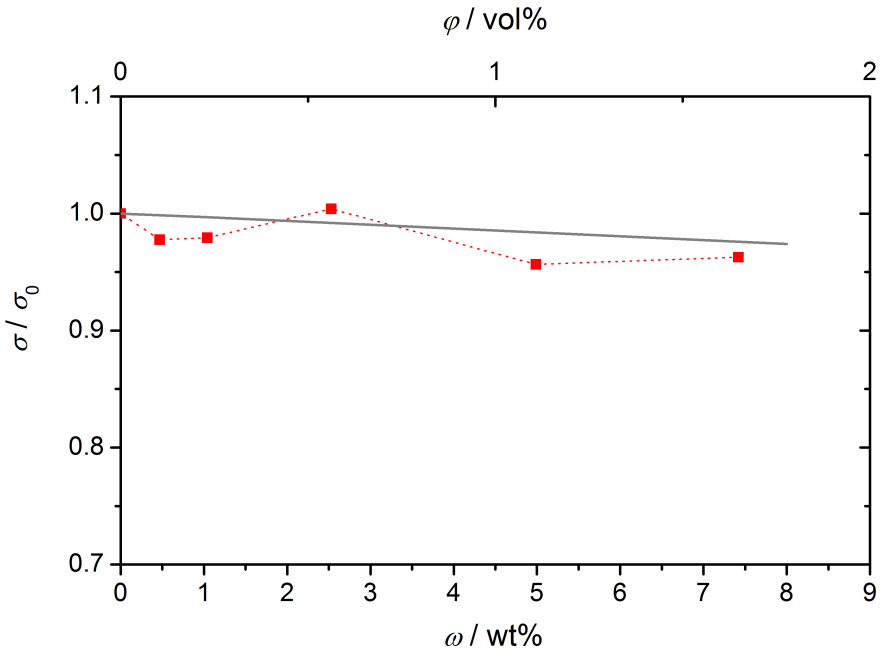

Figure 5.11: Relative conductivity of a dispersion with LLTZO as filler material in EC/DEC 3:7 with 1 mol· L^{-1} $LiPF_6$ dependent on the mass fraction ω of the filler at 25 °C.

favorable as well as unfavorable surface groups for the movement of ions. Not only the size of specific silica surface areas differs but also the morphology and size of particles as well as pore widths for the porous materials. An overall correlation of the pore widths (no graphic shown) of the porous materials and the conductivity shows the same inconsistent behavior like the surface areas, whereas the differences in pore widths are not as big with a maximum of $\sim$ 8.5 nm as the differences in specific surface areas. Due to the morphology and surface chemistry differences more detailed information can be obtained by correlation within individual groups of silica materials which do not differ in morphology.

Hence, observing the correlation between surface and conductivity within the diverse silica groups, a correlation can partially be seen. For the MCM-41 silica materials without any surface modification but with the highest specific surface areas within all materials and the lowest conductivity in dispersion,

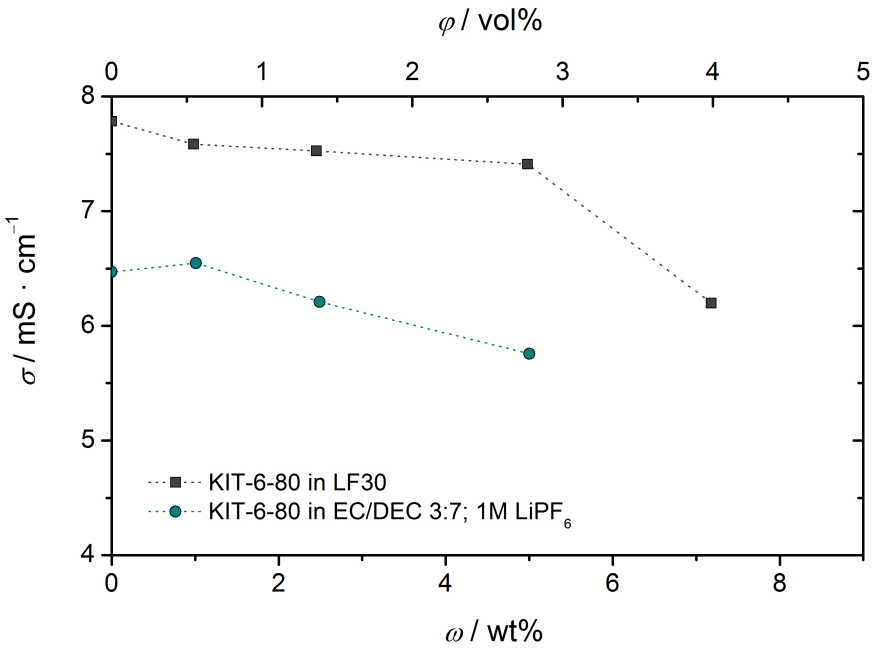

Figure 5.12: Comparison between the dispersion conductivities of KIT-6-80 in the electrolytes 1 M LiFAP in EC/DMC 1:1 and 1 M $LiPF_6$ in EC/DEC 3:7.

a connection between surface area and conductivity can be assumed. In fig. 5.14 the conductivity increases with increasing specific surface area. The increase of conductivity is even nearly in the same range as the increase in specific surface area, except for the MCM-41-C18. Here, the increase of conductivity is clearly higher. This phenomenon might be due to the different pore width of the materials. In fig. 5.15 it is graphically shown that the MCM-41-C14 material shows a noticeable behavior, as it has smaller pores ($\sim$ 1 nm smaller) but higher surface area than MCM-41-C18 but nearly the same conductivity. This leads to the assumption, that a combination of pore width and surface area may play a role for the conductivity behavior of MCM-41 materials as filler material in the used non-aqueous electrolyte. This means a favorable combination of pore width and surface area for a special silica has to be found allowing good ion migration in disperse electrolytes.

Differences between the silica material groups like KIT-6, SBA-15 and

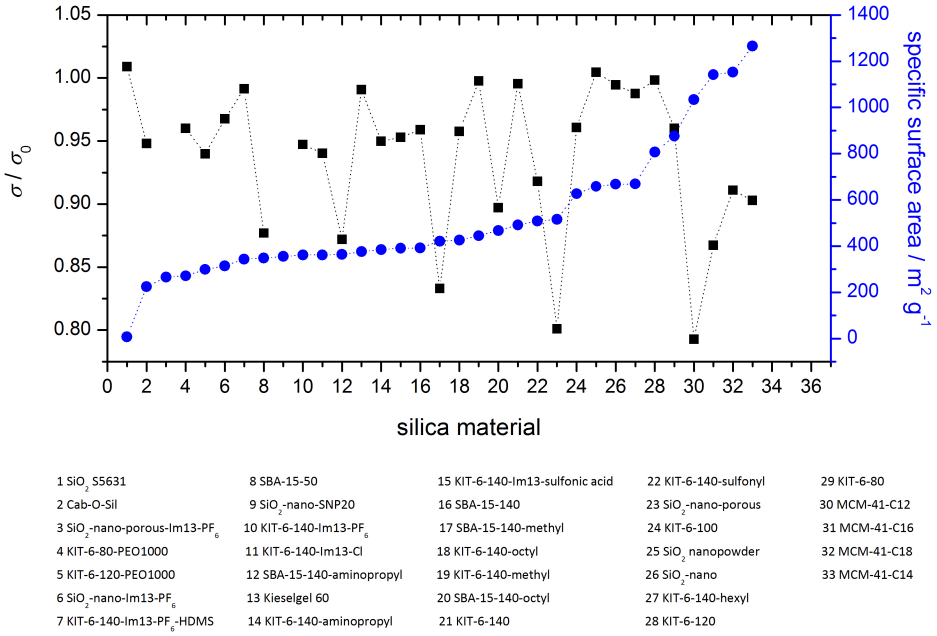

Figure 5.13: Correlation of the specific surface area (blue dots) of all used silica materials with the relative conductivity (black squares) at 25 °C of the composite electrolyte with 2.5 wt% silica mass fraction.

MCM-41 can be found in the morphology, the particle size, the pore geometry and especially the surface chemistry. The pore width and specific surface area of filler materials does not seem to be the main criterion for the conductivity in dispersion, as in most silica material groups there is no clear correlation.

The influence of surface groups can be seen, when conductivities and pore widths within KIT-6 material with and without modification of the surface (see fig. 5.16) are correlated. For the silica materials 1-4 with non-modified surfaces it seems as if bigger pore widths are better for a conductivity enhancement, whereas it has to be mentioned that the difference in conductivity is small with maximum 4 %. For the KIT-6 materials with functionalized surfaces and nearly the same pore diameter, stronger disparities are obvious. Thereby, the surface groups are supposed to have the main influence. The sulfonyl-group, for example, has negative influence on the conductivity

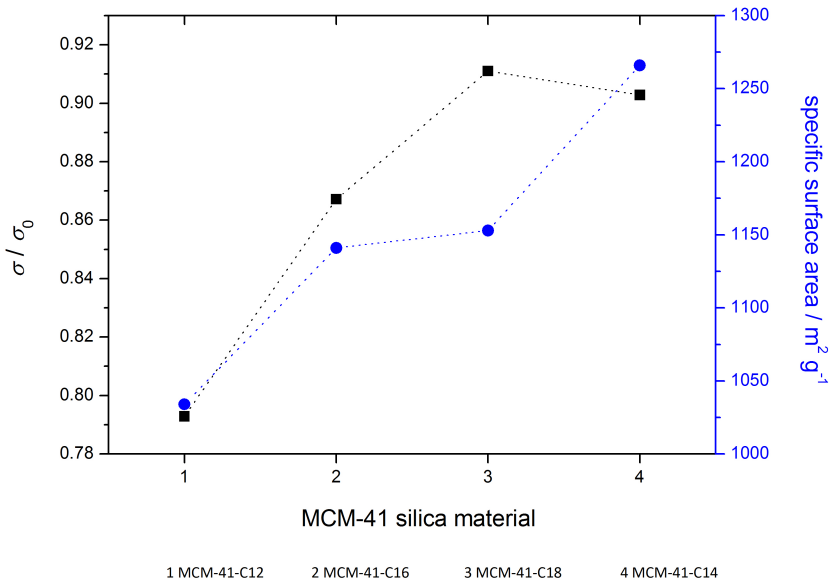

Figure 5.14: Relative conductivity (black squares) at 25 °C of MCM-41 electrolyte dispersions with the filler amount of 2.5 wt% correlated with the specific surface areas (blue dots) of the MCM-41 materials.

in the electrolyte and the methyl-group has positive influence on the conductivity of the electrolyte as it is nearly not decreased by the filler material.

For the commercially available silica materials an interesting correlation between the specific surface area and the relative conductivity in a 2.5 wt% dispersion is found (cf. fig. 5.17). The materials Cab-O-Sil, silica gel 60 and SiO_2 nanopowder show a good connection between increasing silica specific surface area and increasing relative conductivity. The SiO_2 S5631 shows exceptional behavior with a very small specific surface area and high conductivity. In order to assess this, other influencing parameters like zeta potential or network structures have to be taken into account.

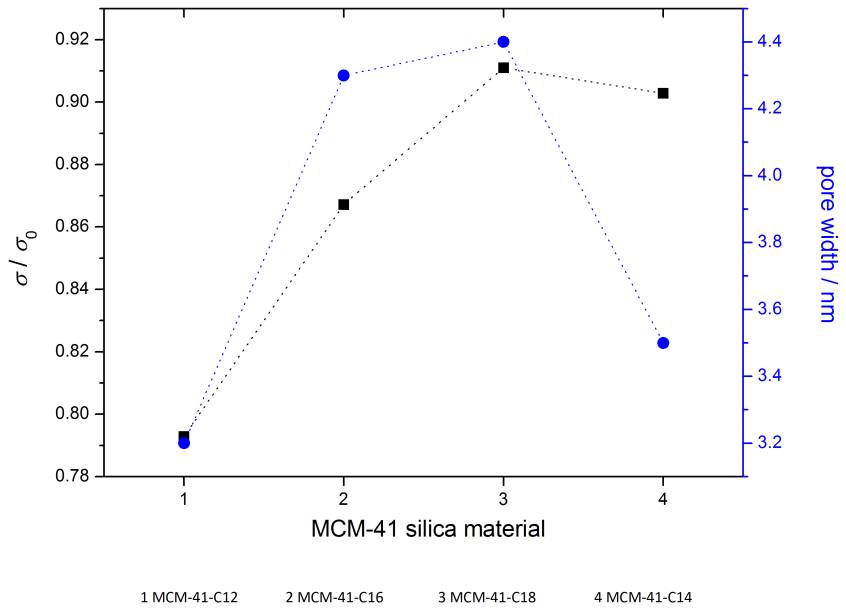

Figure 5.15: Relative conductivity (black squares) at 25 °C of MCM-41 electrolyte dispersions with the filler amount of 2.5 wt% correlated with the pore size (blue dots) of the MCM-41 materials.

5.2.2 Calculation of the activation energy

The activation energy E_A, needed for the migration of ions through a solution has been determined. Variations in activation energies indicate that different conduction mechanisms may be present. The temperature-dependent conductivity of solutions can be described with an Arrhenius-type equation (cf. section 3.1.1). All investigated dispersions, however, do not show a simple Arrhenius behavior, i. e. the ln σ vs. T^{-1} graph deviates significantly from linearity (cf. 5.18).

Accordingly, it is known in the literature [169, 170], that the simple Arrhenius equation often describes the temperature-dependent conductivity for liquid and polymer electrolytes above the glass transition temperature inadequately, therefore the empirical equation of Vogel-Fulcher-Tammann (VFT) is applied (eq. 3.6). This equation was introduced to describe the viscos-

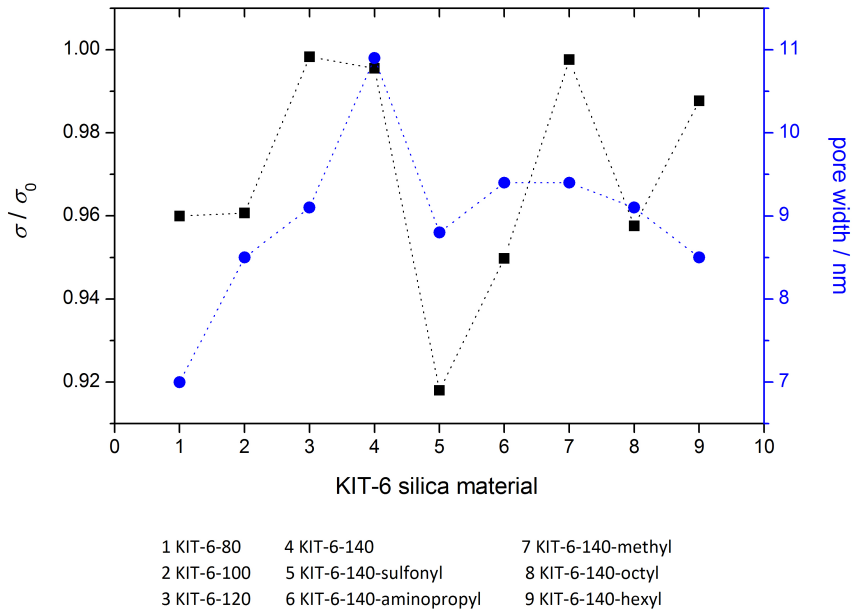

Figure 5.16: Relative conductivity (black squares) at 25 °C of KIT-6 electrolyte dispersions with the filler amount of 2.5 wt% correlated with the pore size (blue dots) of the KIT-6 materials with and without surface modification.

ity of glasses and polymers dependent on temperature, but is also used to describe the temperature dependence of the conductivity. The additional value in the VFT equation compared to the Arrhenius equation is the glass temperature T_g, at which the mechanical and thermodynamic properties of polymers and glasses change substantially. This equation was found to fit well for the measured silica dispersions as a formation of networks like in polymers is assumed.

Instead of an experimental determination, the glass temperature was obtained by a non-linear fit of ln σ vs. 1/T values (using the software OriginPro8). A resulting VFT diagram is shown for the SiO_2 S5631 material as an example in fig. 5.19. Here, the temperature dependence of the prefactor is considered as $T^{-1/2}$. As can be seen, a linear dependency results including the glass temperature T_g. The corresponding glass temperatures

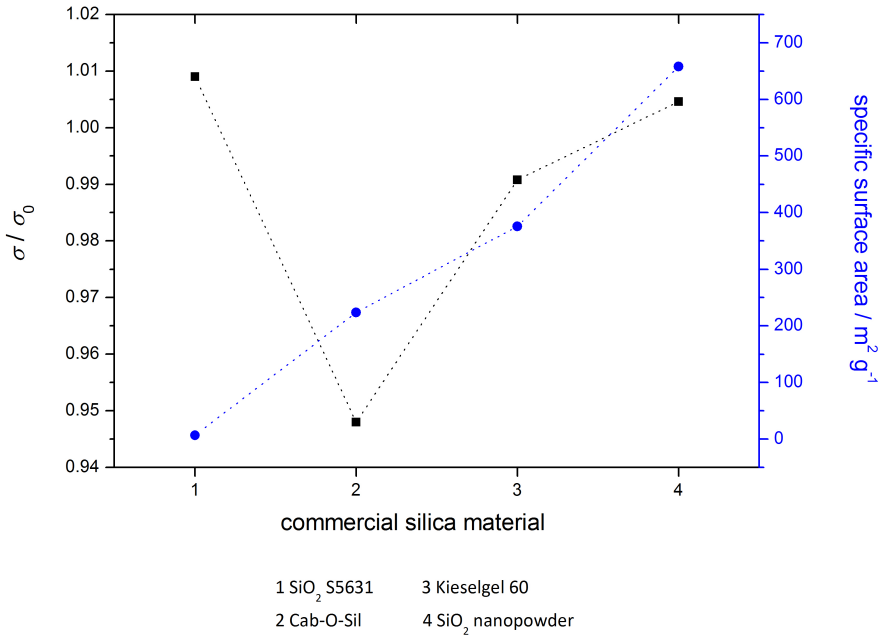

Figure 5.17: Relative conductivity (black squares) at 25 °C of commercial available silica materials in electrolyte dispersions with the filler amount of 2.5 wt% correlated with the specific surface area (blue dots) of the materials.

are mostly between 150 K and 200 K. Actually, the physical meaning of the glass temperature for the observed dispersions remained unclear. Maybe, a transition in the used silica material occurs, but no network or gelation could be observed due to segregation of the particles.

The activation energies were estimated, to see whether the conductivity in the dispersions shows different T dependance. Therefore, the activation energies of the dispersions are compared to the activation energy of the pure electrolyte, whereby the yellow array marks the activation energy of the pure electrolyte in fig. 5.20 and fig. 5.21 with correlated errors. It is noted, that the absolute values of activation energies are not indicative as the calculation with three unknown variables is rather vague, whereas the differences are crucial. No comparison with literature values of activation energies is possible, as no values for activation energies of the movement of Li^+ ions in organic electrolytes could be found in the literature. There is

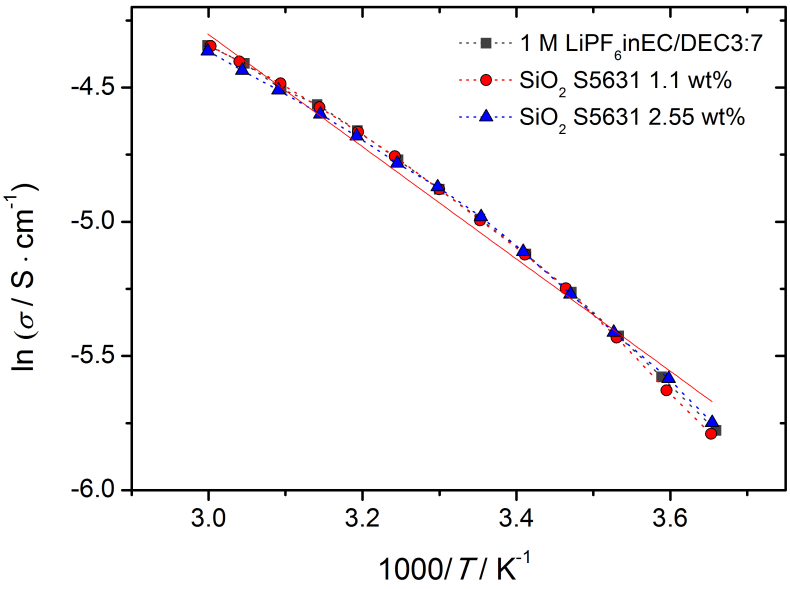

Figure 5.18: Exemplary presentation of the Arrhenius diagram with silica material S5631 for different mass fractions in 1 M $LiPF_6$ in EC/DEC 3:7 compared to the pure electrolyte. A deviance from linearity (red line) is obvious. The dotted line is just an guide to the eye and no correlation between conductivity and temperature.

a review on conduction phenomena in Li^+ ion batteries by Park et al. [170], but only conductivity values are discussed.

As can be seen in fig. 5.20, the activation energies of several dispersions are located in the range of the actication energy of the pure electrolyte 1 M $LiPF_6$ in EC/DEC 3:7, when the calculation uncertainties are taken into account. Especially the commercial materials S5631, Cab-O-Sil and silica gel 60 as well as the the silica nanoparticles almost do not affect the activation energy of the electrolyte. The activation energies are even little less than that of the pure electrolyte. A decreased activation energy indicates easier ionic motion, but it should be noticed, that this difference is small. So it can be deduced, that these particles do not or only slightly influence the ionic motion of ions in the composite electrolytes. This find-

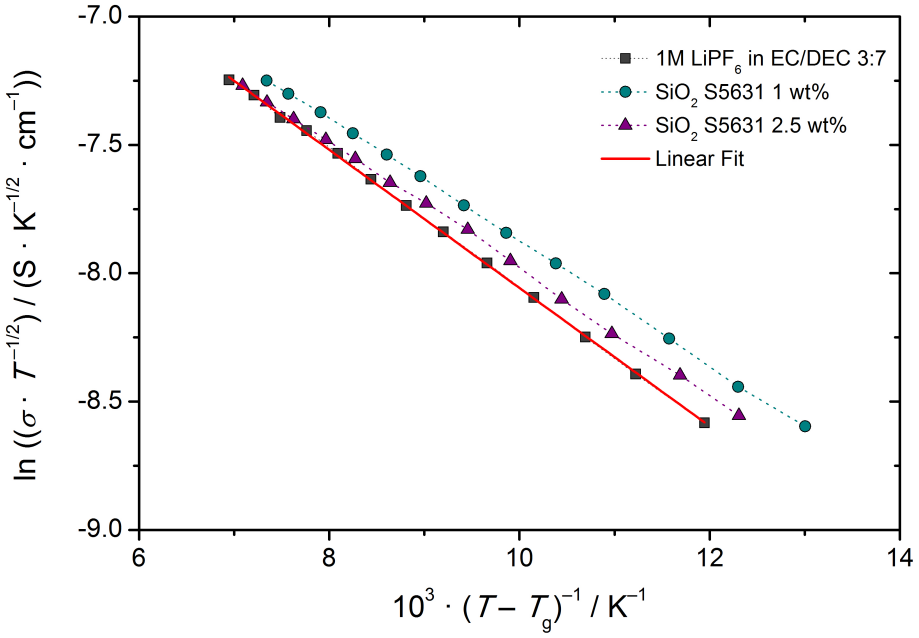

Figure 5.19: Exemplary presentation of the calculation with the Vogel-Fulcher-Tamman equation (VFT). The SiO_2 S5631 material is shown as reference besides the pure electrolyte. Temperature dependence of the prefactor is considered and the glass temperature, received from a non-linear adjustment, is taken into account. Accordingly, this results in a linear dependence.

ing supports the conductivity measurements shown in fig. 5.6 and fig. 5.7. Except of the Cab-O-Sil the other commercial materials have nearly stable conductivities, especially in higher mass fractions and do not decrease the conductivity as much as expected by Maxwell calculations. Within the results for the nanoparticles, the SiO_2-nano particles have an outstanding position in conductivity measurements, as the conductivity of the pure electrolyte is not affected with an amount of 7 wt% of particles. Moreover, the nanoporous SiO_2-particles had very bad impact on the conductivity and could not be measured in higher mass fractions due to strong decrease of conductivity. This is not in accordance with the calculated activation energies, as they show almost no difference.

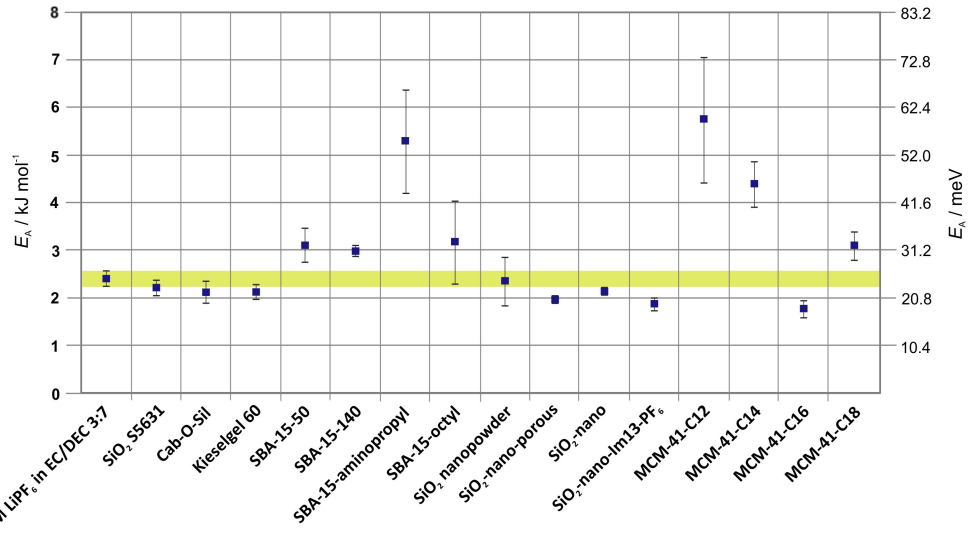

Figure 5.20: Activation energies of various silica dispersions with 1 mol·L^{-1} $LiPF_6$ in EC/DEC 3:7 received from a non-linear adjustment of the Arrhenius plot with the VFT equation. Dispersions with 2.5 wt% mass fraction of silica are compared. Actually, the absolute values are not crucial, but rather the differences. Special attention must be paid to the yellow array marking the activation energy of the pure electrolyte with numerical uncertainties involved. Hence, all dispersions are analyzed with this as benchmark.

Some materials show large uncertainties in activation energy anyhow, resulting from the calculation and measuring inaccuracies. The segregation of the particles influenced the conductivity measurements the most and thus the calculated activation energies. Basically, major differences compared to the pure electrolyte can be seen for SBA-15-aminopropyl and the two MCM-41-materials C12 and C14. These materials exhibit far greater activation energies by approximately 30 meV, indicating hindrance of the ionic conduction. Accordingly, the MCM-41-C12 material shows a strong fall-off in conductivity (cf. fig. 5.5) and could not be measured in higher silica mass fractions. The SBA-15-aminopropyl also shows a stronger decrease of conductivity in dispersion than other functionalized materials, which was shown

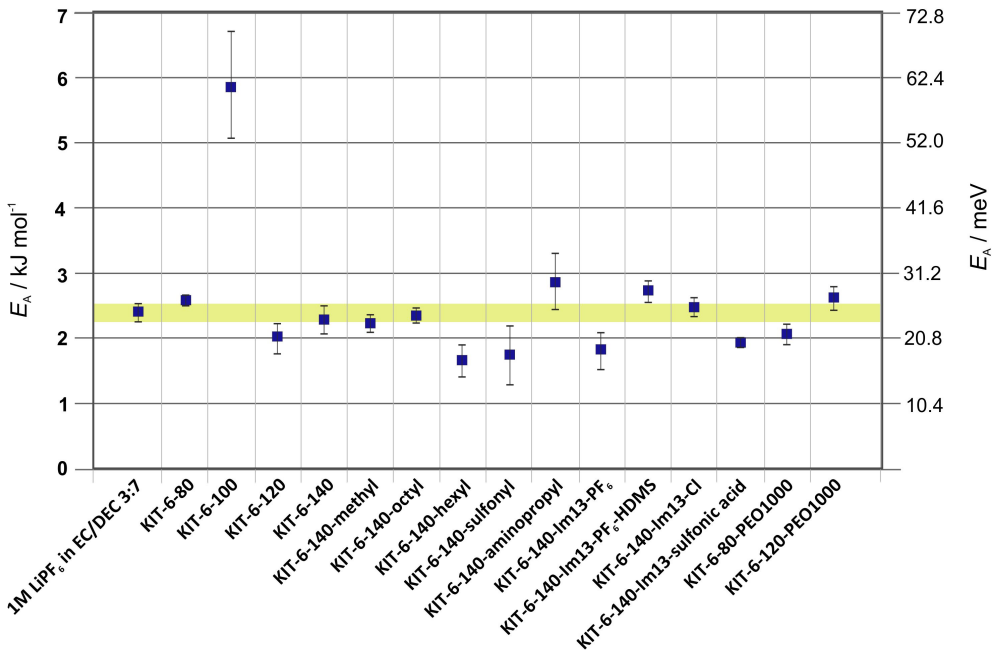

Figure 5.21: Activation energies of KIT-6 silica dispersions with 1 mol·L^{-1} $LiPF_6$ in EC/DEC 3:7 received from a non-linear adjustment of the Arrhenius plot. Dispersions with 2.5 wt% mass fraction of silica are compared. Actually, the absolute values are not crucial, but rather the differences. Special attention must be paid to the yellow array marking the activation energy of the pure electrolyte with calculated errors involved. Hence, all dispersions are analyzed with this as benchmark.

in prior works ([12, 168]). However, the MCM-41-C16 material does not show an obvious difference in the conductivity measurement compared to the other MCM-41 materials, although it has a lower calculated activation energy. All in all, the MCM-41 materials in dispersion reduce the conductivity of the pure electrolyte stronger (minimum 10 % with 2.5 wt% silica) than other investigated silica materials, which is in line with the calculated activation energies, except of the MCM-C16 material.

Within the KIT-6 materials shown in fig. 5.21, only one strong deviation is obvious. The KIT-6-100 material has more than double the activation en-

ergy of the pure electrolyte. This strong deviation does not fit to the measured conductivities shown in fig. 5.4. Hence, this seems to be an error in the measurement. The KIT-6 materials nearly have the activation energy of the pure electrolyte. The materials KIT-6-hexyl, KIT-6-sulfonyl and KIT-6-140-Im13-PF_6 exhibit minimally smaller activation energies, referring to a favored conduction mechanism. In the conductivity diagrams this favored process would not become obvious, as the modified KIT-6-silica have only small variations in conductivity. The KIT-6-140-Im13-Cl has approximately the same influence on conductivity as the KIT-6-140-Im13-PF_6. So again, these differences in activation energy do not fit to the measured conductivities or it does not get obvious. Maybe this is due to the small differences in activation energy, when the measuring errors are taken into account. In conclusion these calculations show, that the surface modification of KIT-6-silica seem to have no influence on the activation energies of these materials in dispersion.

The connection of the discussed deviations with the fitting process becomes more obvious, when a constant glass temperature T_g for the silica materials is considered. As T_g should not vary much between the silica materials, the average glass temperature was determined, so that the calculation with only two variables was possible. With the average T_g of 178 K the activation energies for all dispersions were calculated again as can be seen in fig. 5.22 and fig. 5.22. The activations energies of the dispersions have then only small differences as expected. The scattering is much smaller with two variables. In the calculation with three variables the influence of the curvature of the data was too pronounced. This shows, that the deviations may be fitting artifacts as the glass temperature and the activation energy are opposing in value. The overall conclusion, that silica materials have less influence and only small differences on the activation energy for the movement of ions in a liquid lithium electrolyte is hereby confirmed. One additional observation is, that all of the functionalized KIT-6 silica materials seem to have minimal higher activation energies.

5.3 Zeta potential measurements

Zeta potentials were determined in this work to get a picture of adsorption phenomena at the surface and influences of surface charge on the stability of

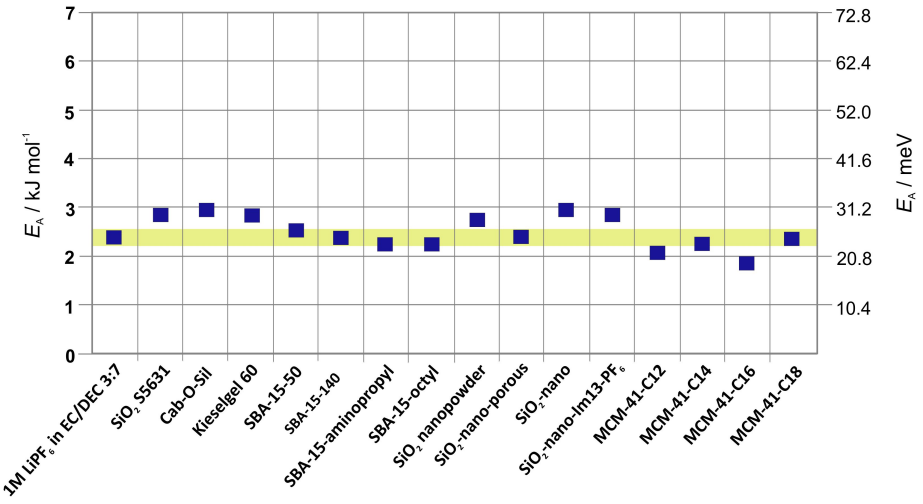

Figure 5.22: Activation energies of various silica dispersions with silica mass fractions of 2.5 wt% and 1 mol·L^{-1} $LiPF_6$ in EC/DEC 3:7 received from a non-linear adjustment of the Arrhenius plot with the VFT equation are shown. The calculation was done with two variables as a constant T_g of 178 K was assumed. The yellow array marks the activation energy of the pure electrolyte as benchmark. Calculation deviations do not exceed the dimensions of the data points.

the dispersions. This is possible because the zeta potential in particular systems is dependent on the surface chemistry and also on the interaction with the surrounding environment as the zeta potential is related to the charge density arising from the surface of particles or species attached to it. Hence, the electrical potential depends on the ionic composition of the medium.

As the absolute value did not seem to be the decisive value, zeta potentials of the silica materials were additionally measured in the solution of EC/DEC with the ratio 3:7 (without the conducting salt) besides the dispersions in the electrolyte 0.002 M $LiPF_6$ in EC/DEC 3:7. In solvents with moderate permittivity ε_r ($\varepsilon_r > 0$) a certain degree of ionization is possible whereas in non-polar media with low permittivity no full ionization is possible. In such media, particles can acquire charge and electrostatic force due to acid-base interactions between particle surface and dispersing agent. The permittivity

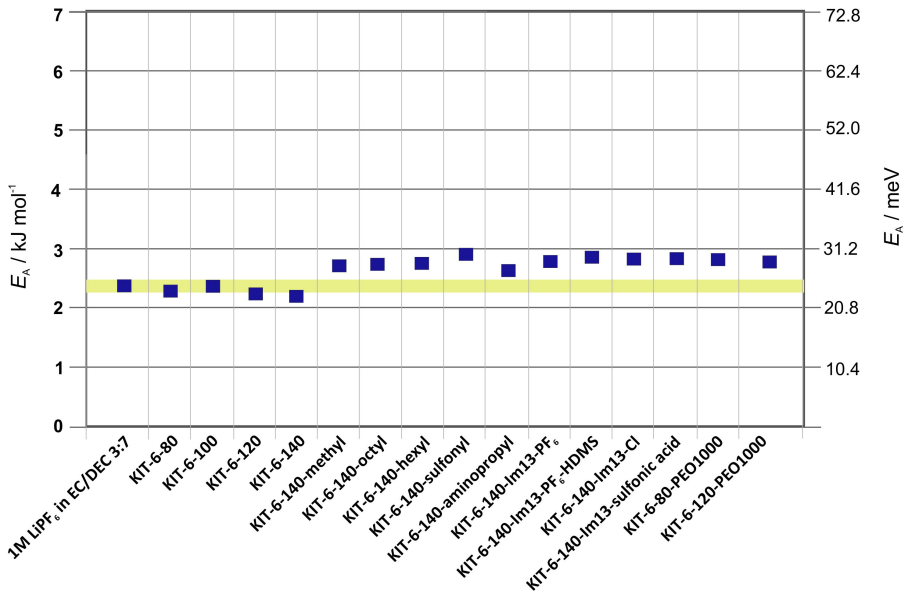

Figure 5.23: Activation energies of KIT-6 silica dispersions with 1 mol·L^{-1} $LiPF_6$ in EC/DEC 3:7 and a silica mass fraction of 2.5 wt% received from a non-linear adjustment of the Arrhenius plot with the VFT equation are shown. Calculation deviations are included in the dimensions of the data points and the yellow array marks the activation energy of the pure electrolyte for comparison.

of EC/DEC with the ratio 3:7 is approximately ε_r = 29.

Basically, the absolute values of the zeta potentials are difficult to interpret, as the variation of particles and heterogeneous distribution of the surface charge can lead to misleading conclusions. Anyhow, oxide surfaces may be stabilized by ionic dispersants, as the surface charge density is increased. In the specific adsorption process, counter ions of the charged surface are adsorbed, resulting in final sign and magnitude of the zeta potential.

The difference between the zeta potential in the electrolyte (with Li-ions) and the solvent mixture (no Li-ions) is a hint for adsorption of the anions or cations of the conducting salt. The favored adsorption process at the oxide surface, also described in the literature, is the adsorption of the anions [104,

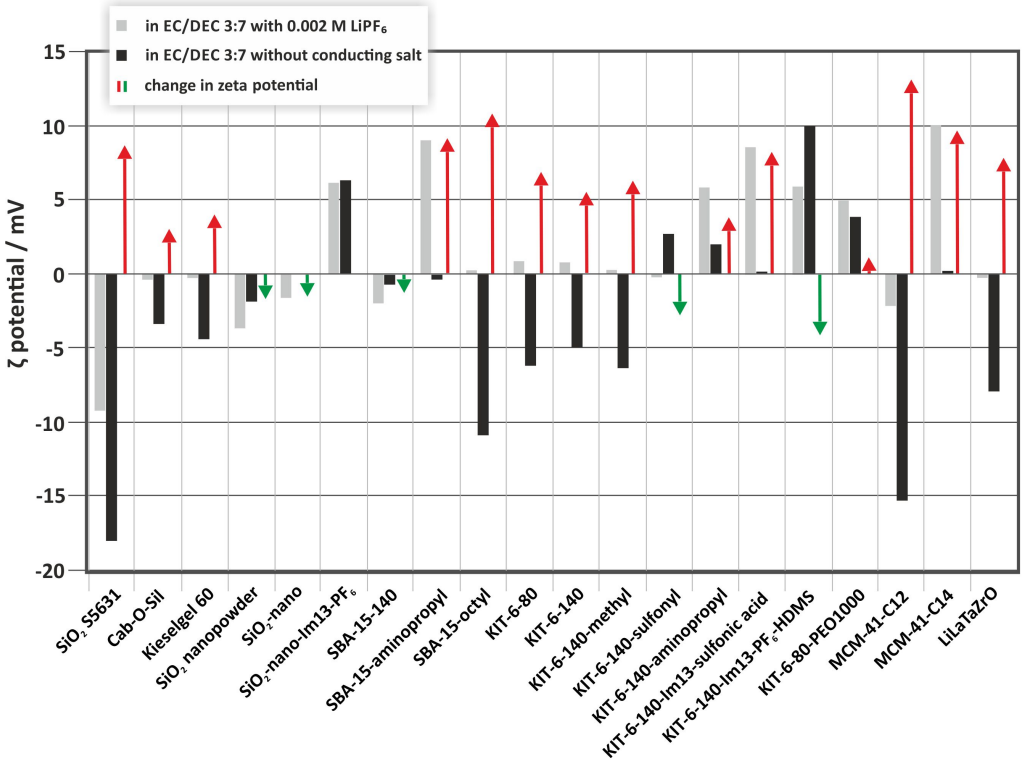

Figure 5.24: Zeta potentials of several silica materials in the electrolyte 0.002 M $LiPF_6$ in EC/DEC 3:7 (gray) and in the solvent mixture EC/DEC 3:7 (black) without conducting salt and therefore without Li^+ ions. The red and green arrows symbolize the change in zeta potential when adding the salt ions (green: decreasing potential to more negative values; red: increasing potential to more positive values).

105], in this case of PF_6^- ions on the silica surface, so that the dissociation of the Li^+ ions out of ion pairs is enabled. This would lead to an enhanced concentration of the essential charge carriers Li^+ in space charge regions. However, pure silica surfaces often have negative surface charges, which leads to adsorption of the positively charged Li^+ ions. Hence, the silica surfaces were modified with special surface groups.

The results of the zeta-potential-measurements are shown graphically in fig. 5.24. The measurements had to be done fast and each with a new cuvette, otherwise the measurement was affected by obfuscation of the cuvette material, as the solvents have probably reacted with the polymer material of the cuvettes.

One interesting observation is that eight silica materials (mainly KIT-6 materials) have a zeta potential of approximately 0 mV in the electrolyte solution. The free ions in the solution shield the potential even more with higher concentration and the double layer is confined. Therefore, the electrolyte solutions have to be very diluted to measure a zeta potential different from 0 mV. For most of these materials, the surface potential in the solvent mixture was slightly negative without conducting salt. This suggests a negatively charged surface of the silica material.

Five of the materials (SiO_2 S5631, SiO_2 nanopowder, SiO_2-nano, SBA-15-140 and MCM-41-C12) have a negative zeta potential in the electrolyte, whereas seven materials show a positive zeta potential and hence surface potential. This would mean, that the materials with a negative zeta potential have positively charged particle surfaces, which adsorb negative ions ($PF_6{}^-$) at the surface. The opposite applies to the silica with positive zeta potential, meaning the Li^+ ions are preferably adsorbed at the silica surface instead of the $PF_6{}^-$ anions.

As already mentioned, the differences in the zeta potential in the two solutions with and without conducting salt seems to offer more meaningful information, therefore this change is marked with arrows in fig. 5.24. Thereby, change of zeta potential viewing from the solution without conducting salt to the electrolyte solution is analyzed. The red arrows mark a zeta potential that gets more positive by addition of conducting salt ions, concluding that the Li^+ ions are adsorbed at the silica surface. The green arrows mark a more negative zeta potential with addition of $LiPF_6$, concluding that the desired adsorption of $PF_6{}^-$ ions is present at these silica surfaces.

The dispersions with SBA-15-aminopropyl, KIT-6-140-Im13-sulfonic acid and the MCM-41-C14 show a zeta potential of nearly zero in the solution mixture without conducting salt and a clearly positive (+6 mV to +10 mV) potential in the electrolyte and therefore an enhancement of the zeta potential. This might be interpreted as adsorption of lithium ions at the silica surface which is the adverse than desired. The zeta potential of the SBA-15-aminopropyl confirms the strong conductivity decrease in the dispersion

compared to the pure electrolyte (see fig. 7.1). Within several surface-functionalized silica materials the SBA-15-aminopropyl shows the strongest decrease of conductivity. This behavior could be expected as the amino group favors the conversion with a proton, and therefore the amount of free charge carriers is reduced.

Additionally, the amount of surface modification especially in the SBA-15 material with aminopropyl was very high, as in the IR spectra the characteristic band for Si-OH groups around 900 cm^{-1} had disappeared (cf. [168]), which was not the case for other functionalized SBA-15 materials. In contrast, the KIT-6-140-aminopropyl silica does not show any significant difference in conductivity behavior compared to the other simple functionalized silica (cf. fig. 5.8) like KIT-6-140-methyl or -sulfonyl. Especially the KIT-6-140-sulfonyl shows a very different zeta potential behavior as the zeta potential gets more negative in the ionic solution.

The KIT-6-140-Im13-sulfonic acid, however, involves OH-groups again, like the pure silica surface. These OH-groups favor the reaction with cations like Li^{+}. Therefore, this increase in surface potential from solvents to electrolyte could be expected. In the conductivity behavior of KIT-6-140-Im13-sulfonic acid (cf. fig. 5.9) nothing conspicuous can be observed. Especially compared to the KIT-6-140-Im13-PF_6-HDMS no significant difference is obvious, although this material has a positive zeta potential, but decreasing (less positive potential) with addition of ions. The post-treatment with HDMS was carried out to saturate remaining silianol groups, but this was not effective. In the mass fraction of 2.5 wt% the KIT-6-140-Im13-PF_6-HDMS has a 4 % higher conductivity, but nearly the same like KIT-6-140, which shows a more positive zeta potential in the electrolyte. Hence, no clear surface potential influence on the conductivity behavior in dispersions is identifiable here.

All the MCM-41 materials show a stronger decrease of the electrolyte's conductivity by addition of filler than other silica materials. Both of the measured MCM-41 materials show a more positive zeta potential in the electrolyte solution than in the solvent solution. An unexpected phenomenon is the zeta potential of nearly zero in the solvents without salt ions for the MCM-41-C14 in contrast to the clearly negative surface potential of -15 mV for the MCM-41-C12. The synthesis procedure for the MCM-41 materials is the same, they only differ in pore width and specific surface area due to different chain length of the used precursor. Hence, a similar surface po-

tential was expected. However, the change in zeta potential is high for both materials and it gets more positive with addition of $LiPF_6$. Therefore, the possible adsorption of a significant number of Li^+ ions can cause the decrease of conductivity beyond the simple Maxwell calculation in dispersion of approximately 5%, with addition of 1 wt% MCM-41 material (cf. fig. 5.5).

Several other materials show a more positive zeta potential in the electrolyte than in the solvent mixture, but in the conductivity measurements no noticeable difference or influence is obvious. Actually, the commercially available silica materials S5631 and silica gel 60 show good conductivity behavior with nearly no decrease until mass fractions of 5 wt%, although the zeta potential indicates an adsorption of Li^+ ions.

Moreover, the differences in zeta potential for the KIT-6-80 and KIT-6-140 materials are only half of the differences for the MCM-41-materials, and the conductivity behavior of the KIT-6 materials is nearly that expected from the Maxwell calculation.

A lowering of the zeta potential and therefore adsorption of the anions is shown by the nanomaterials and besides the already mentioned KIT-6-140-Im13-PF_6-HDMS, the KIT-6-140-sulfonyl. These changes in zeta-potential are small and therefore do not strongly influence the conductivity behavior. However, the nano materials SiO_2-nano and SiO_2 nanopowder show a good conductivity behavior in dispersion, as they almost do not affect the electrolyte conductivity and hence show conductivities higher than expected by the Maxwell calculation.

Actually, most of the materials do not show an improved conductivity, probably because the differences in the zeta potential in the two solutions are too small. Furthermore, the absolute values of the zeta potentials are also small; although it has to be taken into account that zeta potentials are normally measured in water, where the dielectric constant is higher ($\varepsilon_r(H_2O) \approx 80$ $(20\,^\circ C)$, ε_r(EC/DEC 3:7) ≈ 29 $(25\,^\circ C)$; ε_r for the pure EC and DEC can be found in tab. 3.1). Therefore, smaller zeta values are expected in the electrolyte. It has to be pointed out, that the electrophoresis techniques can only be applied to extremely diluted systems, like it was done, but there is an uncertainty in extrapolating the diluted results to concentrated systems in reality. The method of acustophoresis seems to be the better tool to study the adsorption of dipersants [171].

Generally, the greater the magnitude of the zeta potential, the more likely

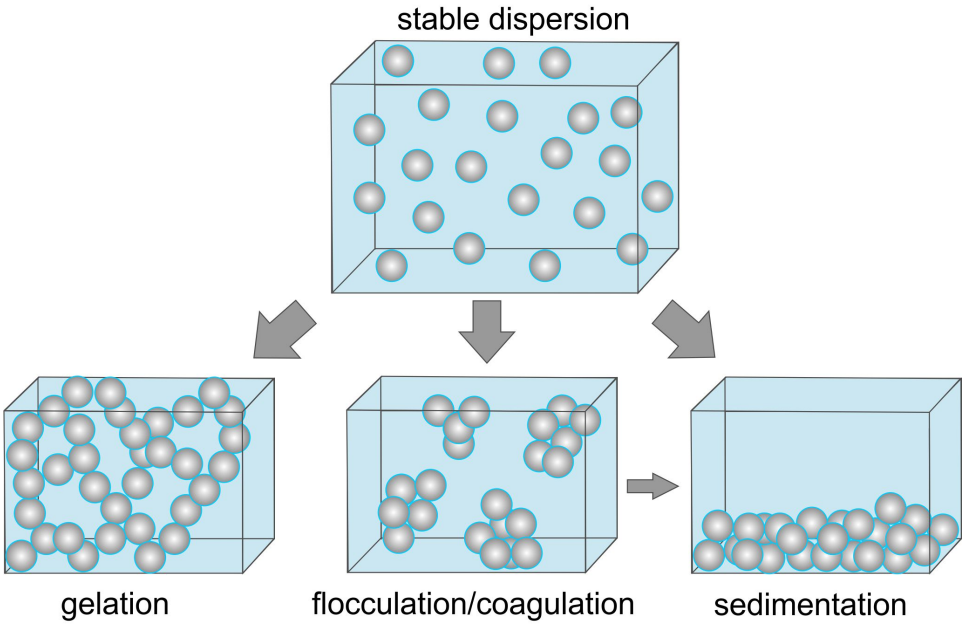

Figure 5.25: Effect of surface charge on particles in colloids and the resulting particle distance or behavior.

is the suspension to be stable (see fig. 5.25) and the smaller is the probability of flocculation or sedimentation occurring. This is due to the greater repulsive forces introduced into the system which help to overcome the tendency to aggregate. This simplest model of these phenomena arise from the DLVO (Deryaguin-Landau-Verwey-Overbeek) theory. It is stated, that the stability of a colloid is a balance between attractive van-der-Waals forces and electrical repulsion due to surface charge. As the zeta potential approaches zero, the electrostatic repulsion becomes small compared to the van-der-Waals forces and the colloid will aggregate and accumulate (flocculation) followed by sedimentation due to the attractive forces. In the case of gelation, the particles built up a network structure, with possible percolation path. Besides the stable dispersion the gelation would have been a desired effect for the investigated composite electrolytes. A full dispersion of ceramic powder is therefore essential for the processing of the composite electrolytes, meaning that no aggregates form.

In colloids the attractive forces can be encountered by repulsive forces to separate particles. The specifically adsorbed ions can cause charge reversal which may lead to a re-stabilization of the colloid. This is achieved either by addition of charge to the particles (electrostatic stabilization, mostly done with altering the pH) or by addition of polymeric molecules. Both ways were tested firstly by introducing imidazolium groups and secondly by the addition of PEO groups on the surface. The goal was to achieve a gelation of the particles in the electrolyte. Unfortunately, no stable dispersion could be reached.

The higher zeta potential values in the electrolyte solution with conducting salt, independent of the sign, show that the surfaces of these silica materials have a higher effective particle charge and therefore these particles are stabilized a bit more in the used electrolyte. Higher zeta potentials of approximately 10 mV in the electrolyte are shown by MCM-41-C14, KIT-6-Im13-sulfonic acid, SBA-15-aminopropyl and the SiO_2 S5631. These materials had indeed partially more gel-type characteristics and appearance than the other materials.

The overall measured potentials are in the range of +10 mV to -18 mV. Stable dispersions are obtained with zeta-potentials starting with +/$-$30 mV as shown in tab. 5.1. This may also be a cause for the sedimentation of the particles in the dispersions. As the zeta potentials are a good reference for the stability of colloidal dispersions, tab. 5.1 gives an overview of zeta potential ranges and the associated stability. This table acts just as an indication and is accurate especially for aqueous solutions. The stability of the investigated silica dispersions is mainly influenced by the particle size, the concentration and the pH. The surface charging in non-aqueous media is extremely complex as even polar impurities, mainly water, are a great influencing factor in magnitude and sign of the zeta potential. Again, the determination of water impurities is essential. As the zeta potential for the composite electrolytes continuously declines with higher concentration of electrolyte solutions, it would have been helpful to measure the zeta potential in even lower concentrated electrolyte solutions.

Table 5.1: Assessment of the colloid stability dependent on the zeta potential (source: [172]).

zeta potential [mV]	Assessment of colloid stability
0 to ± 3	Maximal agglomeration and precipitation
around ± 5	Region of strong agglomeration
± 10 to ± 15	Beginning of agglomeration
± 16 to ± 30	Incipient stability
± 30 to ± 40	Moderate stability
± 40 to ± 60	Good stability
> 60	Excellent stability

5.3.1 Possibility of an adsorption mechanism

To review the numeric possibility of a specific adsorption mechanism of conducting salt ions on the silica surface, a rough estimation of the amount of Si-OH groups on several silica surfaces, which are supposed to act as adsorption positions, was done. Additionally, the number of ions in an electrolyte solution with 1 mol·L^{-1} $LiPF_6$ was calculated.

Therefore, the first assumption is the presence of 1.5 Si-OH groups on 1 nm^2 of the silica surface (this was assumed as a realistic number). For several specific surface areas of silica materials and different silica mass fractions the total number of adsorption positions was estimated in table 5.2:

Table 5.2: Number of adsorption positions (OH-groups) on various silica surfaces in different silica mass fractions.

specific surface area / $m^2 \cdot g^{-1}$	silica mass fraction / wt%	number of adsorption positions / g
300 (SBA-15)	2.5	$1.2 \cdot 10^{19}$
	10	$4.5 \cdot 10^{19}$
	50	$4.5 \cdot 10^{20}$
600 (SiO_2 nanopowder)	2.5	$2.3 \cdot 10^{19}$
	10	$9.0 \cdot 10^{19}$
1266 (MCM-41)	2.5	$4.9 \cdot 10^{19}$
	10	$1.9 \cdot 10^{20}$

The number of ions in an electrolyte with $LiPF_6$ are considered for 4 g of the electrolyte with a densitiy of ρ=1.165 $g \cdot cm^{-3}$. For an electrolyte with a concentration of 1 $mol \cdot L^{-1}$ the following number of ions is calculated:
$N(Li^+) = N(PF_6^-) = n \cdot N_A = 2.58 \cdot 10^{20}$.

For an electrolyte with a concentration of 0.1 $mol \cdot L^{-1}$ the number of ions is one order of magnitude smaller:
$N(Li^+) = N(PF_6^-) = n \cdot N_A = 2.58 \cdot 10^{19}$.

This calculation confirms the possible impact of adsorption on the conductivity. The number of ions in the 1 M electrolyte are one order of magnitude higher than the number of possible adsorption positions, but the the influence of adsorption on the conductivity should be still noticeable. With 50 wt% of silica mass fraction for a silica with a specific surface area of 300 $m^2 \cdot g^{-1}$, the adsorption positions and the number of ions in a 1 M electrolyte are in the same order of magnitude. However, this mass fraction was not possible to disperse homogeneously in the used electrolyte. Therefore, the easier approach was to reduce the number of ions by reducing the concentration of the electrolyte. In a 0.1 $mol \cdot L^{-1}$ $LiPF_6$ electrolyte the number of ions is one order of magnitude smaller and hence is in the range of adsorption position of silica mass fractions between 2.5 % and10 wt%. Nevertheless, this low concentrated electrolyte was not possible to measure at temperatures below $10\,^{\circ}C$, as the used solvent EC crystallized.

For further examination of the adsorption concept, special segregation experiments were done (see fig. 5.26). Here, the conductivity of the electrolyte

was measured before the addition of silica material. Then a defined amount of silica material was added and dispersed for a certain amount of time. After resting for some time, the filler material had sedimented. In the end, the conductivity of the solvent was measured again.

In fig. 5.26, the results of this simple experiment are shown. As can be seen, the conductivity of the electrolyte was not affected by the silica addition and therefore, there is no hint for the adsorption of ions on the silica surface.

As in the conductivity measurements the overall conductivity is measured, a decrease in conductivity with addition of filler material has to be observed, regardless of whether the anions or cations of the salt are adsorbed on the silica surface, because the amount of charge carrier is reduced. The conductivity of the electrolyte is reduced with addition of silica material, but this seems to be more a volume exclusion phenomenon due to isolating particles, as the electrolyte reaches the original conductivity with segregation of the silica material. However, for the conduction in lithium ion electrolytes, the amount of Li^+ ions is decisive, and cation-catching surface groups are obstructive. An enhanced conductivity can only be observed, if one sort of charge carrier concentration is enhanced in the space charge regions and these space charge regions overlap, so that fast conducting path (percolation paths) are created.

5.4 Rheology

The rheological measurements were performed to determine viscosity variations and the possible formation of network structures. Therefore, the dispersions were sheared between two plates and changes compared to the pure electrolyte were observed. The electrolyte shows Newtonian behavior, as the viscosity of the material does not change after increasing the shear rate. The viscosity is a characteristic of a material that expresses the internal friction of fluid systems. Newtonian fluids obey the Newtonian law (eq. 4.7), meaning that there is a linear dependence between the shear stress τ and the shear rate $\dot{\gamma}$ as well as unaltered viscosity η with change of the shear rate. Hence, the viscosity is a material constant for Newtonian fluids and the constant viscosity is sufficient to describe the rheological behavior. Systems with elasticity and plasticity characteristics besides the viscosity

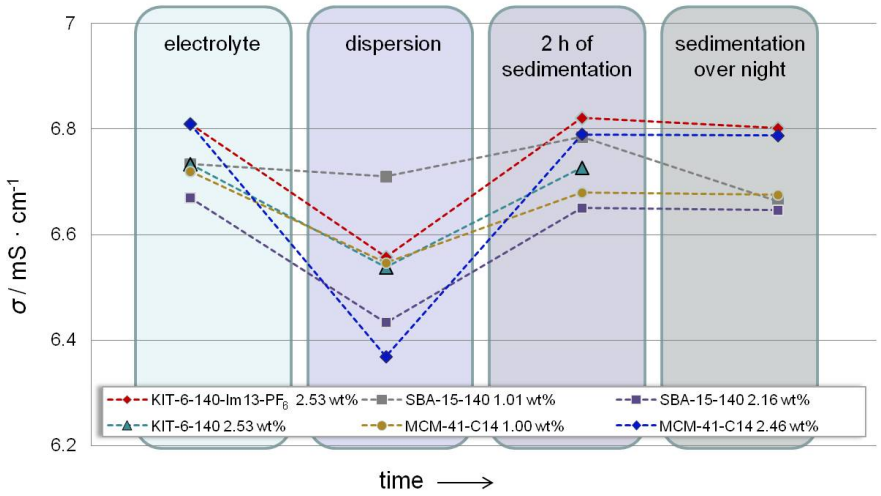

Figure 5.26: Results of a segregation experiment to clarify possible adsorption phenomena. The conductivities of electrolytes with various segregated silica materials were observed over time.

are non-Newtonian fluids as these characteristics lead to deviation from this linear proportionality.

The rheological measurements showed, that no network is formed in the case of silica particles dispersed in the organic electrolyte 1 M $LiPF_6$ in EC/DEC 3:7 as the dispersions show Newtonian behavior. Predominantly, the dispersions showed the same viscosity behavior dependent on shear rate like the pure electrolyte as shown exemplary for some materials in fig. 5.27 and the viscosity is independent of the shear rate. As was expected, the materials segregated in the dispersions. Within the investigated materials, the Cab-O-Sil and the SBA-15-140-octyl materials show special behavior in dispersions. They both have higher viscosities than the pure electrolyte at small shear rates of 1 s^{-1}, which decrease with increasing shear rate. Even the overall viscosities are higher. In theory, shear thinning materials show a decrease of viscosity with increasing shear rates as can be seen in the general classification diagram (fig. 5.29). In a diagram with a linear plotted viscosity (fig. 5.28), it is obvious, that the behavior of Cab-O-Sil differs from the other dispersions with shear thinning behavior and the SBA-15-140-octyl differs also, but less pronounced. Shear thinning materials become more liq-

uid with increasing shear stress as can be seen in fig. 5.29, which is often correlated with a destruction of networks. A further explanation is the orientation or deformation of particles in the fluid flow so that they cause small flow resistances (see fig. 5.30). This pseudoplasticity or shear thinning is a known characteristic of wet sand. Hence, these two materials show superior behavior compared to most other investigated materials.

A main characteristic of the Cab-O-Sil is the synthesis as aerogel. With a filigree network structure and big, open pores it differs in morphology from the other investigated materials, which have mainly mesoporous or nonporous structures. Due to the high porosity, the volume densities are extremely small (ρ = 0.004 g·cm^{-1} - 0.5 g·cm^{-1}) and the gel structure is inherent. Hence, a special orientation of these particles under shear stress is plausible (cf. fig. 5.30). Anisotropic particles, for example, align themselves in the direction of flow, whereas isotropic particles arrange in parallel shear zones. Deformable particles will be deformed under the flow dependent on their elasticity. Knots of polymer chains can possibly dissolve into individual chains by shearing. This also applies to aggregates, which can be decomposed to individual particles. In SEM pictures (cf. fig. 5.2) the fluffy and agglomerate structure of Cab-O-Sil is evident.

With examination of the morphology of SBA-15-140-octyl particles shown in fig. 5.2, it gets obvious that they have a lamella structure unlike the mostly spherical dimensions of the other silica materials. These materials are expected to have special orientation under shear stress, but normally show a decrease in viscosity and not the seen increase (cf. fig. 5.28). Moreover, this special behavior of SBA-15-octyl is not seen for the KIT-6-140-octyl, although it has to be taken into account, that the spherical appearance of the KIT-6-140 particles is different (cf. fig. 5.1). However, this is not convincing enough, as all the other SBA-15 materials with the same flat particle morphology show Newtonian behavior in the rheological measurements. Perhaps the octyl-functionality leads to special behavior of these SBA-15-particles, as these alkyl-groups have a chain structure compared to the other surface groups. A comparison with a hexyl-surface-group would have been decisive.

The application of the shear stress (τ) against the shear rate ($\dot{\gamma}$) is shown in fig. 5.31, as this is another typical diagram to identify material classes in rheological experiments. Here, the gradient of the straight line is characteristic for the used liquid. The comparison of the results with the theoretical

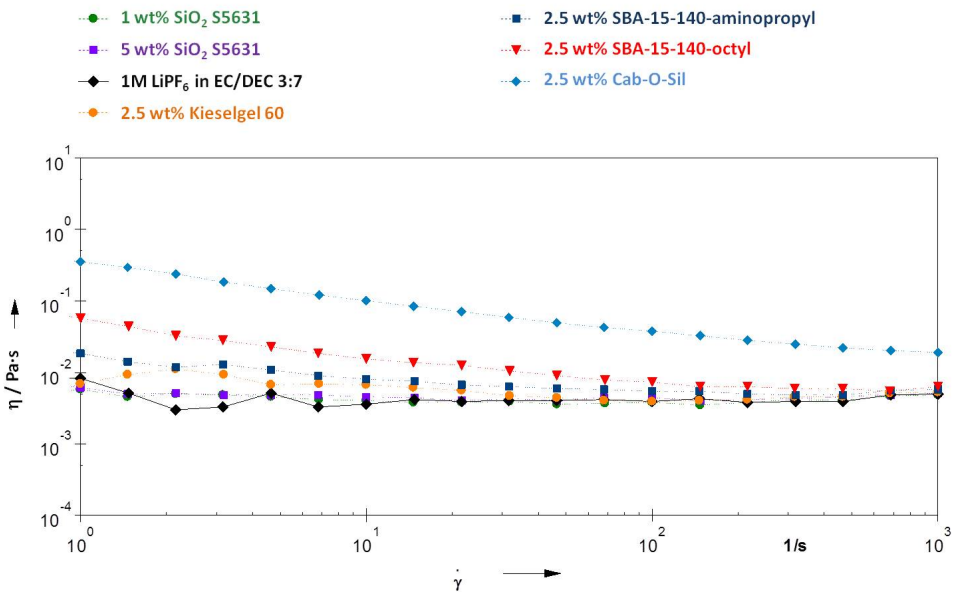

Figure 5.27: Logarithmic plot of the room temperature viscosity η with the shear rate $\dot{\gamma}$ for several composite electrolytes. Dispersions with different silica and varying silica mass fractions are shown. This graphic is not a complete survey; only some materials are shown exemplary. The dotted lines do not represent a functional relation between the viscosity and the shear rate, they are rather added as guide to the eye.

classification supports the assumption of Cab-O-Sil as shear thinning material. For the SBA-15-140-octyl it is not as obvious. Especially for the Cab-O-Sil the gradient of the straight line is less than for the other materials with Newtonian behavior and the beginning shear stress is higher.

With these experiments and comparison with general classification of materials, it can be assumed that the major part of the examined materials show Newtonian behavior except of the Cab-O-Sil, which show shear thinning behavior. The behavior of SBA-15-140 is not as clear as for the Cab-O-Sil. In real experiments, there can be deviations from the linearity of Newtonian fluids in the theoretical diagrams. Therefore, the specification of SBA-15-140-octyl as shear thinning material or Newtonian fluid is debatable.

In fig. 5.3, the viscosity values of several dispersions with 1 wt% and 2.5 wt% silica mass fraction at the shear rate of 100 s^{-1} as standard are

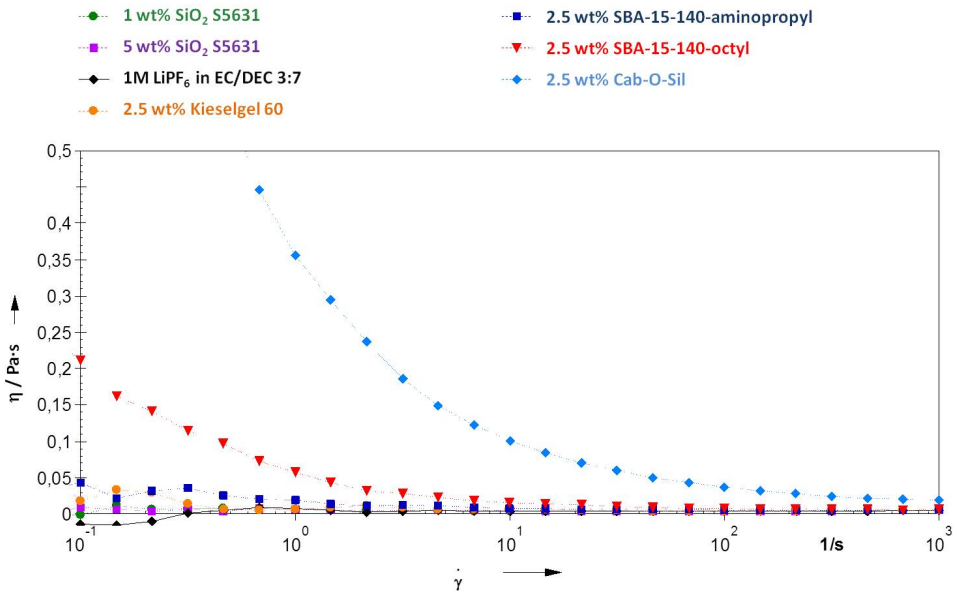

Figure 5.28: Linear plot of the variation of room temperature viscosity η with the shear rate $\dot{\gamma}$ for several composite electrolytes.

Table 5.3: Viscosities of composite electrolytes in comparison to the pure electrolyte 1 M $LiPF_6$ in EC/DEC 3:7 at a shear rate of 100 s^{-1} as standard. Materials with a silica mass fraction of 1 wt% (left) and 2.5 wt% (right) are each compared with the viscosity of the pure electrolyte (gray field).

material (1 wt%)	η / mPa · s
MCM-41-C18	2.98
MCM-41-C14	3.06
SBA-15-50	3.47
SiO_2 S5631	3.81
SBA-15-140	3.90
KIT-6-80	3.90
1M $LiPF_6$ in EC/DEC 3:7	3.91
KIT-6-140	4.08
KIT-6-80-PEO1000	4.27
KIT-6-100	4.34
SiO_2 nanopowder	4.53
SBA-15-100	5.24

material (2,5 wt\%)	η / mPa · s
SBA-15-140	3.15
1M $LiPF_6$ in EC/DEC 3:7	3.91
Kieselgel 60	3.91
KIT-6-140-Im13-PF_6	4.11
LiLaTaZrO	4.19
KIT-6-140-aminopropyl	4.36
KIT-6-140-Im13-sulfonic acid	4.50
KIT-6-140-octyl	4.74
SiO_2-nano-Im13-PF_6	4.86
KIT-6-140-sunfonyl	5.32
SBA-15-140-aminopropyl	5.38
SBA-15-140-octyl	7.33
Cab-O-Sil	37.30

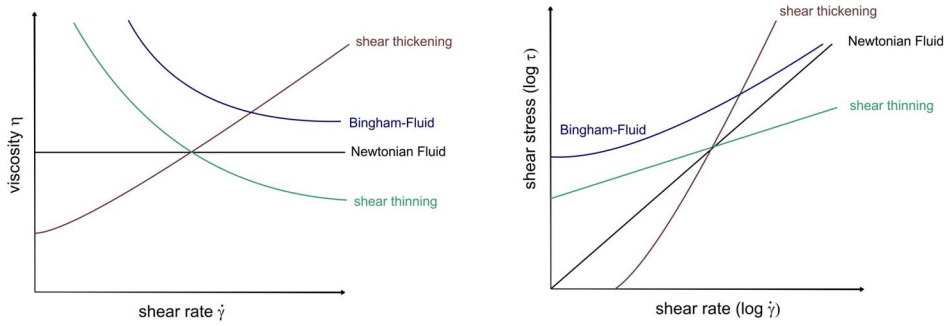

Figure 5.29: General classification of materials behavior under shear stress. On the left side the dependence of the viscosity trend on the shear rate (flow curve) is the criterion for classification of materials. On the right side the shear stress as logarithmic scale against the logarithmic shear rate is shown for the materials classes. This is also a typical diagram, as the gradient of the straight parts are characteristic for the used liquid. This gradient is also a measure for the shear viscosity.

compared in tabular form. The non-modified materials show nearly the viscosity of the pure electrolyte in both mass fraction, which is low with η = 3.91 mPa·s. Small variations may depend on the measurement. The surface-functionalized particles have a marginally higher viscosity with 2.5 wt% silica mass fraction depending on the surface group. The

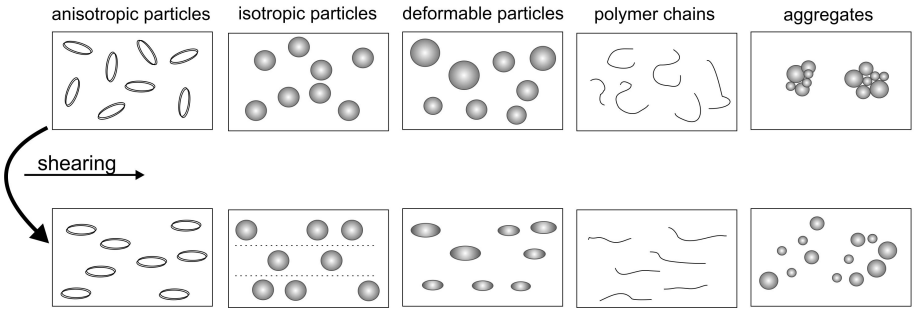

Figure 5.30: Influence of shearing on the disposition of various shear thinning materials with different morphologies (source: [166]).

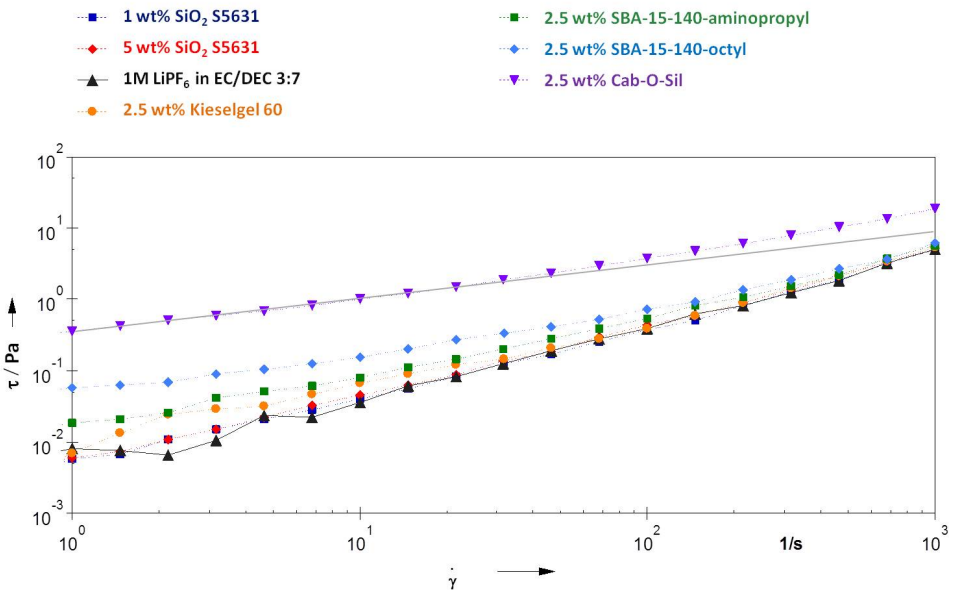

Figure 5.31: Dependence of shear rate $\dot{\gamma}$ on the shear stress τ of some selected materials with special behavior.

SBA-15-140-octyl exhibits the highest viscosity of the modified materials (η = 7.33 mPa·s) may be due to the organic rest. Interestingly, the PEO1000 chain does not influence the viscosity with 1 wt% of mass fraction. Actually, this long polymer chain was expected to build up a network in order to reach higher viscosities, even in small silica mass fractions. Within the silica materials measured in 1 wt% silica mass fraction, no significant differences in viscosity have occurred.

What is evident is the decrease of viscosity of MCM-41 materials compared to the pure electrolyte. This may be a hint for the bad influence on the conductivity in electrolyte dispersions with MCM-41 materials as filler, because of fast sedimentation and instability. Normally, a decrease in viscosity leads to a higher conductivity due to higher ion mobility. Another inconstancy is the difference in viscosity values for the SBA-15-50 (η = 3.47 mPa·s) and the SBA-15-100 material (η = 5.24 mPa·s). Hence, the data in tab. 4.1 show, that the SBA-15-100 material has a higher specific surface area than the other examined SBA-15 materials. This is the only obvious difference between these materials. However, the comparison of viscosity values with the

specific surface area of all materials does not show a clear trend. The highest specific surface areas are found for the MCM-41 materials with approximately 1200 m^2g^{-1} followed by KIT-6 materials (491 m^2g^{-1} - 876 m^2g^{-1}) and the SiO_2 nanopowder (658 m^2g^{-1}). Though, these materials have distributed viscosity values around that of the pure electrolyte.

In the silica mass fraction of 2.5 wt% the viscosities of the dispersions are higher than that of the pure electrolyte. Again, the non-modified silica materials like SBA-15-140 and silica gel 60 reproduce the viscosity of the pure electrolyte and the functionalized materials show an increase in viscosity. As already analyzed, especially the modified SBA-15-140 materials show a different behavior compared to the pure SBA-15-140 material and the viscosities are also higher. Therefore, the surface groups on silica materials have decisive influence on the behavior of filler materials in dispersions.

The most obvious fact is the viscosity of commercial Cab-O-Sil, which is nearly ten times higher in value compared to the electrolyte. In contrast to all the other silica materials, this material showed a gel-like behavior already visibly with bare eyes. The Cab-O-Sil has a wide pore distribution and a small surface area compared to the other silica materials (cf. tab. 4.1) besides the different morphology, which seems to be decisive for the stability and network of dispersions.

The comparison with the conductivity behavior of Cab-O-Sil in the electrolyte dispersion shows, that this positive mechanical behavior has a negative influence on the electrolyte conductivity, as the conductivity decreases rapidly with addition of small amounts of Cab-O-Sil (cf. fig. 5.6). For higher silica mass fractions than 2.5 wt% a homogenous dispersion could not be reached. Unfortunately, a higher viscosity leads to a decrease in conductivity. Hence, the structure of Cab-O-Sil particles in electrolyte dispersions seems to block the mobility of charge carriers, although the calculated activation energy (shown in fig. 5.20), is in the same range as in the pure electrolyte or even slightly smaller. The zeta potential of Cab-O-Sil (cf. fig. 5.24) is very low but seems to get a little more positive with addition of conducting salt ions. Consequently, the reduced conductivity of Cab-O-Sil seems to be more the result of blocked ions pathways and high viscosity, rather than adsorption phenomenons.

The viscosity trend in various mass fractions of the same silica was examined for the silica KIT-6-80. In graphic 5.32 the increase in viscosity with increasing silica mass fraction is shown. With 1 wt% silica mass fraction no

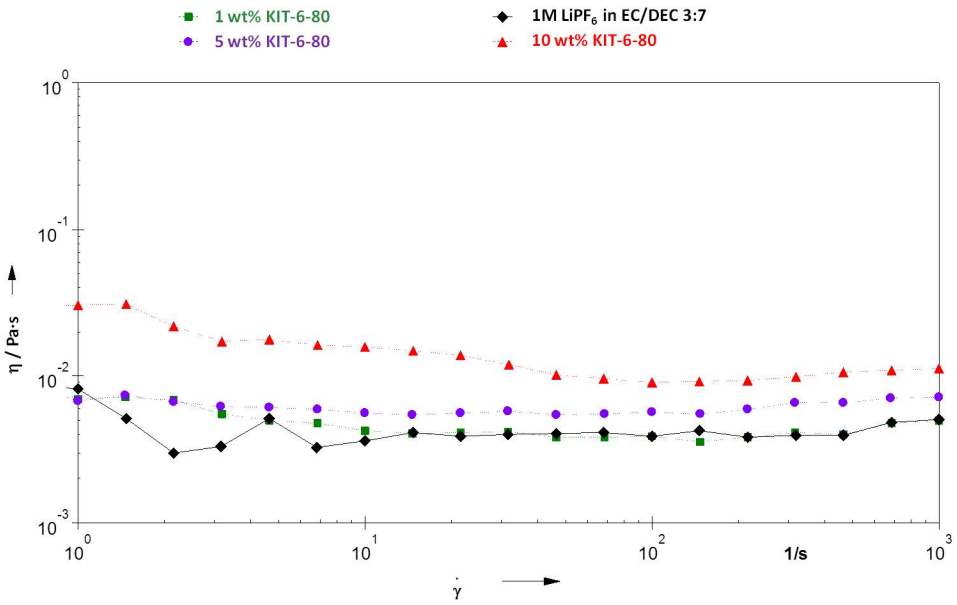

Figure 5.32: Influence of the added amount of silica mass fraction on the viscosity for the silica material KIT-6-80.

change in viscosity (η = 5.24 mPa·s at 100 s^{-1}) is observed compared with the electrolyte. For a silica mass fraction of 5 wt% the viscosity increases about 45 % (η = 5.67 mPa·s at 100 s^{-1}; $\Delta\eta$ = 1.77 mPa·s) and with a silica mass fraction of 9.9 wt% this increase is with 60 % and a viscosity value of η = 9.08 mPa·s at 100 s^{-1} ($\Delta\ \eta$ = 3.41 mPa·s) even higher. Graphically shown in fig. 5.33 this results in an approximately linear (taking measurement errors into account) increase of viscosity with silica mass fraction, as expected.

The correlation between the viscosity increase and the conductivity decrease (cf. fig. 5.4) with increasing silica mass fraction shows that the conductivity also decreases linearly between mass fractions of 1 wt% and 5 wt% with an amount of 12 %. Unfortunately, the conductivity was not determined in higher mass fractions for KIT-6-80. However, in higher mass fraction the other KIT-6 materials show irregularities, as there was a fast segregation and decomposition. All in all, the decrease in conductivity is not as strong as the increase of viscosity. Therefore, it can be expected, that other effects beside

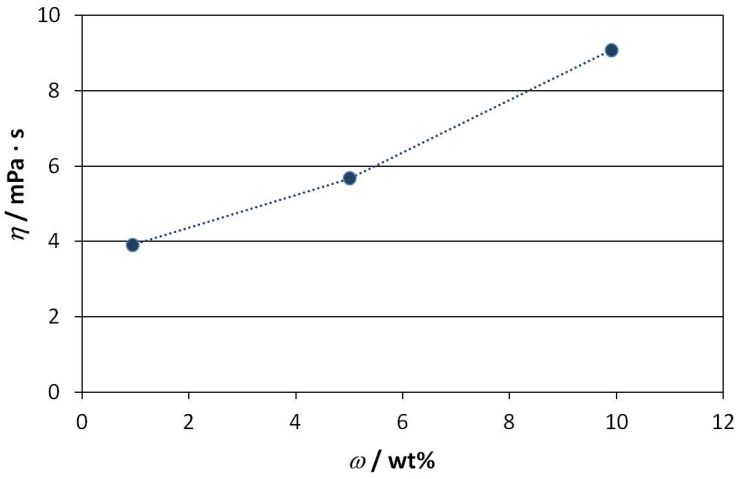

Figure 5.33: Connection of viscosity increase with added silica mass fraction for KIT-6-80 material.

the viscosity have an influence on the conductivity in the observed disperse electrolytes.

Nevertheless, the SiO_2 nanopowder also exhibits a special viscosity behavior in dispersion (fig. 5.34). The viscosity of the dispersion with 5 wt% silica material is twice as high (η = 13.8 mPa·s at 100 s^{-1}) than the viscosities of other silica dispersions. This higher value may be due to the small particle size and therefore special orientation or networking in higher mass fraction. The constant viscosity with increasing shear rate indicates a Newtonian fluid. This changes in the dispersion at a higher temperature of $50\,^{\circ}\mathrm{C}$ and 5 wt% mass fraction. There, viscosity decreases with increasing shear rate. This characteristic is referred to a shear thinning behavior and was also observed for the Cab-O-Sil material and can be due to fast segregation or special orientation of the particles at higher temperature in this case.

Time-dependent conductivity and rheology measurements, meaning long time as well as very fast measurements (without stirring), also gave no hint for the appearance of time-dependent particle networks.

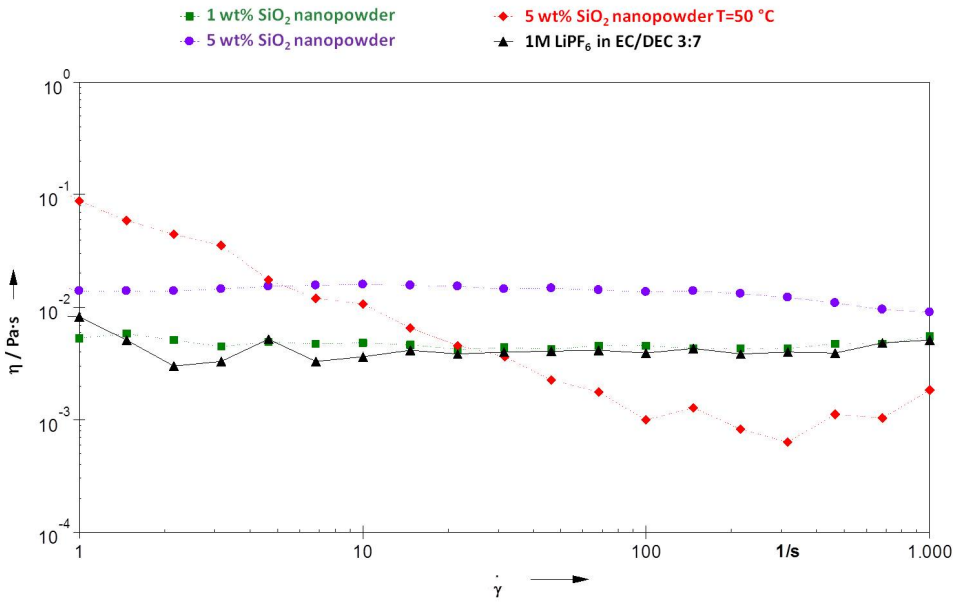

Figure 5.34: Logarithmic plot of the variations in viscosity for the SiO_2 nanopowder in different mass fraction at 25 °C and at higher temperature dependent on the shear rate.

5.5 Electrochemical window

The electrochemical window is an important property of electrolytes for the use in lithium ion batteries. A wide voltage range, in which the electrolyte is stable is required to reach high voltage batteries.

The measured current with increasing voltage is the limiting factor to decide whether decomposition has started. Thus, the limiting current has to be defined in order to determine the electrochemical stability range. Fig. 5.35 shows the electrochemical stability range for several disperse electrolytes dependent on different limiting currents. Only a selected number of filler materials was examined to provide an overview. As there is no standard definition which current value limits the electrochemical stability, the change in size of the electrochemical window with three different current densities was observed. Relatively small current values of 10 µA, 2 µA and 1 µA were chosen, as a starting decomposition reaction was already assumed.

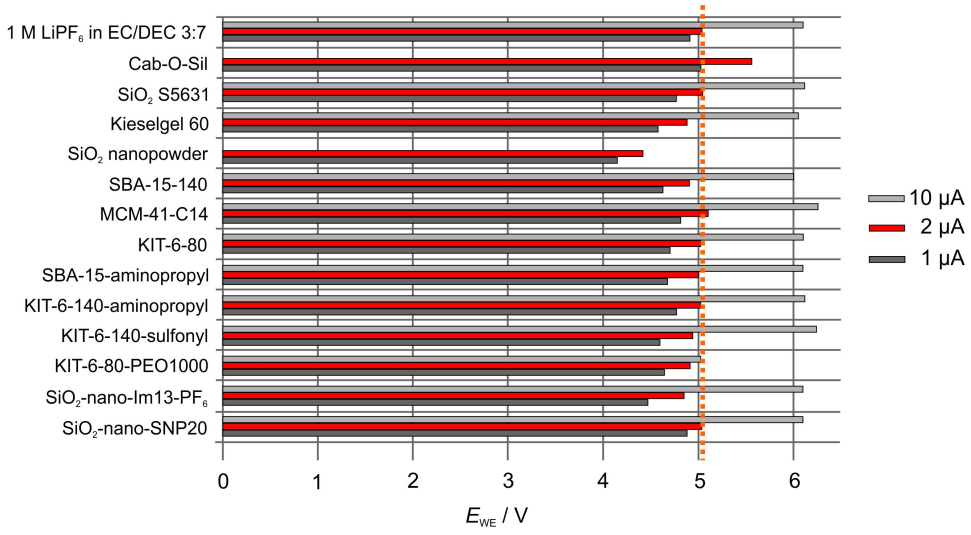

Figure 5.35: Electrochemical stability measured vs. glassy carbon of composite electrolytes with varying filler material. The silica mass fraction of all materials was 2.5 wt%. Three different limiting currents as stop criterion were chosen for comparison of the size of electrochemical windows. The currents correspond to current densities of 1.4 A·m^{-2}, 0.28 A·m^{-2} and 0.14 A·m^{-2}.

These were current densities of 1.4 A·m^{-2}, 0.28 A·m^{-2} and 0.14 A·m^{-2}, as the diameter of the electrode was 3 mm.

Between 2 µA and 10 µA as limiting current, the electrochemical window of the electrolyte increased by 1 V, which is a decisive difference for the use of an electrolyte. At 10 µA (1.4 A·m^{-2}) the decomposition was obviously reached, as the current then increased rapidly. This current was reached by all filler materials at approximately the same voltage around 6 V. All dispersions had an amount of 2.5 wt% silica. At the top of the diagram the electrochemical window of the pure electrolyte is shown, to compare the change of electrochemical stability with addition of filler material.

For the comparison of the composite electrolytes a current of 2 µA (red lines) is chosen, because it seems to be a realistic current value for the starting decomposition reaction of the electrolyte and interesting differences are most obvious. The electrolyte 1 M $LiPF_6$ in EC/DEC 3:7 exhibits a stability

window of 5.05 V vs. glassy carbon.

Changes in the electrochemical window compared to the pure elctrolyte are obvious for the SiO_2 nanopowder and the Cab-O-Sil material. The 0.5 V lower electrochemical stability of the SiO_2 nanopowder can be attributed to the higher reactivity of small particles. Hence, the other nanoparticles SNP20 and SiO_2-nano-Im13-PF_6 do not affect the electrochemical stability of the electrolyte concluding that there is another influencing factor than just the particle size. The dispersion with Cab-O-Sil as filler material shows with 5.56 V a 0.5 V higher electrochemical window compared to the pure electrolyte. Therefore, it can be concluded that the formation of an interparticle network, as it was recognized with rheological measurements, may lead to a higher electrochemical stability. The current of 10 µA was not reached by Cab-O-Sil in the scanned voltage range.

To sum up, the silica materials mostly do not change the electrochemical stability window of the pure electrolyte, which may be due to a missing network formation. The electrochemical characteristics of the composite electrolytes are therefore dominated by the liquid fraction. The only exception is the Cab-O-Sil, which has poor conductivity performance. However, these characteristics fit to the enhanced viscosity of this material.

5.6 Supplementary measurements

Several additional measurements with no crucial results for the clarification of conductivity phenomenons of silica materials in the electrolyte 1 M $LiPF_6$ in EC/DEC 3:7 were done. A short overview is given in the following.

The conductivity measurements were also performed in an electrolyte with 0.1 mol·L^{-1} $LiPF_6$ in EC/DEC 3:7, hence a lower concentrated electrolyte. The basic consideration was the number of adsorption positions on a silica surface: with a smaller amount of ions and therefore a better ratio of adsorption positions on a silica surface, a more notable effect on the electrolyte conductivity was expected. Problematic with these measurements was the instant flocculation and immediate sedimentation of the filler material in the same mass fraction used in the 1 M electrolyte (1 wt%, 2.5 wt%). For silica mass fractions of 0.3 wt% a measurement was possible, but no change in the conductivity of the low concentrated electrolyte could be observed with

different silica materials including nanoparticles. To reach a higher viscosity and therefore a slower sedimentation of the silica the ratio of solvents was changed to EC/DEC 1:1 with 0.1 mol·L^{-1} $LiPF_6$. The temperature-dependent measurements of these dispersions were only possible for temperatures higher than $25\,^{\circ}\mathrm{C}$, because the EC crystallized at lower temperatures. Again, immediate measurements were only possible with very low silica mass fraction due to fast sedimentation. Consequently, a direct comparison between the 1 M and the 0.1 M electrolyte and the influences of the electrolyte concentration on conductivity was not possible.

In the field of battery safety the filler materials were thought to have a positive influence on the liquid electrolyte. One assumption was that the flash point of the highly inflammable solvents is affected in dispersions and therefore, enhanced safety due to higher flash points could be reached. The basic idea was, that the amount of liquid is reduced and bound at inert silica particles which are not easily flammable. Hence, the flash points of several silica dispersions with various amounts of silica were tested. Especially the dispersions with gel-like appearance were measured and, if possible, high silica mass fractions up to 10 wt% were added.

For all tested dispersions no change in flash point was observed. This might be due to the missing network formation within the particles and therefore, the amount of liquid electrolyte was dominating for the flash point. A change in flash point is supposed to occur in a stable colloidal dispersion which was not reached with these materials.

6 Conclusion and Outlook

Composite electrolytes consisting of the liquid organic electrolyte 1 M $LiPF_6$ in EC/DEC with the ratio 3:7 and various dispersed silica filler materials therein, were investigated with systematic electrochemical measurements concerning conductivity, surface potentials, viscosity, network structures and the electrochemical window.

Within all the performed measurements there is no clear trend in the behavior of silica filler materials dispersed in the liquid lithium electrolyte 1 M $LiPF_6$ in EC/DEC 3:7.

- **Conductivity**: The silica filler materials decrease the conductivity of the liquid lithium battery electrolyte. The magnitude of this decrease is dependent on the surface characteristics of the silica. An improvement of mechanical characteristics could be observed with only small loss of conductivity.

The conductivity measurements show predominantly a decrease in conductivity with addition of filler material. Only with low silica mass fractions of maximum 1 wt% there is a small conductivity increase, but this is not consistent within the whole examined temperature range. Possibly, there is a weak network formation at room temperature of a small amount of silica particles, which is destroyed with increasing temperature due to the increasing energy of the silica particles.

As the silica materials sedimented quickly stirring was necessary, hence, leading to prohibition of possible percolation paths. However, for the occurrence of percolation paths higher filler concentrations than the used are actually required, as the particles need to have small distances. Dispersions with higher filler concentrations (silica mass fractions) than 10 wt%, sometimes even less, could not be reached with a homogenous distribution of the silica materials in the electrolyte. Moreover, with longer dispersing times decomposition reactions appeared.

To prevent fast decomposition the silica materials surfaces were modified, as the adsorbed amount of water on the silica surfaces led to decomposition of the disperse electrolytes. This modification resulted in a reduced amount of OH surface groups on the silica surface. Therefore, active surface groups in terms of possible adsorption mechanisms could be reached. Due to the faster decomposition reactions in higher filler mass fractions (> 5 wt%) and sedimentation of particles, strong deviations in the conductivity measurements of disperse electrolytes with high filler amount were observed. Hence, the measurements of disperse electrolytes were more error-prone with increasing silica mass fraction.

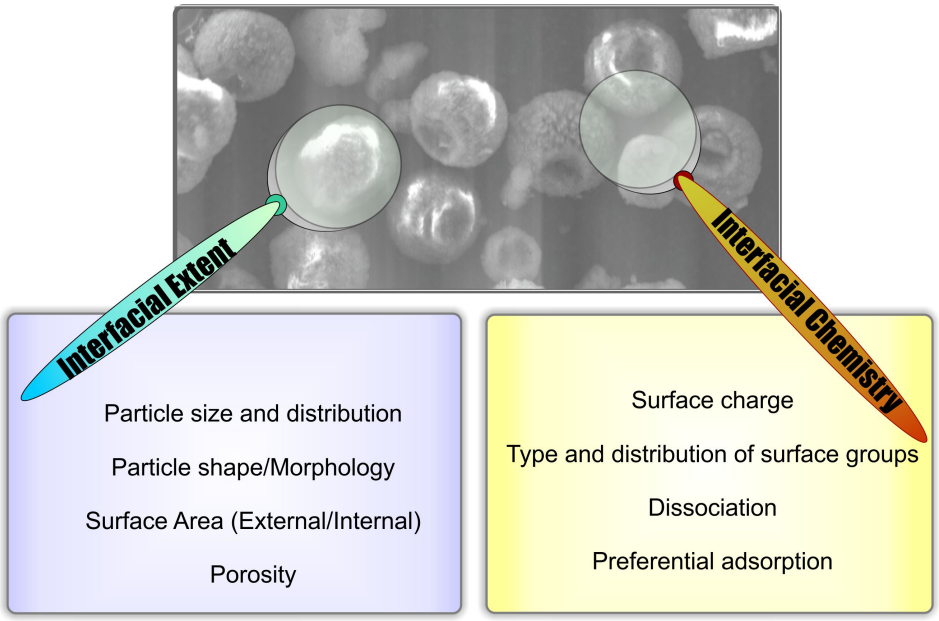

Figure 6.1: Overview of fundamental parameters that control the behavior of particulate suspensions.

Possible overlapping space-charge regions with addition of more filler material or even blocking effects, if the particles are too close, could rarely be observed. As expected, the overall conductivity increased with increasing temperature and decreased with increasing silica mass fraction as assumed by Maxwell exclusion assumptions. For many dispersions an approximately

linear conductivity decrease with increasing silica mass fraction is obvious, but in some cases the decrease is stronger than expected by the Maxwell model and in other cases the conductivity seems to be unaffected even by silica mass fractions of 7.5 wt%. These variations around the conductivity decrease expected within the Maxwell model lead to the assumption, that other effects than only an exclusion volume are relevant. For more significant results, it is necessary to reach stable dispersions with a network formation between particles. Only then, reliable information about the conductivity of disperse electrolytes can be gained. Moreover, stirring could then be avoided so that potentially percolation phenomena could occur.

The correlation of conductivity of the disperse electrolytes with the surface area and the pore width of the silica materials showed, that inconsistencies are present. Within some material groups like MCM-41 materials, a dependence of increasing conductivity with increasing specific silica surface area could be assumed. Bigger pore widths also seem to be favorable for higher conductivities. The important step forward would be a correlation with particle sizes which vary in a range of nm and μm but this was not measured in this work and is therefore not determined for most of the silica. The particle size is decisive for the stability of dispersions and should be noticed for further measurements.

The calculation of the activation energies out of the conductivity measurements on basis of the VFT equation showed that a few silica materials in dispersion lead to a much higher activation energy for the movement of ions. The hindrance in the movement of the electrolyte ions was not obvious in the conductivity measurements, as a stronger decrease of conductivity would have been expected in these cases. The appliance of the VFT equation, usually used for polymer electrolytes and ionic liquids, was a compromise. This equation fits better to the dispersions than the Arrhenius equation, but the meaning of the glass temperature for the dispersions is not clear.

- **Surface potential**: Zeta potentials are small and therefore colloidal stability was not achieved. Several silica materials with special surface groups show more positive zeta potentials with addition of conducting salt, suggesting that Li^+ ions are adsorbed at the silica surface.

A closer look to the silica surface charges with zeta potential measurements showed small zeta potential values. Stability of dispersions increases

with increase of zeta potential, whereas dispersions with low sedimentation rates are reached with zeta potentials starting from 30 mV.

Most of the silica materials had zeta potentials around 10 mV or less, but the overall values were not the essential value; the absolute value could not reliably be measured. Hence, changes of the zeta potential in dispersions with the electrolyte was observed in comparison to dispersions with the solvent mixture without conducting salt and therefore without lithium ions. Many silica materials (e.g. SiO_2 S5631, KIT-6-140, SBA-15-aminopropyl, KIT-6-140 sulfonic acid) showed a more positive zeta potential in the electrolyte solution than in the solvent mixture, indicating an adsorption of Li^+ ions at the surface. This would be the undesired adsorption of ions, as the Li^+ ions are the essential charge carriers. The favorable adsorption would be that of $PF_6{}^-$, leading to a more negative surface potential with addition of lithium salt. This more negative zeta potential in the electrolyte dispersions is shown by materials like KIT-6-140-sulfonyl and the nanomaterials SiO_2 nano and SiO_2 nanopowder. It has to be noticed, that the differences were only in a small range and therefore not significant.

A rough estimate of the number of silanol groups (adsorption positions) on several silica surfaces showed that dependent on the specific surface area the ratio of one of the ion species (concentration of 1 mol/L for the electrolyte) to the adsorption position differs one order of magnitude. Ratios in the same range would be reached with a silica mass fraction of 50 wt%. Nevertheless, an adsorption effect should be notable even in silica mass fraction smaller than 5 wt%. Due to the highest specific surface areas MCM-41 materials have the highest number of adsorption positions. This can be one reason for the strong deviation from volume exclusion assumptions and the strongest decrease in conductivity within the different silica material groups.

- **Rheology**: The missing of a particulate network in the silica dispersions was confirmed in the rheological measurements as they showed mainly Newtonian behavior. Cab-O-Sil showed a special characteristic with a clearly higher viscosity.

Most of the silica dispersions showed Newtonian behavior in rheological measurements except of Cab-O-Sil and SBA-15-octyl. These two materials had higher viscosities and approaches of shear thinning behavior. As expected, all dispersions had higher viscosity with higher amount of filler

material. The overall problem of non-stable dispersions with fast sedimentation was crucial for the rheology and the measurements confirmed that no particle network was present in the dispersions. The special behavior of Cab-O-Sil is considered to be due to the morphology of an aerogel.

- **Electrochemical window**: With the exception of Cab-O-Sil (larger electrochemical window) and SiO_2 nanopowder (smaller electrochemical window), all materials showed the same electrochemical window as the electrolyte without filler material, which might be due to the missing particulate network.

The outstanding behavior of Cab-O-Sil was also present in determination of the electrochemical window. Except of Cab-O-Sil and SiO_2 nanopowder all other silica materials showed in dispersion the same electrochemical window as the pure electrolyte. The smaller electrochemical window of SiO_2 nanopowder might be due to the smaller and more reactive particles. The higher electrochemical window of Cab-O-Sil is considered to be due the special morphology an therefore better dispersion stability. The physical reason for the change of the electrochemical window is unclear.

- **Assessment**: Several different characteristics of silica materials and the constitution of the materials surface have influence on the electrochemical behavior of liquid lithium electrolytes in dispersion.

In conclusion (cf. fig. 6.1), the electrochemical behavior of lithium electrolyte dispersions with silica materials is dependent on the particle morphology and the particle size. The interaction of the ions in the electrolyte with the filler material is influenced by the surface area and the surface charge as well as the porosity. The preferential adsorption of ions and the dissociation of ion pairs can be influenced by the type of surface group.

Summarizing the results of this work, with special design/modification/ functionalization of the surface of silica materials the electrochemical behavior of these materials as filler materials in hybrid electrolytes can be changed. The influence of the nanofillers can be positive and negative for the characteristics of an electrolyte. No hybrid electrolyte with completely positive effect of the filler material on the liquid electrolyte and a noticeable effect on the conductivity, stability (electrochemically and mechanically) and safety could

be reached. Considering the experimental results, a highly conductive liquid lithium electrolyte can only be improved marginally, thus not yet in the way, that the nanofiller concept becomes relevant in practice.

- **Further work**: There is much potential for further work covering different aspects like the network formation and stable dispersions as well as the lithium transference number or safety aspects.

All in all, for future experiments stable dispersions with a network between the particles are essential. Maybe this can be achieved with special gelating additives or addition of electrolytes (mixtures) with higher viscosity like ionic liquids. The challenge is to use materials with a volume fraction such that the good conductivity of the basic electrolyte is only marginally affected. Other approaches are to synthesize materials with a predetermined network or to reach a particle network with the polymerization of special surface groups on the silica surface. The approach of polymerization of surface groups on the silica particle surface was partially realized with PEO surface groups, but needs to be further investigated in a systematic way. As first measurement with predetermined network structure, the investigation of the conductivity behavior of the electrolyte in monoliths with straight channels would be helpful. Yet, the preparation of a monolith with straight channels is a challenge.

Another interesting study in terms of particle networks would be the observation of formation and distribution of particles in the liquid electrolyte. Therefore, SEM investigations are suitable, but the liquid component cannot be examined in the vacuum of the SEM. Considerations in this direction are the investigation of frozen dispersions in the SEM to get a picture of the particle distribution and the potential particle ordering. An alternative is the marking of the particles with fluorescent groups and viewing of the in situ particle formation with a fluorescence microscope like done by Pfaffenhuber et al. [173], where hints for a percolating network might be found.

Of special interest is the determination of the Li^+ transference number in the dispersions. Since only the overall conductivity of anions and cations in the dispersion was measured until now, the interesting information would be, whether the mobility of Li^+ ions can be increased with addition of a filler material. Considering the space charge regions a higher lithium transference number in dispersions can be assumed, if an adsorption process of the anions takes place. So far, it is impossible to measure the lithium transference

number in a reliable way. There are several methods for the determination of t_{Li^+} published, but they are all riddled with errors or not usable for the dispersions. And again, for measurements of this type, stable dispersions are the basic precondition to get reliable information. This was also the problem for the estimation of the lithium transference number by pulsed-field-gradient-NMR (pfg-NMR) measurements. There, the lithium transference number can be estimated by determination of the diffusion coefficient. This measurement was tested in this work, but as the particles sedimented too quickly no reliable values of diffusion coefficients in the dispersions could be achieved.

In terms of safety calorimetry experiments would give information about the influence of filler material on the risk potential of exothermic reaction of the organic electrolyte. Especially, the Accelerating Rate Calorimetry (ACR) enables the investigation of temperature and pressure trends as well as decomposition points under real conditions. Dispersions of the liquid electrolyte with a filler material seemed to have advantages concerning safety aspects, as the liquid component is reduced or even bound in the ideal case. Moreover, as the mechanical characteristics can be changed with addition of filler, the handling of the electrolyte is safer and leakage of batteries may be prohibited with retain of the good conductivity of liquid electrolytes. Hence, the inserting of the electrolyte into the battery during the assembling process requires more effort as for liquid electrolytes. A pasty or gel-like electrolyte need to be placed directly on the active material of the electrodes probably, before insertion of the electrodes into a battery stack.

Finally, there is much potential in the search of appropriate materials for electrolyte dispersions. Although a lot of systematic measurements were done in this work with silica material as filler and an electrolyte with $LiPF_6$ as conducting salt, it is necessary to find more stable filler materials or other conducting salts as well as surface modifications with better surface groups. Filler materials that do not decompose in reaction with the electrolyte, especially with the fluoride containing conducting salt, need to be investigated. Besides the already examined Al_2O_3 or TiO_2 in literature, new inert filler materials can be found. Maybe a closer look to the solid electrolytes like garnets is worthwhile. If the silica material shall be maintained because of advantages like easy preparation and designing of the material, other conducting salts that have comparable conductivity to the $LiPF_6$, but with less or even without release of fluoride need to be synthesized. One promising salt is Li-

FAP. It has shown less release of fluoride and therefore less decomposition reaction, but it was not possible to further examine the salt in this work. The search for modified surface groups on the filler surface that show effects like effective adsorption of the anions PF_6^-, high zeta potentials and leading to a built-up of a particulate network has only started with the presented work.

7 Appendix

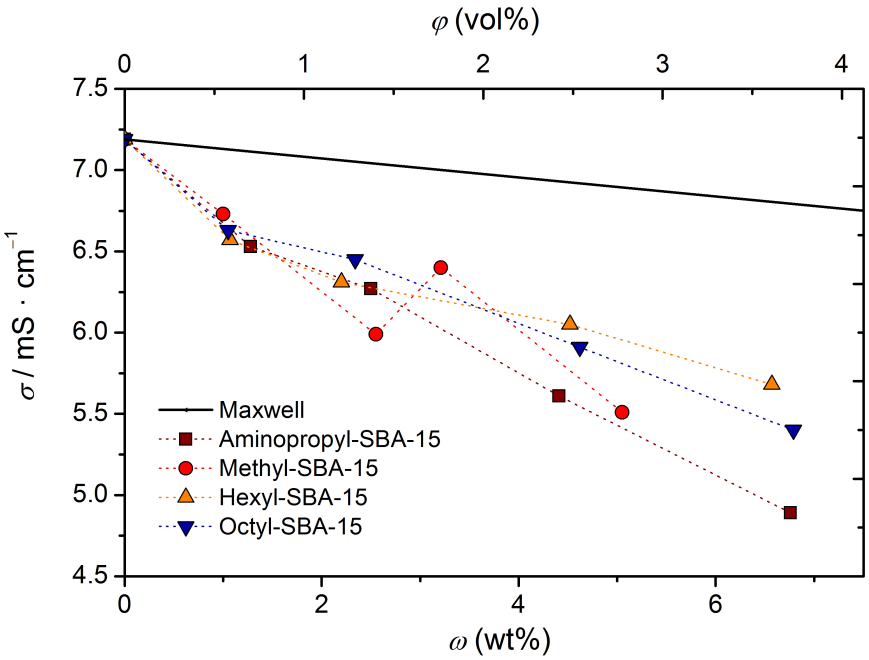

Figure 7.1: Conductivity trend of dispersions with functionalized SBA-15 silica materials at room temperature dependent on the added silica mass fraction.

material	ζ-potential	
	in EC/DEC 3:7 with 0.002 M $LiPF_6$	in EC/DEC 3:7
0.002 M $LiPF_6$ in EC/DECF 3:7	0.4	
EC/DEC 3:7		3.0
SiO_2 S5631	-9.1	-18.0
Cab-O-Sil	-0.3	-3.3
Kieselgel 60	-0.2	-4.3
SiO_2 nanopowder	-3.6	-1.8
SiO_2-nano	-1.5	0.2
SiO_2-nano-Im13-PF_6	6.1	6.3
SBA-15-140	-1.9	-0.7
SBA-15-aminopropyl	8.9	-0.3
SBA-15-octyl	0.1	-10.8
KIT-6-80	0.8	-6.1
KIT-6-140	0.7	-4.9
KIT-6-140-methyl	0.2	-6.3
KIT-6-140-sulfonyl	-0.1	2.7
KIT-6-aminopropyl	5.8	2.0
KIT-6-140-Im13-sulfonic acid	8.5	0.1
KIT-6-140-Im13-PF_6-HDMS	5.8	10.0
KIT-6 -80-PEO1000	4.8	3.8
MCM-41-C12	-2.1	-15.3
MCM-4-C14	9.9	0.1
LiLaTaZrO	-0.1	-7.9

Figure 7.2: Values of the zeta potentials of the dispersions measured with LDV in an electrolyte with 0.0002M $LiPF_6$ in EC/DEC 3:7 and in the pure solvent mixture EC/DEC 3:7.

added filler material	E_a / J · mol^{-1}	ΔE_a / J · mol^{-1}
1M LiPF6 in EC/DEC 3:7	2403.8	131.2
SiO_2 S5631	2211.6	155.0
Cab-O-Sil	2114.2	230.6
Kieselgel 60	2121.1	156.6
SBA-15-50	3104.2	379.5
SBA-15-140	2987.2	109.3
SBA-15-140-aminopropyl	5291.4	1095.8
SBA-15-140-octyl	3172.0	879.0
SiO_2 nanopowder	2352.0	540.2
SiO_2-nano-porous	1958.0	75.4
SiO_2-nano	2140.3	87.0
SiO_2-nano-Im13-PF_6	1880.2	134.5
MCM-41-C12	5751.6	1316.9
MCM-41-C14	4392.2	486.1
MCM-41 C16	1783.9	182.2
MCM-41-C18	3100.3	305.8
KIT-6-80	2583.5	90.2
KIT-6-100	5831.5	832.7
KIT-6-120	2020.4	240.0
KIT-6-140	2282.6	203.9
KIT-6- methyl	2221.7	134.0
KIT-6-140-octyl	2345.5	103.0
KIT-6-hexyl	1663.2	238.3
KIT-6-140-sulfonyl	1750.2	460.4
KIT-6-140-aminopropyl	2861.5	443.8
KIT-6-140-Im-13-PF_6	1825.7	285.4
KIT-6-140-Im13-PF_6-HDMS	2718.8	160.3
KIT-6-140-Im13-Cl	2468.4	118.4
KIT-6-140-Im13-sulfonic acid	1927.8	39.8
KIT-6-80-PEO1000	2067.0	140.1
KIT-6- 120-PEO1000	2616.9	167.9

Figure 7.3: Values of calculated activation energies with the VFT equation and three variables.

added filler material	E_a / J · mol^{-1}	ΔE_a / J · mol^{-1}
1M LiPF6 in EC/DEC 3:7	2392.6	27.2
SiO_2 S5631	2862.8	21.7
Cab-O-Sil	2973.0	31.7
Kieselgel 60	2846.9	24.0
SBA-15-50	2538.8	16.4
SBA-15-140	2383.8	10.9
SBA-15-140-aminopropyl	2252.7	36.4
SBA-15-140-octyl	2247.9	34.7
SiO_2 nanopowder	2734.8	36.4
SiO_2-nano-porous	2409.7	12.7
SiO_2-nano	2963.2	22.8
SiO_2-nano-Im13-PF_6	2882.7	32.5
MCM-41-C12	2089.6	39.0
MCM-41-C14	2271.7	27.6
MCM-41 C16	1880.1	12.9
MCM-41-C18	2369.1	16.6
KIT-6-80	2306.7	1.6
KIT-6-100	2378.5	36.2
KIT-6-120	2263.8	1.8
KIT-6-140	2201.2	12.6
KIT-6- methyl	2744.9	16.6
KIT-6-140-octyl	2761.4	12.9
KIT-6-hexyl	2770.2	46.1
KIT-6-140-sulfonyl	2917.9	61.4
KIT-6-140-aminopropyl	2654.9	25.8
KIT-6-140-Im-13-PF_6	2806.3	43.9
KIT-6-140-Im13-PF_6-HDMS	2892.6	11.9
KIT-6-140-Im13-Cl	2848.8	13.0
KIT-6-140-Im13-sulfonic acid	2869.6	8.0
KIT-6-80-PEO1000	2840.3	24.9
KIT-6- 120-PEO1000	2804.1	12.8

Figure 7.4: Values of calculated activation energies with the VFT equation and a fixed glass temperature of 178 K.

Acknowledgement

First, I would like to thank Prof. Dr. Jürgen Janek for giving me this interesting research theme to work on, for guiding me through my doctoral research studies and the chance to work independently between great scientists, colleagues and friends.

I would like to thank Dr. Bjoern Luerssen for fruitful discussions, funny and serious conversations and strong support. Besides the scientific work you teached me a lot about human behavior, especially talking about the "Lithium Lab". It was a pleasure to work with you. Moreover, I would like to thank you for correcting this dissertation work. This thank also goes to my brother Joachim Sann and my good friend Mareike Wagner in London. Thank you so much.

Many thanks to all the group members of the working group of Prof. Janek at the University Gießen. Thank you for a good time during my PhD thesis. Especially, I would like to thank Nasti for a good work together and the great discussions and conversations. I also want to thank Kveta and Mrs. Majdandzik for their great technical support and encouraging words. Steffie, Alex, Klaus, Marcus, Timo - thank you for a lot of unforgettable memories and much fun. In this context the biggest thank goes to Rabea and Sven for being real good friends over the time. I am so happy to have you both in my life and without you the PhD thesis would have been much harder.

I also would like to thank Prof. Dr. Michael Fröba and his group for the great cooperation, good meetings and helpful discussions. Special thanks to Dr. Jan Roggenbuck and Jan W. Vogel for the preparation of the silica materials.

To my "Semester" - thank you very much for a great time together and I hope we stay in contact.

Many thanks to my best friends Christiane, Mareike, Sarah, Sarvi, Swantje and Verena. Girls, you are amazing and I hope we will have fun and unforgettable moments until we are very old.

Thanks to my partner Tim (and also to his family) - you know me for half of my life. You always believed in me, supported me and calmed me down when I was worried. Thank you so much for being there for me since such a long time.

The most and very special thanks go to my family:

Mama and Papa - thank you so much for your support in every way over the years, for always being there and your encouraging words. To my sister Carolin and my brother Joachim and also their partners - many thanks for your unconditional support and always being there at the right time. I am very grateful to have you as my family as you are the best family one can wish for.

Bibliography

[1] B. Scrosati, J. Hassoun, and Y.-K. Sun. Lithium-ion batteries. A look into the future. *Energy Environ. Sci.*, 4(9):3287–3295, 2011.

[2] V. S. Kolosnitsyn and E. V. Karaseva. Lithium-sulfur batteries: Problems and solutions. 44(5):506–509–, 2008.

[3] X. Ji and L. F. Nazar. Advances in Li-S batteries. *J. Mater. Chem.*, 20(44):9821–9826, 2010.

[4] G. Girishkumar, B. McCloskey, A. C. Luntz, S. Swanson, and W. Wilcke. Lithium-Air Battery: Promise and Challenges. *J. Phys. Chem. Lett.*, 1(14):2193–2203, July 2010.

[5] V. Etacheri, R. Marom, R. Elazari, G. Salitra, and D. Aurbach. Challenges in the development of advanced Li-ion batteries: a review. *Energy Environ. Sci.*, 4(9):3243–3262, 2011.

[6] J. Cabana, L. Monconduit, D. Larcher, and M. R. Palacon. Beyond Intercalation-Based Li-Ion Batteries: The State of the Art and Challenges of Electrode Materials Reacting Through Conversion Reactions. *Adv. Mater.*, 22(35):E170–E192, 2010.

[7] R. A. Huggins. *Advanced Batteries*. Springer, 2009.

[8] B. Scrosati and J. Garche. Lithium batteries: Status, prospects and future. *J. Power Sources*, 195(9):2419–2430, 2010.

[9] D. Aurbach, Y. Talyosef, B. Markovsky, E. Markevich, E. Zinigrad, L. Asraf, J. S. Gnanaraj, and H.-J. Kim. Design of electrolyte solutions for Li and Li-ion batteries: a review. *Electrochim. Acta*, 50(2-3):247–254, November 2004.

[10] J. M. Tarascon and M. Armand. Issues and challenges facing rechargeable lithium batteries. *Nature*, 414(6861):359–367, November 2001.

[11] J. W. Fergus. Ceramic and polymeric solid electrolytes for lithium-ion batteries. *J. Power Sources*, 195(15):4554–4569, August 2010.

[12] K. Sann, J. Roggenbuck, N. Krawczyk, H. Buschmann, B. Luerßen, M. Fröba, and J. Janek. Conductivity of liquid lithium electrolytes with dispersed mesoporous silica particles. *Electrochim. Acta*, 60(0):1–6, January 2012.

[13] N. Kamaya, K. Homma, Y. Yamakawa, M. Hirayama, R. Kanno, M. Yonemura, T. Kamiyama, Y. Kato, S. Hama, K. Kawamoto, and A. Mitsui. A lithium superionic conductor. *Nat Mater*, 10(9):682–686, September 2011.

[14] J. Li, C. Daniel, and D. Wood. Materials processing for lithium-ion batteries. *Journal of Power Sources*, 196(5):2452–2460, March 2011.

[15] A. Lewandowski and A. Swiderska-Mocek. Ionic liquids as electrolytes for Li-ion batteries: an overview of electrochemical studies. *J. Power Sources*, 194(2):601–609, 2009.

[16] V. Aravindan, J. Gnanaraj, S. Madhavi, and H.-K. Liu. Lithium-Ion Conducting Electrolyte Salts for Lithium Batteries. *Chem. Eur. J.*, 17(51):14326–14346, 2011.

[17] S. S. Zhang. A review on electrolyte additives for lithium-ion batteries. *J. Power Sources*, 162(2):1379–1394, 2006.

[18] J. Maier. Enhancement of ionic conductivity in solid-solid-dispersions by surface induced defects. *Ber. Bunsenges. Phys. Chem*, 88:1057–1062, 1984.

[19] C. C. Liang. Conduction Characteristics of the Lithium Iodide-Aluminum Oxide Solid Electrolytes. *J. Electrochem. Soc.*, 120:1289–1292, 1973.

[20] J. Maier. Space charge regions in solid two-phase systems and their conduction contribution - I. Conductance enhancement in the system ionic conductor-'inert' phase and application on AgCl:Al_2O_3 and AgCl:SiO_2. *J. Phys. Chem. Solids*, 46(3):309–320, 1985.

[21] J. Maier. Defect chemistry and conductivity effects in heterogeneous solid electrolytes. *J. Electrochem. Soc.*, 134:1524–1535, 1987.

[22] A. J. Bhattacharyya, M. Dollé, and J. Maier. Improved Li-Battery Electrolytes by Heterogeneous Doping of Nonaqueous Li-Salt Solutions. *Electrochem. Solid-State Lett.*, 7:A432–A434, 2004.

[23] A. J. Bhattacharyya and J. Maier. Second Phase Effects on the Conductivity of Non-Aqueous Salt Solutions: "Soggy Sand Electrolytes". *Adv. Mater.*, 16(9-10):811–814, 2004.

[24] A. J. Bhattacharyya, J. Maier, R. Bock, and F. F. Lange. New class of soft matter electrolytes obtained via heterogeneous doping: Percolation effects in "soggy sand" electrolytes. *Solid State Ionics*, 177(26-32):2565–2568, October 2006.

[25] U.-H. Lee, T. Kudo, and I. Honma. High-ion conducting solidified hybrid electrolytes by the self-assembly of ionic liquids and TiO_2. *Chem. Commun.*, (21):3068–3070, 2009.

[26] P. Raghavan, X. Zhao, J. Manuel, G. S. Chauhan, J.-H. Ahn, H.-S. Ryu, H.-J. Ahn, K.-W. Kim, and C. Nah. Electrochemical performance of electrospun poly(vinylidene fluoride-co-hexafluoropropylene)-based nanocomposite polymer electrolytes incorporating ceramic fillers and room temperature ionic liquid. *Electrochim. Acta*, 55(4):1347–1354, January 2010.

[27] J. Le Bideau, L. Viau, and A. Vioux. Ionogels, ionic liquid based hybrid materials. *Chem. Soc. Rev.*, 40(2):907–925, 2011.

[28] A. Wittmar, D. Ruiz-Abad, and M. Ulbricht. Dispersions of silica nanoparticles in ionic liquids investigated with advanced rheology. 14(2):1–10, 2012.

[29] N. Krawczyk, K. Sann, S. Kraas, A. Schlifke, J. W. Vogel, B. Luerßen, M. Fröba, and J. Janek. Electrochemical Characterization of Ionic Liquid Based Composite Electrolytes for Lithium-Ion Batteries. In *Meeting Abstracts*, number 12, pages 1209–1209. The Electrochemical Society, 2012.

[30] S. Ramesh and C.-W. Liew. Exploration on nano-composite fumed silica-based composite polymer electrolytes with doping of ionic liquid. *J. Non-Cryst. Solids*, 358(5):931–940, 2012.

[31] J. Syzdek, R. Borkowska, K. Perzyna, J. M. Tarascon, and W. Wieczorek. Novel composite polymeric electrolytes with surface-modified inorganic fillers. *J. Power Sources*, 173(2):712–720, November 2007.

[32] H. Mazor, D. Golodnitsky, E. Peled, W. Wieczorek, and B. Scrosati. A search for a single-ion-conducting polymer electrolyte: Combined effect of anion trap and inorganic filler. *J. Power Sources*, 178(2):736–743, April 2008.

[33] X.-L. Wang, Q. Cai, L.-Z. Fan, T. Hua, Y.-H. Lin, and C.-W. Nan. Gel-based composite polymer electrolytes with novel hierarchical mesoporous silica network for lithium batteries. *Electrochim. Acta*, 53(27):8001–8007, November 2008.

[34] J. Kim, S.-J. Park, and S. Kim. Electrochemical properties of composite electrolytes based on poly (ethylene oxide)/poly (ethylene imine) containing the inorganic silica fillers. *J. Nanosci. Nanotechnol.*, 12(1):685–689, 2012.

[35] C. Tang, K. Hackenberg, Q. Fu, P. M. Ajayan, and H. Ardebili. High ion conducting polymer nanocomposite electrolytes using hybrid nanofillers. *Nano Lett.*, 12(3):1152–1156, 2012.

[36] C. Pfaffenhuber, F. Hoffmann, M. Fröba, J. Popovic, and J. Maier. Soggy-sand effects in liquid composite electrolytes with mesoporous materials as fillers. *J. Mater. Chem. A*, 1(40):12560–12567, 2013.

[37] Y. L. Yap, A. H. You, L. L. Teo, and H. Hanapei. Inorganic Filler Sizes Effect on Ionic Conductivity in Polyethylene Oxide (PEO) Composite Polymer Electrolyte. *Int. J. Electrochem. Sci.*, 8:2154–2163, 2013.

[38] F. Croce, L. Persi, B. Scrosati, F. Serraino-Fiory, E. Plichta, and M. A. Hendrickson. Role of the ceramic fillers in enhancing the transport properties of composite polymer electrolytes. *Electrochim. Acta*, 46(16):2457–2461, May 2001.

[39] Q. Li, J. Chen, L. Fan, X. Kong, and Y. Lu. Progress in electrolytes for rechargeable li-based batteries and beyond. *Green Energy & Environment*, 2016 (in press).

[40] M. Marcinek, J. Syzdek, M. Marczewski, M. Piszcz, L. Niedzicki, M. Kalita, A. Plewa-Marczewska, A. Bitner, P. Wieczorek, and T. Trzeciak. Electrolytes for li-ion transport - review. *Solid State Ionics*, 276:107–126, 2015.

[41] K. Xu. Electrolytes and interphases in li-ion batteries and beyond. *Chemical reviews*, 114(23):11503–11618, 2014.

[42] J. Scheers, S. Fantini, and P. Johansson. A review of electrolytes for lithium-sulphur batteries. *Journal of Power Sources*, 255:204–218, 2014.

[43] M. Balaish, A. Kraytsberg, and Y. Ein-Eli. A critical review on lithium-air battery electrolytes. *Physical Chemistry Chemical Physics*, 16(7):2801–2822, 2014.

[44] H. Buschmann. *Charakterisierung mesodisperser Komposit-Elektrolyte für Lithiumionen-Hochleistungsbatterien*. Justus-Liebig-Universität Gießen, 2008.

[45] J. B. Goodenough and Y. Kim. Challenges for Rechargeable Li Batteries. *Chem. Mater.*, 22(3):587–603, August 2009.

[46] C. P. Rhodes, M. Mullings, and R. Lopez. Advanced Non-Flammable Electrolytes for Li-Ion Batteries. *Meeting Abstracts*, MA2012-01(9):539, 2012.

[47] K. Xu, Y. Lam, S. S. Zhang, T. R. Jow, and T. B. Curtis. Solvation Sheath of Li^+ in Nonaqueous Electrolytes and Its Implication of Graphite/Electrolyte Interface Chemistry. *J. Phys. Chem. C*, 111(20):7411–7421, May 2007.

[48] J. M. Tarascon and D. Guyomard. New electrolyte compositions stable over the 0 to 5 V voltage range and compatible with the $Li_{1+x}Mn_2O_4$/carbon Li-ion cells. *Solid State Ionics*, 69(3-4):293–305, August 1994.

[49] C. A. Vincent and B. Scrosati. *Modern Batteries*. Butterworth-Heinemann, 1997.

[50] J. O. Besenhard and H. P. Fritz. Cathodic reduction of graphite in organic solutions of alkali and $NR_4{}^+$ salts. *J. Electroanal. Chem.*, 53(2):329–333, 1974.

[51] K. Xu. Nonaqueous liquid electrolytes for lithium-based rechargeable batteries. *Chemical reviews*, 104(10):4303–4418, 2004.

[52] K. Xu, S. Zhang, T. R. Jow, W. U. Xu, and C. A. Angell. LiBOB as salt for lithium-ion batteries: A possible solution for high temperature operation. *Electrochem. Solid-State Lett.*, 5(1):A26–A29, 2002.

[53] J. S. Gnanaraj, M. D. Levi, Y. Gofer, D. Aurbach, and M. Schmidt. $LiPF_3(CF_2CF_3)_3$: A Salt for Rechargeable Lithium Ion Batteries. *J. Electrochem. Soc.*, 150(4):A445–A454, 2003.

[54] S. E. Sloop, J. K. Pugh, S. Wang, J. B. Kerr, and K. Kinoshita. Chemical Reactivity of PF_5 and $LiPF_6$ in Ethylene Carbonate/Dimethyl Carbonate Solutions. *Electrochem. Solid-State Lett.*, 4(4):A42–A44, 2001.

[55] D. Aurbach, K. Gamolsky, B. Markovsky, G. Salitra, Y. Gofer, U. Heider, R. Oesten, and M. Schmidt. The study of surface phenomena related to electrochemical lithium intercalation into Li_xMO_y host materials (M=Ni, Mn). *J. Electrochem. Soc.*, 147(4):1322–1331, 2000.

[56] K. Ozawa. *Lithium Ion Rechargeable Batteries: Materials, Technology, and New Applications*. Wiley. com, 2012.

[57] D. E. Fenton, J. M. Parker, and P. V. Wright. Complexes of alkali metal ions with poly(ethylene oxide). *Polymer*, 14(11):589, 1973.

[58] A. M. Stephan and K. S. Nahm. Review on composite polymer electrolytes for lithium batteries. *Polymer*, 47(16):5952–5964, 2006.

[59] F. M. Gray. *Polymer electrolytes*. Springer Verlag, 1997.

[60] M. Armand. Polymer solid electrolytes - an overview. *Solid State Ionics*, 9:745–754, 1983.

[61] J. Y. Song, Y. Y. Wang, and C. C. Wan. Review of gel-type polymer electrolytes for lithium-ion batteries. *J. Power Sources*, 77(2):183–197, 1999.

[62] A. Fernicola, B. Scrosati, and H. Ohno. Potentialities of ionic liquids as new electrolyte media in advanced electrochemical devices. *Ionics*, 12(2):95–102, 2006.

[63] A. Basile, A. F. Hollenkamp, A. I. Bhatt, and A. P. O'Mullane. Extensive charge-discharge cycling of lithium metal electrodes achieved using ionic liquid electrolytes. *Electrochem. Commun.*, 27:69–72, 2012.

[64] M. J. Marczewski, Y. J. Choi, J. Scheers, A. Matic, P. Jacobsson, and P. Johansson. Ionic Liquid-In-Salt: Characterization of Electrolytes for High Temperature Lithium Batteries. In *Meeting Abstracts*, number 12, pages 1226–1226. The Electrochemical Society, 2012.

[65] J. Hassoun, A. Fernicola, M. A. Navarra, S. Panero, and B. Scrosati. An advanced lithium-ion battery based on a nanostructured Sn-anode and an electrochemically stable LiTFSI-Py_{24} TFSI ionic liquid electrolyte. *J. Power Sources*, 195(2):574–579, 2010.

[66] M. Armand, F. Endres, D. R. MacFarlane, H. Ohno, and B. Scrosati. Ionic-liquid materials for the electrochemical challenges of the future. *Nat. Mater.*, 8(8):621–629, 2009.

[67] A. Fernicola, F. Croce, B. Scrosati, T. Watanabe, and H. Ohno. LiTFSI-BEPyTFSI as an improved ionic liquid electrolyte for rechargeable lithium batteries. *J. Power Sources*, 174(1):342–348, 2007.

[68] H. Matsumoto, H. Sakaebe, K. Tatsumi, M. Kikuta, E. Ishiko, and M. Kono. Fast cycling of Li/$LiCoO_2$ cell with low-viscosity ionic

liquids based on bis(fluorosulfonyl)imide[FSI]$^-$. *J. Power Sources*, 160(2):1308–1313, 2006.

[69] S. Seki, Y. Kobayashi, H. Miyashiro, Y. Ohno, A. Usami, Y. Mita, N. Kihira, M. Watanabe, and N. Terada. Lithium secondary batteries using modified-imidazolium room-temperature ionic liquid. *J. Phys. Chem. B*, 110(21):10228–10230, 2006.

[70] A. Guerfi, M. Dontigny, P. Charest, M. Petitclerc, M. Lagacè, A. Vijh, and K. Zaghib. Improved electrolytes for Li-ion batteries: Mixtures of ionic liquid and organic electrolyte with enhanced safety and electrochemical performance. *J. Power Sources*, 195(3):845–852, 2010.

[71] R. S. Kühnel, N. Bückenfeld, S. Passerini, M. Winter, and A. Balducci. Mixtures of ionic liquid and organic carbonate as electrolyte with improved safety and performance for rechargeable lithium batteries. *Electrochim. Acta*, 56(11):4092–4099, April 2011.

[72] S. Berendts, H. Buschmann, J. Reinacher, and J. Janek. Li-Ion Conducting Garnet-Type Materials: Structure and Electrochemical Characterization. *Z. anorg. allg. Chem.*, 638(10):1623–1623, 2012.

[73] P. Hartmann, T. Leichtweiss, M. R. Busche, M. Schneider, M. Reich, J. Sann, P. Adelhelm, and J. Janek. Degradation of NASICON-Type Materials in Contact with Lithium Metal: Formation of Mixed Conducting Interphases (MCI) on Solid Electrolytes. *J. Phys. Chem. C*, 117(41):21064–21074, October 2013.

[74] C. Czeslik, H. Seemann, and R. Winter. *Basiswissen Physikalische Chemie*. Teubner, 2001.

[75] C. H. Hamann and W. Vielstich. *Elektrochemie, 3. Auflage*. Wiley-VCH, 1998.

[76] S. Zugmann, M. Fleischmann, M. Amereller, R. M. Gschwind, H. D. Wiemhöfer, and H. J. Gores. Measurement of transference numbers for lithium ion electrolytes via four different methods, a comparative study. *Electrochim. Acta*, 56(11):3926–3933, April 2011.

[77] H. Schmalzried. Point defects in ternary ionic crystals. *Prog. Solid State Chem.*, 2(0):265–303, 1965.

[78] J. Frenkel. Über die Wärmebewegung in festen und flüssigen Körpern. *Zeitschrift für Physik*, 35(8-9):652–669, 1926.

[79] C. Wagner and W. Schottky. Theorie der geordneten Mischphasen. *Z. Phys. Chem. B*, 11:163–210, 1930.

[80] C. Wagner. Über den Mechanismus der Bildung von Ionenverbindungen höherer Ordnung (Doppelsalze, Spinelle, Silikate). *Z. phys. Chem*, 1936.

[81] W. H. Meyer. Polymer Electrolytes for Lithium-Ion Batteries. *Adv. Mater.*, 10:439–448, 1998.

[82] H. Vogel. Das Temperaturabhängigkeitsgesetz der Viskosität von Flüssigkeiten. *Phys. Z*, 22(645):645–646, 1921.

[83] G. S. Fulcher. Analysis of recent measurements of the viscosity of glasses. *Journal of the American Ceramic Society*, 8(6):339–355, 1925.

[84] G. Tammann and W. Hesse. Die Abhängigkeit der Viscosität von der Temperatur bei unterkühlten Flüssigkeiten. *Z. Anorg. Allg. Chem.*, 156(1):245–257, 1926.

[85] M. L. Williams, R. F. Landel, and J. D. Ferry. The temperature dependence of relaxation mechanisms in amorphous polymers and other glass-forming liquids. *Journal of the American Chemical Society*, 77(14):3701–3707, 1955.

[86] A. Killis, J.-F. LeNest, H. Cheradame, and A. Gandini. Ionic conductivity of polyether-polyurethane networks containing $NaBPh_4$: A free volume analysis. *Die Makromolekulare Chemie*, 183(11):2835–2845, 1982.

[87] M. Armand. Polymers with Ionic Conductivity. *Adv. Mater.*, 2(6-7):278–286, 1990.

[88] C. Wagner. The electrical conductivity of semi-conductors involving inclusions of another phase. *J. Phys. Chem. Solids*, 33(5):1051–1059, 1972.

[89] J. C. Maxwell. *A treatise on electricity and magnetism*. Dover Publications Inc., 1891.

[90] J. B. Wagner Jr. Transport in compounds containing a dispersed second phase. *Mater. Res. Bull.*, 15(12):1691–1701, December 1980.

[91] J. E. Weston and B. C. H. Steele. Effects of inert fillers on the mechanical and electrochemical properties of lithium salt-poly(ethylene oxide) polymer electrolytes. *Solid State Ionics*, 7(1):75–79, August 1982.

[92] S. A. Khan, G. L. Baker, and S. Colson. Composite polymer electrolytes using fumed silica fillers: Rheology and ionic conductivity. *Chem. Mater.*, 6(12):2359–2363, 1994.

[93] F. Capuano, F. Croce, and B. Scrosati. Composite polymer electrolytes. *J. Electrochem. Soc.*, 138(7):1918–1922, 1991.

[94] E. Quartarone, P. Mustarelli, and A. Magistris. PEO-based composite polymer electrolytes. *Solid State Ionics*, 110(1):1–14, 1998.

[95] J. Zhang, X. Huang, H. Wei, J. Fu, Y. Huang, and X. Tang. Enhanced electrochemical properties of polyethylene oxide-based composite solid polymer electrolytes with porous inorganic-organic hybrid polyphosphazene nanotubes as fillers. *J. Solid State Electrochem.*, 16(1):101–107, 2012.

[96] S. Kalnaus, A. S. Sabau, W. E. Tenhaeff, N. J. Dudney, and C. Daniel. Design of composite polymer electrolytes for Li ion batteries based on mechanical stability criteria. *J. Power Sources*, 201:280–287, 2012.

[97] G. Katsaros, T. Stergiopoulos, I. M. Arabatzis, K. G. Papadokostaki, and P. Falaras. A solvent-free composite polymer/inorganic oxide electrolyte for high efficiency solid-state dye-sensitized solar cells. *Journal of Photochemistry and Photobiology A: Chemistry*, 149(1):191–198, 2002.

[98] J. H. Kim, M.-S. Kang, Y. J. Kim, J. Won, N.-G. Park, and Y. S. Kang. Dye-sensitized nanocrystalline solar cells based on composite polymer electrolytes containing fumed silica nanoparticles. *Chem. Commun.*, (14):1662–1663, 2004.

[99] Y. Wang. Recent research progress on polymer electrolytes for dye-sensitized solar cells. *Solar Energy Materials and Solar Cells*, 93(8):1167–1175, 2009.

[100] Q. Li, R. He, J. O. Jensen, and N. J. Bjerrum. Approaches and recent development of polymer electrolyte membranes for fuel cells operating above $100\,^{\circ}\mathrm{C}$. *Chem. Mater.*, 15(26):4896–4915, 2003.

[101] K. Stewart. TiO_2 Nanotubes based composite polymer electrolytes for Fuel cells. *Project work*, 2012.

[102] A. Kumar and M. Deka. PEO/P (VdF-HFP) blend based Li^+ ion-conducting composite polymer electrolytes dispersed with dedoped (insulating) polyaniline nanofibers. *J. Solid State Electrochem.*, 16(1):35–44, 2012.

[103] M. Osinska, M. Walkowiak, A. Zalewska, and T. Jesionowski. Study of the role of ceramic filler in composite gel electrolytes based on microporous polymer membranes. *J. Membr. Sci.*, 326(2):582–588, January 2009.

[104] W. V. Edwards, A. J. Bhattacharyya, A. V. Chadwick, and J. Maier. An XAS study of the local environment of ions in soggy sand electrolytes. *Electrochemical and solid-state letters*, 9(12):A564–A567, 2006.

[105] A. J. Bhattacharyya, M. Patel, and S. K. Das. Soft matter lithium salt electrolytes: ion conduction and application to rechargeable batteries. *Monatshefte für Chemie-Chemical Monthly*, 140(9):1001–1010, 2009.

[106] Y. Lu, S. S. Moganty, J. L. Schaefer, and L. A. Archer. Ionic liquid-nanoparticle hybrid electrolytes. *J. Mater. Chem.*, 22(9):4066–4072, 2012.

[107] L. Suo, Y.-S. Hu, H. Li, M. Armand, and L. Chen. A new class of Solvent-in-Salt electrolyte for high-energy rechargeable metallic lithium batteries. *Nature communications*, 4:1481, 2013.

[108] K. Ueno, K. Yoshida, M. Tsuchiya, N. Tachikawa, K. Dokko, and M. Watanabe. Glyme-Lithium Salt Equimolar Molten Mixtures: Concentrated Solutions or Solvate Ionic Liquids? *J. Phys. Chem. B*, 116(36):11323–11331, 2012.

[109] L. Rayleigh. LVI. On the influence of obstacles arranged in rectangular order upon the properties of a medium. *The London, Edinburgh, and Dublin Philosophical Magazine and Journal of Science*, 34(211):481–502, 1892.

[110] K. Feitosa, S. Marze, A. Saint-Jalmes, and D. J. Durian. Electrical conductivity of dispersions: from dry foams to dilute suspensions. *J. Phys.: Condens. Matter*, 17(41):6301, 2005.

[111] H. L. Duan, B. L. Karihaloo, J. Wang, and X. Yi. Effective conductivities of heterogeneous media containing multiple inclusions with various spatial distributions. *Phys. Rev. B*, 73(17):174203–, May 2006.

[112] R. Lemlich. A theory for the limiting conductivity of polyhedral foam at low density. *J. Colloid Interface Sci.*, 64(1):107–110, March 1978.

[113] C. Korte, N. Schichtel, D. Hesse, and J. Janek. Influence of interface structure on mass transport in phase boundaries between different ionic materials. *Monatshefte für Chemie-Chemical Monthly*, 140(9):1069–1080, 2009.

[114] T. Jow and J. B. Wagner Jr. The Effect of Dispersed Alumina Particles on the Electrical Conductivity of Cuprous Chloride. *J. Electrochem. Soc.*, 126:1963–1972, 1979.

[115] K. L. Kliewer and J. S. Koehler. Space Charge in Ionic Crystals. I. General Approach with Application to NaCl. *Phys. Rev.*, 140(4A):A1226–A1240, November 1965.

[116] K. Shahi and J. B. Wagner Jr. Ionic Conductivity and Thermoelectric Power of Pure and Al_2O_3 Dispersed AgI. *J. Electrochem. Soc.*, 128:6–13, 1981.

[117] A. M. Stoneham, E. Wade, and J. A. Kilner. A model for the fast ionic diffusion in alumina-doped LiI. *Mater. Res. Bull.*, 14(5):661–666, May 1979.

[118] S. Jiang and J. B. Wagner Jr. A theoretical model for composite electrolytes - II. Percolation model for ionic conductivity enhancement. *J. Phys. Chem. Solids*, 56(8):1113–1124, August 1995.

[119] J. Maier. Ionic conduction in space charge regions. *Prog. Solid St. Chem.*, 23:171–263, 1995.

[120] J. Maier. Composite electrolytes. *Materials chemistry and physics*, 17(5):485–498, 1987.

[121] J. W. Essam. Percolation theory. *Rep. Prog. Phys.*, 43(7):833–912, 1980.

[122] S. R. Broadbent and J. M. Hammersley. Percolation processes, I. Crystals and mazes. *Proc. Camb. Phil. Soc.*, 53:629–641, 1957.

[123] P. Balaya, A. J. Bhattacharyya, J. Jamnik, Y. F. Zhukovskii, E. A. Kotomin, and J. Maier. Nano-ionics in the context of lithium batteries. *J. Power Sources*, 159(1):171–178, September 2006.

[124] S. Kirkpatrick. Percolation and Conduction. *Rev. Mod. Phys.*, 45(4):574–588, October 1973.

[125] M. E. Fisher and J. W. Essam. Some Cluster Size and Percolation Problems. *J. Math. Phys.*, 2(4):609–619, July 1961.

[126] A. Bunde and W. Dieterich. Percolation in Composites. *J. Electroceram.*, 5(2):81–92, 2000.

[127] A. Kapitulnik, A. Aharony, G. Deutscher, and D. Stauffer. Self similarity and correlations in percolation. *Journal of Physics A: Mathematical and General*, 16(8):L269, 1983.

[128] D. Stauffer. Scaling theory of percolation clusters. *Physics Reports*, 54(1):1–74, July 1979.

[129] Y. Gefen, A. Aharony, B. B. Mandelbrot, and S. Kirkpatrick. Solvable Fractal Family and Its Possible Relation to the Backbone at Percolation. *Phys. Rev. Lett.*, 47:1771–1774, 1981.

[130] A. Kapitulnik and G. Deutscher. Percolation Characteristics in Discontinuous Thin Films of Pb. *Phys. Rev. Lett.*, 49(19):1444–1448, November 1982.

[131] A. Jarosik, U. Traub, J. Maier, and A. Bunde. Ion conducting particle networks in liquids: modeling of network percolation and stability. *Phys. Chem. Chem. Phys.*, 13(7):2663–2666, 2011.

[132] F. Hoffmann, M. Cornelius, J. Morell, and M. Fröba. Silica-Based Mesoporous Organic-Inorganic Hybrid Materials. *Angewandte Chemie International Edition*, 45(20):3216–3251, 2006.

[133] J. Fan and P. S. Fedkiw. Composite electrolytes prepared from fumed silica, polyethylene oxide oligomers, and lithium salts. *J. Electrochem. Soc.*, 144(2):399–408, 1997.

[134] S. R. Raghavan, M. W. Riley, P. S. Fedkiw, and S. A. Khan. Composite Polymer Electrolytes Based on Poly(ethylene glycol) and Hydrophobic Fumed Silica:Dynamic Rheology and Microstructure. *Chem. Mater.*, 10(1):244–251, January 1998.

[135] H. J. Walls, J. Zhou, J. A. Yerian, P. S. Fedkiw, S. A. Khan, M. K. Stowe, and G. L. Baker. Fumed silica-based composite polymer electrolytes: synthesis, rheology, and electrochemistry. *J. Power Sources*, 89(2):156–162, August 2000.

[136] X. He, Q. Shi, X. Zhou, C. Wan, and C. Jiang. In situ composite of nano SiO_2-P (VDF-HFP) porous polymer electrolytes for Li-ion batteries. *Electrochim. Acta*, 51(6):1069–1075, 2005.

[137] K.-H. Lee, Y.-G. Lee, J.-K. Park, and D.-Y. Seung. Effect of silica on the electrochemical characteristics of the plasticized polymer electrolytes based on the P(AN-co-MMA) copolymer. *Solid State Ionics*, 133(3):257–263, August 2000.

[138] J. T. Park, K. J. Lee, M.-S. Kang, Y. S. Kang, and J. H. Kim. Nanocomposite polymer electrolytes containing silica nanoparticles: Comparison between poly (ethylene glycol) and poly (ethylene oxide) dimethyl ether. *J. Appl. Polym. Sci.*, 106(6):4083–4090, 2007.

[139] X.-W. Zhang, Y. Li, S. A. Khan, and P. S. Fedkiw. Inhibition of lithium dendrites by fumed silica-based composite electrolytes. *J. Electrochem. Soc.*, 151(8):A1257–A1263, 2004.

[140] J. Xi, X. Qiu, X. Ma, M. Cui, J. Yang, X. Tang, W. Zhu, and L. Chen. Composite polymer electrolyte doped with mesoporous silica SBA-15 for lithium polymer battery. *Solid State Ionics*, 176(13):1249–1260, 2005.

[141] X.-L. Wang, A. Mei, M. Li, Y. Lin, and C.-W. Nan. Effect of silane-functionalized mesoporous silica SBA-15 on performance of PEO-based composite polymer electrolytes. *Solid State Ionics*, 177(15):1287–1291, 2006.

[142] H.-M. Kao, Y.-Y. Tsai, and S.-W. Chao. Functionalized mesoporous silica MCM-41 in poly (ethylene oxide)-based polymer electrolytes: NMR and conductivity studies. *Solid State Ionics*, 176(13):1261–1270, 2005.

[143] Y.-S. Lee, S. H. Ju, J.-H. Kim, S. S. Hwang, J.-M. Choi, Y.-K. Sun, H. Kim, B. Scrosati, and D.-W. Kim. Composite gel polymer electrolytes containing core-shell structured $SiO_2(Li^+)$ particles for lithium-ion polymer batteries. *Electrochem. Commun.*, 17:18–21, 2012.

[144] G. Jiang, S. Maeda, H. Yang, Y. Saito, S. Tanase, and T. Sakai. All solid-state lithium-polymer battery using poly(urethane acrylate)/nano-SiO_2 composite electrolytes. *J. Power Sources*, 141(1):143–148, February 2005.

[145] Y. Fu, X. Ma, Q. Yang, and X. Zong. The effect of fumed silica on the interfacial stability in the polymer gel electrolyte. *Mater. Lett.*, 57(11):1759–1764, 2003.

[146] P. L. Antonucci, A. S. Aricò, P. Cretì, E. Ramunni, and V. Antonucci. Investigation of a direct methanol fuel cell based on a composite

Nafion®-silica electrolyte for high temperature operation. *Solid State Ionics*, 125(1-4):431–437, October 1999.

[147] P. Wang, S. M. Zakeeruddin, P. Comte, I. Exnar, and M. Grätzel. Gelation of Ionic Liquid-Based Electrolytes with Silica Nanoparticles for Quasi-Solid-State Dye-Sensitized Solar Cells. *J. Am. Chem. Soc.*, 125(5):1166–1167, January 2003.

[148] Y. Fang, J. Zhang, X. Zhou, Y. Lin, and S. Fang. A novel thixotropic and ionic liquid-based gel electrolyte for efficient dye-sensitized solar cells. *Electrochim. Acta*, 68:235–239, 2012.

[149] S. Sambandam and V. Ramani. SPEEK/functionalized silica composite membranes for polymer electrolyte fuel cells. *J. Power Sources*, 170(2):259–267, 2007.

[150] Y. Fan, J. Wang, Z. Tang, W. He, and J. Zhang. Effects of the nanostructured SiO_2 coating on the performance of $LiNi_{0.5}Mn_{1.5}O_4$ cathode materials for high-voltage Li-ion batteries. *Electrochim. Acta*, 52(11):3870–3875, 2007.

[151] J. Zhou, P. S. Fedkiw, and S. A. Khan. Interfacial stability between lithium and fumed silica-based composite electrolytes. *J. Electrochem. Soc.*, 149(9):A1121–A1126, 2002.

[152] T. Echelmeyer, H. W. Meyer, and L. van Wüllen. Novel Ternary Composite Electrolytes: Li Ion Conducting Ionic Liquids in Silica Glass. *Chem. Mater.*, 21(11):2280–2285, April 2009.

[153] M.-A. Nèouze, J. Le Bideau, P. Gaveau, S. Bellayer, and A. Vioux. Ionogels, new materials arising from the confinement of ionic liquids within silica-derived networks. *Chem. Mater.*, 18(17):3931–3936, 2006.

[154] Y. Lu, S. S. Moganty, J. L. Schaefer, and L. A. Archer. Ionic liquid-nanoparticle hybrid electrolytes. *J. Mater. Chem.*, 22(9):4066–4072, 2012.

[155] D. Zhao, J. Feng, Q. Huo, N. Melosh, G. H. Fredrickson, B. F. Chmelka, and G. D. Stucky. Triblock Copolymer Syntheses of Mesoporous Silica

with Periodic 50 to 300 Angstrom Pores. *Science*, 279(5350):548–552, January 1998.

[156] F. Kleitz, S. Hei Choi, and R. Ryoo. Cubic Ia3d large mesoporous silica: synthesis and replication to platinum nanowires, carbon nanorods and carbon nanotubes. *Chem. Commun.*, 17(17):2136–2137, 2003.

[157] J. C. Vartuli, K. D. Schmitt, C. T. Kresge, W. J. Roth, M. E. Leonowicz, S. B. McCullen, S. D. Hellring, J. S. Beck, and J. L. Schlenker. Effect of Surfactant/Silica Molar Ratios on the Formation of Mesoporous Molecular Sieves: Inorganic Mimicry of Surfactant Liquid-Crystal Phases and Mechanistic Implications. *Chem. Mater.*, 6(12):2317–2326, December 1994.

[158] J. C. Moreira and Y. Gushikem. Preconcentration of metal ions on silica gel modified with 3(1-imidazolyl)propyl groups. *Anal. Chim. Acta*, 176(0):263–267, 1985.

[159] A. M. Lazarin, Y. Gushikem, and S. C. de Castro. Cellulose aluminium oxide coated with organofunctional groups containing nitrogen donor atoms. *J. Mater. Chem.*, 10(11):2526–2531, 2000.

[160] M.-H. Kim, H.-K. Na, Y.-K. Kim, S.-R. Ryoo, H. S. Cho, K. E. Lee, H. Jeon, R. Ryoo, and D.-H. Min. Facile Synthesis of Monodispersed Mesoporous Silica Nanoparticles with Ultralarge Pores and Their Application in Gene Delivery. *ACS Nano*, 5(5):3568–3576, March 2011.

[161] W. Stöber, A. Fink, and E. Bohn. Controlled growth of monodisperse silica spheres in the micron size range. *J. Colloid Interface Sci.*, 26(1):62–69, January 1968.

[162] D. Ende and K.-M. Mangold. Impedanzspektroskopie. *Chemie in unserer Zeit*, 27(3):134–140, 1993.

[163] Arbeitskreis Prof. Dr. Christian Hess. *Impedanzspektroskopie an einem Sauerstoffionenleiter*. practical course notes (Praktikumsskript), TU Darmstadt.

[164] J. Fleig and J. Maier. Rough electrodes in solid and liquid electrochemistry: impact of morphology on the impedance. *Solid State Ionics*, 94(1-4):199–207, February 1997.

[165] Malvern. Zeta Potential theory. In *user manual Zetasizer nano, Man 0317*, chapter 16.

[166] Physikalische Chemie Universität Bayreuth. Rheologie von kolloidalen Suspensionen. In *Praktikumsskript*, 2007.

[167] T. Kawamura, S. Okada, and J. Yamaki. Decomposition reaction of $LiPF_6$-based electrolytes for lithium ion cells. *Journal of Power Sources*, 156(2):547–554, June 2006.

[168] Kerstin Sann. Charakterisierung mesodisperser und gezielt strukturierter Materialien für Lithiumionen-Hochleistungsbatterien. Diploma thesis, 2008.

[169] A. M. Fleshman, M. Petrowsky, J. D. Jernigen, R. S. P. Bokalawela, M. B. Johnson, and R. Frech. Extending the compensated Arrhenius formalism to concentrated alcohol electrolytes: Arrhenius vs. non-Arrhenius behavior. *Electrochimica Acta*, 57(0):147–152, December 2011.

[170] M. Park, X. Zhang, M. Chung, G. B. Less, and A. M. Sastry. A review of conduction phenomena in Li-ion batteries. *Journal of Power Sources*, 195(24):7904–7929, December 2010.

[171] R. Greenwood and K. Kendall. Selection of suitable dispersants for aqueous suspensions of zirconia and titania powders using acoustophoresis. *Journal of the European Ceramic Society*, 19(4):479–488, 1999.

[172] B. Salopek, D. Krasic, and S. Filipovic. Measurement and application of Zeta-Potential. *Rudarsko-geolosko-naftni zbornik*, 4:147–151, 1992.

[173] C. Pfaffenhuber, S. Sörgel, K. Weichert, M. Bele, T. Mundinger, M. Gäbel, and J. Maier. In situ recording of particle network formation

in liquids by ion conductivity measurements. *J. Am. Chem. Soc.*, 133(37):14514–14517, August 2011.